JUKO-Doc-2 (2017)

JUKOLIB-ARC-2017

ATLAS OF AVERAGE RESONANCE CAPTURE DATA

Prepared as internal JUKO report by

J. Kopecky

JUKO Research

Kalmanstraat 4, 1817 HX Alkmaar

The Netherlands

Alkmaar, December 2017

Abstract - Resonance capture is the direct experimental way to determine the partial radiative width in a single-channel reaction mode and to convert it into the gamma-ray strength function. Experimentally, either the capture in discrete resonances (using TOF spectrometry) or in a large number of resonances measured simultaneously (using filtered neutron beam) can be used. In this report the *Average Resonance Capture* (ARC) data, measured at different filter beam facilities, are revisited and re-analyzed. This includes all measurements made between 1970 and 1990 currently recovered, some of which are only partially exploited. The majority of these measurements were devoted to the spectroscopy of low lying final states and only a very limited number addressed the *Photon Strength Function* (PSF) properties. The main aim of this work is to establish a complete data base of ARC measurements. The final Atlas file will include the selection of the best entries converted in PSF format for verification of different strength-function models.

1. Introduction

Photon strength functions (PSF) describe the average response of the nucleus to an electromagnetic probe, and are thus a fundamental quantity of interest for modelling of nuclear reactions, and more particularly radiative capture. They are intimately connected to primary capture intensities, which are, however, a subject to Porter-Thomas fluctuations.

The ARC technique was developed to overcome the Porter-Thomas fluctuations of the primary intensities from thermal or isolated resonance capture. It was realized that by simultaneous averaging over many resonances the Porter-Thomas fluctuations can be reduced and the primary transitions to the final states of given J^{π} have approximately the same intensity and can represent the distribution of partial radiative width.

Three types of experiments are usually used, capture in discrete resonances using TOF spectrometry (DRC), the average resonance capture (ARC) with filtered beams and to a lesser extent thermal neutron-capture data (THC). The last method is preferable for nuclei where the thermal capture is dominated by a single strong s-wave resonance. The instrumental part and the basis of the average resonance capture method have been well documented in a number of previous surveys [1-6]. The principle of the statistical analysis has been covered in the following references [7-11].

The materials, ^{10}B, ^{45}Sc or ^{56}Fe, have been used for ARC experiments where the neutron beams are produced by transmission through filter materials yielding neutron beams with bell-shaped energy distribution having different FWHM at neutron energies of about 150 eV, 2 keV and 24 keV, respectively. The boron-filtered beam primarily removes the thermal component, while for Sc and Fe the neutroncapture cross section interference dips yield quasi mono-energetic beams of a few keV wide. Such facilities have been assembled at four laboratories in the US: the Argonne National Laboratory ANL [1], the National Bureau of Standards [2], the Idaho Nuclear Engineering Laboratory INEL [5] and at Brookhaven National Laboratory BNL [6], during the period between 1970 and 1980. Outside the US, only three laboratories, two in USSR (IAEP/PPEI Obninsk [12] and Kiev [13]) and one in Germany (KfK Karlsruhe [14]), have produced published ARC results. The BNL facility turned out to be the best in all aspects, primarily due to high neutron fluence

and processing tools, and therefore the majority of all adopted data originate from BNL.

The report is organized as follows. In Sect. 1.1 the ARC data from available measurements are presented. The conversion of the data into a strength function with a detailed description of the uncertainties is presented in Sect. 2. In Sect. 3 the re-evaluated final PSF are internally validated against the DRC data. Finally, in Sect. 4 the ARC E1 and M1 data are compared with recent model of the axially-symmetric-deformed HFB+QRPA calculation. Conclusions are presented in Sect. 4.

1.1 Data extraction

We have re-analyzed all available ARC data measured at different beam facilities. The list of data sources used in this re-evaluation is given in the Appendix Table 1. It includes all measurements, which have been recovered from the period after 1970. Corresponding references are quoted. Some of the data, originating from the former collaboration between BNL (R.E. Chrien) and ECN (J. Kopecky), are referred here as *BNL/ECN database* and include some published and unpublished data. The origin of this effort was to form a complete starter file of ARC measurements to be used for PSF data; however, this was not completed at that time. All recovered data are listed, for those not considered in this analysis the reason is quoted in the comment column.

For a data source of ARC publications, the ENDSF and EXFOR data bases have been used. This action resulted in the selection of about 50 references. It includes all measurements which could be recovered. Corresponding references are quoted; some of the data are present in a private data base denoted as *BNL/ECN database*. However, the majority of publications focused on the spectroscopy of low lying final states and only a few publications presented the measured data as PSF results [15-19]. The recommended set of data for the final f(L) data base is shown in Table 2 of Appendix..

The average differential strength function $<f_L>$, determined for primary dipole transitions, is defined as

$$<f_L(E_{\gamma i})> = << \Gamma_{\gamma i} >/ E^3_{\gamma i} > D_0^{-1} , \qquad (1)$$

where $\Gamma_{\gamma i}$ is the partial radiative width, $E_{\gamma i}$ is the transition energy and D_0 is the s-wave resonance spacing. While for DRC the partial radiative width $\Gamma_{\gamma i}$ is experimentally determined, for ARC measurements this quantity has to be derived by the normalization of the measured average gamma-ray intensity $<I_\gamma>$. The E2 transitions are reduced by E_γ^3 too and not by E_γ^5 to place them on the same scale as the dipole ones for easier comparison.

Note that for the DRC measurements the parameters of the initial state are well defined by a single resonance (orbital momentum l and J^π) and the averaging over more

resonances is carried out in the data processing. Contary to this, in the ARC experiment the averaging is carried out in the experiment itself, over the large number of resonances present in the filtered beam neutron window. However, $<\Gamma_{\gamma i}>$ is not available and a normalization procedure has to be applied (see further Sect. 2.3)

The results are usually given in reduced intensities either as $<I\gamma/E_\gamma^3>$ (the phase factor) or as $<I_\gamma/E_\gamma^5>$ values (the assumed energy dependence of the Brink-Axel model) in arbitrary units. All recovered measurements have been reanalyzed and the resulting $<I\gamma/E_\gamma^3>$ values form the starter data base of ARC data (*AtlasIgE3*). The *AtlasIgE3* includes all recovered data, even if the same reaction was studied by several authors. The major part of this action was to convert all results (often presented also as I_γ only) in the common I_γ/E_γ^3 format and furthermore to reconfirm the multipolarity assignments of E1, M1 and E2 groups. For this purpose for every target input the corresponding final states with their $J\pi$ assignmets, taken from the recent ENDSF file, are included and compared with the previous assignments. For some transitions the corresponding final state was not quoted or was in conflict with the assignment, and for these cases the 24 keV data were used as further information. In particular the kinematic shift between 2 and 24 keV data was employed and furthermore the standard 2/24 keV intensity ratio was used for parity assignment. An example of the input file is shown in Table 2 in the Appendix.

All errors quoted in recovered publications have been adopted without any changes as experimental statistical errors of the data base. They include the uncertainty of the gamma ray spectrum analysis, namely the statistical accuracy and absolute intensity calibration. This error is derived from the spectrum fitting and calibration treatment. These errors for moderately large and strong transitions are of the order of 10 - 20%. However, transitions at lower γ-ray energies with a high density of γ-lines or transitions with peak intensity close to the experimental sensitivity limit may be much larger.

2. PSF data processing

2.1 Data dispersion (final state population dependence)

The first reason for data dispersion is due to the dependence of averaged intensities on the spin of the final state. This is due the different population of J_f spin groups ($J_t^{\pm}1/2$ and $J_t^{\pm}3/2$) from the initial s-wave capture state with $J_i = J_t^{\pm}1/2$ (see Fig. 1) and J_t the target spin. For data adopted in the BNL/ECN source, the dependence of averaged reduced intensities on the spin of the final state has been removed using the SPARC or RACA codes [7, 8]. Where such analysis is missing, an approximate factor based on the equation for the statistical factor

$$Q(J_iJ_f) = (J_i + ½) / 2(J_t + ½) \quad (2)$$

has been used. As shown in Ref. [8], such approximation does not significantly influence results compared to the Monte-Carlo approach and the difference still remains within the statistical accuracy of the I_γ/E_γ^3 values.

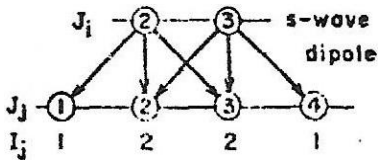

Fig. 1 Schematic picture of double population of $J_i^{+}1/2$ final spin.

The Q(JiJf) correction factors used for f(L) data files are shown in Table1 for different spin configurations involved. The RACA calculated values are combined with a simplified approach, using the statistical factors for the generation of the capture states with spins J_i.

Table 1. The correction factors for the (J_i -> J_f) population dependence on the final spin J_f.

Nucleus	$J_{t\pi}$	Q(JiJf) Stat. factor	Q(JiJf) RACA code
As-76	3/2-	2	
Zr-92	5/2+	2	
Mo-96	5/2+		2.02/1.8
Mo-98	5/2+	2	
Ru-102	5/2+		2.04/1.8
Pd-106	5/2+	2	
Pd-109	0+	1	
Cd-114	1/2+		1.62
Te-124	1/2+	1.33	
I-128	5/2+	2	
Ba-135	0+	1	1
Ba-136	3/2+	2	
Nd-146	7/2-	2	
Sm-148		2	
Sm-150		2	
Sm-155	0+	1	1
Gd-155	0+	1	1
Gd-156	3/2-	2	
Gd-157	0+	1	1
Gd-158	3/2-	2	

Gd-159	0+	1	1
Dy-162	5/2+		2.02/1.9
Dy-163	0+	1	1
Dy-164	5/2-		2.03/1.9
Dy-165	0+	1	1
Ho-166	7/2-	2	
Er-168	7/2+		2.32/1.7
Yb-172	1/2-		1.51
Yb-174	5/2-	2	
Lu-176	7/2+		2.02/1.9
Hf-178	7/2-	2	
Hf-180	9/2+	2	
W-184	1/2-	1.33	
W-185	0+	1	1
W-187	0+	1	1
Os-188	1/2-	1.33	
Os-189	0+	1	1
Os-191	0+	1	1
Os-193	0+	1	1
Ir-192	3/2+	2	
Ir-194	3/2+	2	
Pt-195	0+	1	1
Pt-196	1/2-	1.33	
Pt-197	0+	1	1
Pt-199	0+	1	1
Au-198	3/2+	2	
Th-233	0+	1	1
U-236	7/2-	2	
U-239	0+	1	1
U-239	0+	1	1
Np-238		2	
Pu-240	1/2+	1.33	

2.2 Data dispersion from Porter-Thomas fluctuations

A major source of data dispersion is due to the Porter Thomas fluctuations. In an analysis of the BNL measurements the Porter-Thomas uncertainty is estimated from the Monte-Carlo simulation code RACA [8]. This estimate is applied as an uncertainty band over data points for the same multipolarity and is not added to individual transitions as an additional error. Since the code RACA is not available anymore, we have looked for an

approximation, which was employed before the code RACA was implemented in ARC processing procedure.

A simple approach can be adopted, as a useful approximation. The relative variance is given by the factor 2/□ factor, where □ is number of degrees of freedom. In the present situation is □□is equal to the number of resonances present in the 2 keV window and can be estimated from the FWHM of the Sc filter. In the adopted data the E1, M1 and sometimes E2 groups are clearly separated from each other by the satisfactory experimental averaging and their multipolarity assignments are well known. The full width at half maximum of the BNL Sc filtered beam facility has been determined 900 eV [6] and the number of resonances can be estimated using □ = 900/D_0(eV) leading to the dispersion dPT = √ 2/□. For a boron filter the FWHM is estimated as about 1000 eV [11].

The beam profile has the maximal neutron flux at its centre and decreases at the beam boundaries, reducing the effective number of degrees of freedom, and the number of resonances. This can be compensated by using a smaller effective FWHM value of 600 eV. Further the presence of p-wave resonances may influence the dispersion (see later) but despite all these effects this approximation gives sufficient information to judge the dispersion of the data due to the Porter-Thomas fluctuations within the E1, M1 and E2 experimental data groups. The derived PT dispersion factors for all studied nuclides are shown in Table 2.

Table 2. The estimated PT dispersion for all nuclides, for D_o values data from RIPL-3 have been used [20].

Nucleus	Do	1+dPT =√2/υ	
	[eV]	FWHM n-beam 900keV	600keV
As-76	93	1.44	1.56
Zr-92	536	2.10	2.34
Mo-96	81.4	1.43	1.52
Mo-98	46.5	1.32	1.39
Ru-102	18.5	1.20	1.25
Pd-106	10.9	1.16	1.19
Pd-109	135	1.55	1.66
Cd-114	24.8	1.23	1.29
Te-124	25.1	1.24	1.29
I-128	9.7	1.15	1.18
Ba-135	360	1.89	2.09
Ba-136	40	1.29	1.36
Nd-146	17.8	1.13	1.19

Sm-148	57	1.36	1.38
Sm-150	2.2	1.07	1.14
Sm-155	114	1.50	1.62
Eu-154	1.14	1.05	1.12
Gd-155	13.8	1.17	1.21
Gd-156	1.8	1.06	1.08
Gd-157	30.5	1.26	1.32
Gd-158	87	1.44	1.54
Gd-159	82	1.43	1.52
Dy-162	2.14	1.07	1.09
Dy-163	62.9	1.37	1.46
Dy-164	7.28	1.13	1.16
Dy-165	144	1.57	1.69
Ho-166	4.20	1.07	1.09
Er-168	4	1.10	1.12
Tm-170	7.28	1.13	1.21
Yb-172	6.08	1.12	1.14
Yb-174	8.06	1.13	1.16
Lu-176	3.45	1.09	1.11
Hf-178	2.4	1.07	1.09
Hf-180	4.09	1.10	1.18
Ta-182	4.17	1.10	1.17
W-184	12	1.16	1.20
W-185	81	1.42	1.52
W-187	93	1.46	1.56
Os-188	4.56	1.10	1.12
Os-189	40	1.29	1.36
Os-191	70	1.39	1.48
Os-193	115	1.51	1.62
Ir-192	1.68	1.06	1.07
Ir-194	3.98	1.09	1.11
Pt-195	82.6	1.43	1.53
Pt-196	19.2	1.21	1.25
Pt-197	214	1.69	1.84
Pt-199	340	1.87	2.07
Au-198	15.7	1.19	1.23
Th-233	15.8	1.19	1.23
U-236	0.49	1.03	1.05
U-239	16.4	1.19	1.23
Np-238	0.52	1.04	1.11
Pu-240	2.07	1.07	1.08

For illustration, the PT dispersion band for E1 and M1 transitions of ^{197}Au (n,γ) reaction are shown in Fig. 2. The calculated trend lines were applied to guide the eye and are broadened by the estimated factor (1+dPT) =1.19. It seems that the number of outliers, considering the statistical errors, is reasonably small. The resonances from the tails of the bell shape neutron spectrum are weak and contribute less to the averaging.

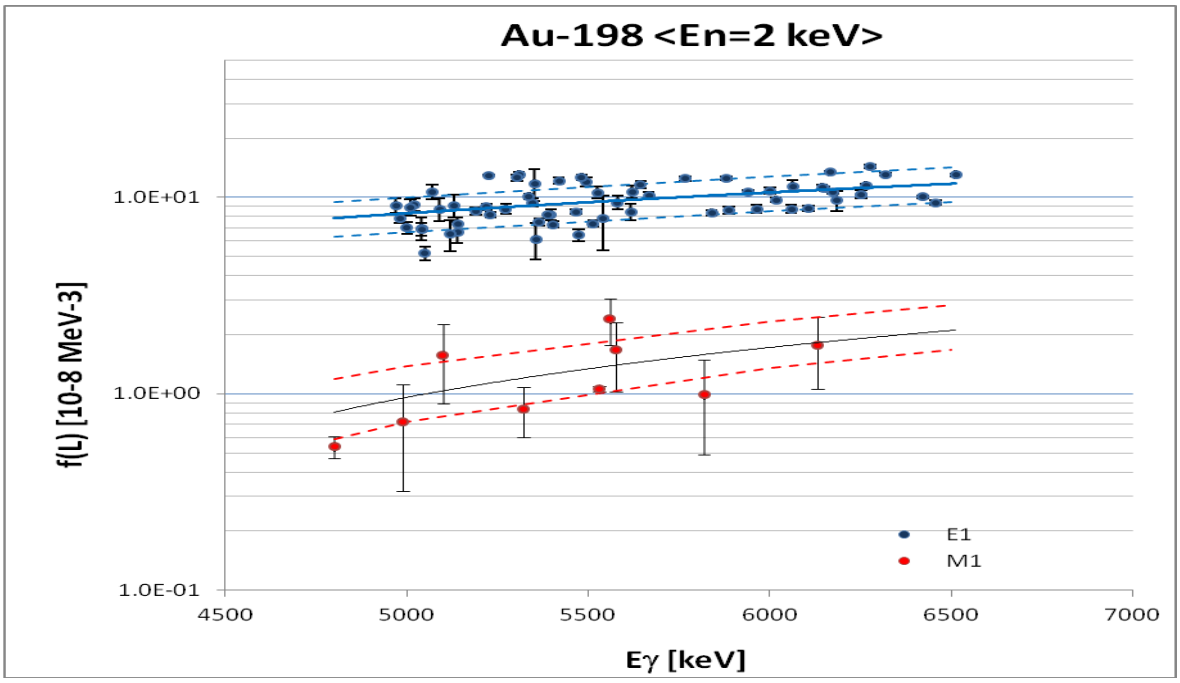

Fig. 2 The PT dispersion estimated from the $\sqrt{2}/\upsilon$ approximation for ^{198}Au. The 2 keV data are taken from*JUKOLIB-ARC-2017* file. The trend fit curves (full and the dashed) describe the PT dispersion boundary around the arbitrary mean value.

To illustrate this effect the dPT is also shown for a smaller window in order to accommodate this effect by smaller effective FWHM. However, the comparison of the $\sqrt{2}/\upsilon$ approximation with the Monte Carlo calculation [9, 21] indicates that the influence is not too significant in the presence of achieved statistical accuracy of measured data.

2.3 Conversion to the absolute PSF scale

When the dispersion was corrected for double population (see Fig. 1), the data are ready for conversion of the adopted $\langle I_\gamma/E_\gamma^3 \rangle$ values in the γ-ray strength function scale of 10^{-8}MeV^{-3}. Because the initial state in the filtered beam experiments is a mixture of many initial states (resonances) and cannot be uniquely defined, some external information has to be applied. This can be done using DRC data. As matter of fact, this normalization procedure using the DRC results, is the only way to generate absolute PSF from ARC filtered beam experiments, because they involve resonances with known Γ_γ. The DRC is the same physical process at similar neutron energy and the resonances have well defined orbital momentum and parity parameters.

The calibration of the reduced intensities is performed using the comparison with DRC data using equations

$$<f(I\gamma/E^3)_{ARC}>/<f(E1)_{DRC}> = C \quad (3)$$

and $$f(E1)_{ARC} = C \times (I\gamma/E^3)_{ARC} \quad (4).$$

The E1 transitions are primarily used because of their superior statistical accuracy and their purity (the negligible effect od p-wave contribution) . The calibration against DRC f(M1) values has not been used for two reasons: firstly the statistical accuracy is inferior to E1 data and secondly the M1 radiation from the capture of 2 keV neutron beam is slightly polluted by E1 radiation from the p-wave capture (see below)

The normalization constant *C* may be derived in two ways. When DRC measurements are available, the information can be taken using the mean value of $f(E1)_{DRC}$, averaged over transitions present in the energy range used (usually of about 1 MeV broad), as documented in Ref. [22]. The advantage of this procedure is that the same transitions measured in both DRC and ARC experiments are used. The DRC then gives the absolute transition strength.

If the DRC measurement is not available, use is made of the f(E1) systematic equation

$$<f(E1)> = 0.0021\, A^{1.69\pm0.17}\ [10^{-8}\ \mathrm{MeV}^{-3}],\quad (5)$$

based on a fit to measured DRC data [22] as a function of the atomic mass A at $E\gamma$ energies around 6.2 ± 0.5 MeV and shown in Fig. 3. This energy may form an additional uncertainty for targets in which the dominant E1 transitions are not in the vicinity of 6.2 MeV. In such a case, the systematic value has to be adjusted assuming an additional E^2 dependence from the Brink-Axel model.

After completion of this re-analysis and re-processing, a recommended value was chosen for the PSF file (*Atlasf(L)*). For targets with more measurements, the quality and the completeness of data were used as a criterion to choose the recommended final source. The preliminary release of *Atlasf(L)* from March 2017 was used in Ref. [19].

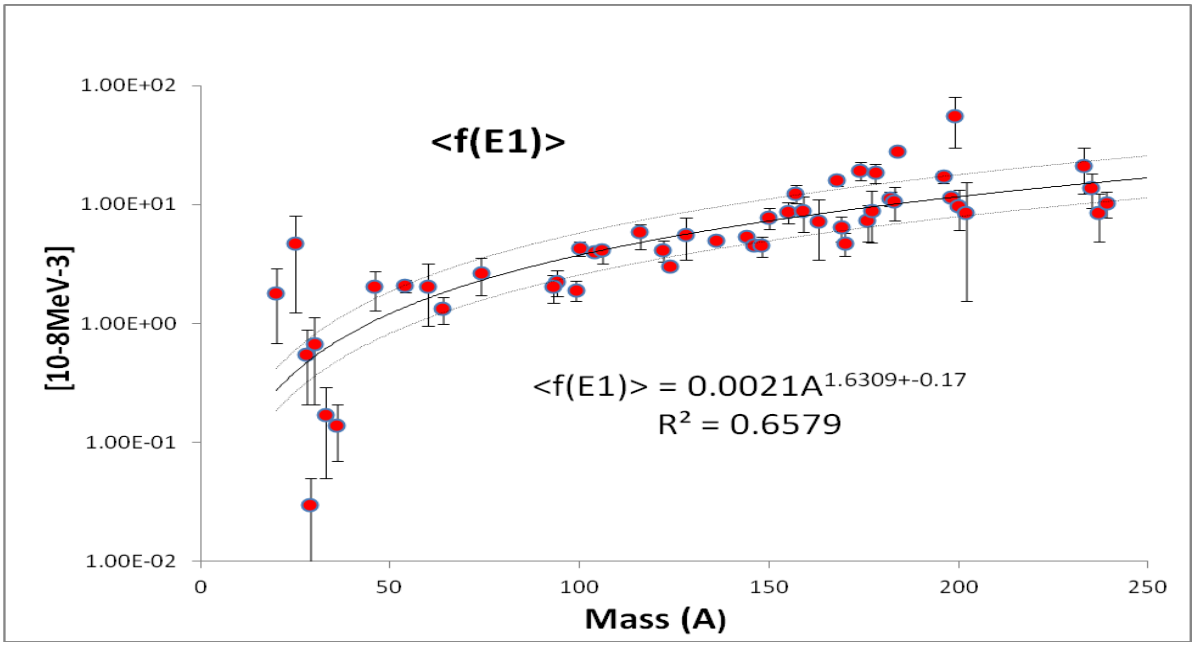

Fig. 3 Plot of $<f(E1)>_{DRC}$ values. The full curve represents the LSQ fit to recent data with the R^2 value. The uncertainty band of f*A and A/f represents the 99% confidence limit. The mean energy $<E_\gamma>$ of transition groups was 6.2 MeV.

An example of such a conversion is shown in in the Appendix (Table 3) for the ^{75}As(n,γ) reaction. The E1 transitions used for the normalization, in this case against the systematic equation, are labelled in red and the M1 transitions, used for E1/M1 ratio analysis, are in blue. Note the energy range has been chosen close to 6-7 MeV and covers both E1 and M1 transitions. The summary of the normalization factors is included in Table 3.

Table 3. List of nuclides with the ARC calibration in to the PSF data

$<E_\gamma>$ - the mean energy of the energy interval of transitions used for the calibration
<f(E1)> - PSF values derived from DRC or systematic, underlined values adopted
M1 - No E1 transitions present, M1 systematic used instead

Nucleus	n-beam	<Eγ> Calib. energy	<f(E1)> E1 Calib. DRC exp.	<f(E1)> E1 Calib. DRC SYS
		MeV	10^{-8}MeV^{-3}	
As-76	Sc	6.7		<u>2.35</u>
Zr-92	Sc	6.2	--	<u>3.20</u> M1)
Mo-96	Sc	6.1		<u>3.43</u>
Mo-98	Sc	6.6		<u>3.55</u>

Ru-102	Sc	6.8		3.78
Pd-106	B	7.2	4.14	(4.03)
Pd-109	Sc	5.9		1.29[M1)]
Cd-114	Sc	6.2		4.53
Te-124	Sc	7.1	--	1.44[M1)]
I-128	Sc	6.6	(1.90)	5.47
Ba-135	Sc	5.1		5.96
Ba-136	Sc	6.6	5.0	(6.03)
Nd-146	B	6.4	4.5	(6.77)
Sm-148	B	6.6	4.5	(7.28)
Sm-150	B	6.3	7.83	(7.44)
Sm-155	Sc	5.4		7.46
Eu-154	Sc	7.9		7.38
Gd-155	Sc	5.9	9.2	(7.46)
Gd-156	B	7.4		7.53
Gd-157	Sc	5.9	12.4	(7.61)
Gd-158	B	6.4		7.69
Gd-159	Sc	5.4	8.81	(7.77)
Dy-162	Sc	6.8		8.01
Dy-163	Sc	5.7	7.26	
Dy-164	Sc	7.2	8.17	(8.09)
Dy-165	Sc	5.4		8.24
Ho-166	B	6.0		8.33
Er-168	B	6.4	15.9	(8.50)
Tm-170	Sc	6.1	(4.72)	8.66
Yb-172	Sc	6.8		8.83
Yb-174	B	6.6	19.4	(8.99)
Lu-176	Sc	5.9	7.4	(9.16)
Hf-178	Sc	6.8	18.5	(9.33)
Hf-180	Sc	6.0		10.01
W-184	B	6.8	28.1	(9.85)
W-185	Sc	5.4		9.93
W-187	Sc	4.6		10.11
Ta-182	Sc	5.8	11.3	(9.67)
Os-188	Sc	6.3		10.20
Os-189	Sc	4.5		10.28
Os-191	Sc	5.4		10.46
Os-193	Sc	5.5		10.60
Ir-192	Sc	6.1		10.55
Ir-194	Sc	5.9		10.73
Pt-195	Sc	4.9		10.82

Pt-196	Sc	6.3	17.4	(10.91)
Pt-197	Sc	4.7		11.00
Pt-199	Sc	4.6		11.18
Au-198	Sc	6.0	11.4	(11.09)
Th-233	Sc	4.1	(20.3)	14.44
U-236	Sc	6.0		15.6
U-239	B	4.0	10.29	(15.04)
Np-238	Sc	5.3		15.71
Pu-240	Sc	5.6	19.9	(15.15)

2.4 The <Eγ> dependence of the normalization

The mean energy of the energy regions (on average about 0.5-1 MeV wide), used for normalization of the $I\gamma/E_\gamma^3$ input data, is shown in the first column of Table 5. They range between 3.6 and 7.2 MeV. In cases where the measured DRC data are used for normalization and the identical transitions are also chosen, no energy difference between DRC and ARC data occurs. However, the situation is different if the ARC data are related to the DRC systematics. The average reference energy of the <f(E1)> systematic equation is 6.2 $\pm$ 0.25 MeV and some of the used energy regions are significantly different and for the renormalization to this energy a correction factor has to be applied. The additional energy behaviour is generally assumed to be E_γ^2 as predicted by the Brink-Axel Giant Resonance model. The resulting <Eγ> listing is given in Table 4.

Table 4. The Eγ dependence correction factor $F=<E\gamma>_{ARC}/<E\gamma>_{DRC}$ for data normalized to the $<f(E1)>_{DRC}$ from DRC measurements or DRC systematic at 6.2 MeV. The 3rd column gives the F^2 ratio for DRC measurements, while the 4th column gives the DRC systematic.

Nucleus	$<E_\gamma>_{ARC}$	<DRC> F^2	< SYS> F^2
		used	used
As-76	6.7		0.86
Zr-92	6.2		1 M1
Mo-96	6.1		1.03
Mo-98	6.6		0.88
Ru-102	6.8		0.83
Pd-106	7.2	0.96	
Pd-109	5.9		1.10
Cd-114	6.2		1
Te-124	7.1	1 M1	
I-128	6.6	1.03	

Ba-135	5.1		1.48
Ba-136	6.6	1	
Nd-146	6.4	1.09	
Sm-148	6.6	0.88	
Sm-150	6.3	0.97	
Sm-155	5.4		1.32
Eu-154	7.9		0.62
Gd-155	5.9	1.20	
Gd-156	7.4		0.7
Gd-157	5.9	0.96	
Gd-158	6.4		0.94
Gd-159	5.4	0.89	
Dy-162	6.8		0.83
Dy-163	5.7		
Dy-164	7.2		0.74
Dy-165	5.4		1.32
Ho-166	6.0		1.07
Er-168	6.4	1	
Tm-170	6.1		1.03
Yb-172	6.8		0.82
Yb-174	6.6	0.95	
Lu-176	5.9	0.98	
Hf-178	6.8	0.95	
Hf-180	5.9		1.05
W-184	6.8	0.94	
W-185	5.4		1.32
W-187	4.6		1.82
Ta-182	5.8		
Os-188	6.3		0.97
Os-189	4.5		1.90
Os-191	5.4		1.32
Os-193	5.5		1.27
Ir-192	6.1		1.03
Ir-194	5.9		1.10
Pt-195	4.9		1.60
Pt-196	6.3		0.97
Pt-197	4.7		1.74
Pt-199	4.6		1.82
Au-198	6.0	1	
Th-233	4.1		2.29
U-236	6.0		1.07

U-239	4.0	0.94	
Np-238	5.3		1.32
Pu-240	5.6	0.92	

The following nuclides, normalized with the systematic equation and with $<E_\gamma>$ outside the 5.7 – 6.7 MeV range, have been chosen for the correction using the factor $(<E_\gamma>_{ARC}/6.2)^2$. They are; ^{135}Ba, ^{155}Sm, ^{154}Eu, ^{156}Gd, ^{164,166}Dy, $1^{85,187}$W, ^{195,197,199}Pt, ^{233}Th and ^{238}Np.

2.5 The p-wave contribution

The ARC experiments use neutron beam energies spreading from about 100 eV (B) through 2 keV (Sc) and up to 24 keV (Fe). The dominance of s-wave capture, close to thermal energies, decreases with increasing neutron energy, so that p-wave resonances start to contribute to the capture process. This effect has been included in the code RACA as the Monte-Carlo modelling of the partial cross sections and is discussed in Refs. [8,9]. In the spectroscopic application of the ARC method, the p-wave capture is primarily used for the parity determination of the final states by means of the intensity ratio of the 24 keV to the 2 keV data. The boron filtered beam with its low neutron mean energy of about 150 eV has negligible p-wave component, except nuclides from the 3p-giant resonance of the p-wave strength around A = 100. This influenced only Pd-106 file in the present PSF data base (see Appendix 1 for details).

However, for PSF application, the *p*-wave capture both at 2 and mainly 24 keV complicates the determination of the absolute strength of M1 radiation, increasing the s- wave M1 strength by the p-wave E1 admixture. In all BNL/ECN data the p-wave admixture at 2 keV was estimated from RACA calculations and the results are shown in Table 4. The size of this contribution follows the distribution of 3p and 4p giant resonances of p-wave neutron strength function. Contrary to that, the E1 s-wave capture is negligibly increased by M1 *p*-waves due the weaker M1 strength. In all calculated cases was the M1 p-wave contribution to E1 transitions was smaller than $^{\pm}$5% (see Table 6).

Table 6. The results of RACA calculations of the p-wave component at 2 keV ARC experiments (from private BNL/ECN collaboration logbook).

Nuclide	$\mathbf{<f(M1)>_{p\text{-}waves}}$ in $\mathbf{<f(E1)>_{s\text{-}waves}}$	$\mathbf{<f(E1)>_{p\text{-}waves}}$ in $\mathbf{<f(M1)>_{s\text{-}waves}}$
Mo-96	0.09	0.66
Ru-102	0.04	0.33
Cd-114	0.04	0.24
Sm-155	0.04	0.21
Gd-157	0.01	0.15

Dy-162	0.01	0.13
Dy-164	0.02	0.18
Yb-172	0.01	0.09
Lu-176	0.01	0.15
Pt-195	0.02	0.31
Th-233	0.02	0.39
U-239	0.03	0.37

For number of the ARC data processed in the *BNL-ECN database*, the E1 component present in the M1 radiation was estimated by the RACA code calculations. For the remaining data, with no correction, this effect is estimated in the following way. The theoretical description of the formula for the ratio of s- and p-wave capture can be found in Refs. [7-11] (Eq. 7 in [9]) and is a function of several ingredients, such as S_0, S_1, $\Gamma_{\gamma 0}$ and $\Gamma_{\gamma 1}$. If we use the following assumptions, $\Gamma_n << \Gamma_{\gamma;;}\Gamma_\gamma$ is independent of the orbital momentum and $D_J = D_0/2J+1$, the approximation of the theoretical equation for average cross section at 2 keV [9] can be simplified as

$$<\sigma_{Jf>} \sim \Sigma_{s\text{-wave}} <\Gamma_{\gamma f}(E1,M1)> + S_1 f/S_0 \; \Sigma_{p\text{-wave}} <\Gamma_{\gamma f}(E1,M1)> . \qquad (5)$$

The factor $f = (ka)^2/(1+(ka)^{2)}$ is the penetrability of p-wave neutrons relative to s-wave neutrons.

The dominant factor in this formalism is the S_1/S_0 ratio. We have plotted the calculated $(f(E1))_{p\text{-wave}}/(f(M1)_{s\text{-wave}})$ ratio against the S_1/S_0 ratio and found it most instructive to estimate the E1 (p-wave) component (see Fig. 4). We used the RACA calculated contributions within the BNL/ECN collaboration for 11 nuclides (no S_1/S_0 value for ^{195}Pt).

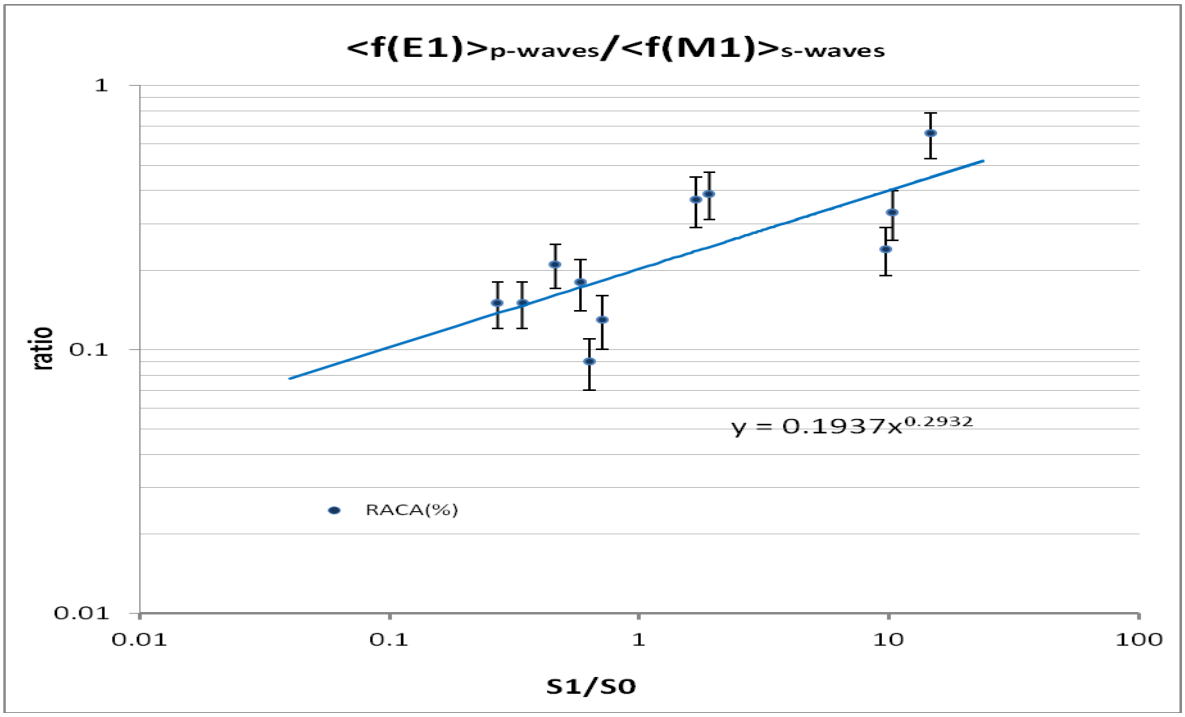

Fig. 4 The calculated $\langle f(E1)\rangle_{p\text{-waves}}/\langle f(M1)\rangle_{s\text{-waves}}$ ratios as a function of S_1/S_0. The fitted trend line is used as a systematic estimate of the p-wave admixture.

The derived trend function of the $\langle f(E1)\rangle_{p\text{-waves}}/\langle f(M1)\rangle_{s\text{-waves}} = 0.19(S_1/S_0)^{0.29}$ ratio was used to estimate this effect for all remaining nuclei. The applied corrections to the M1 strength are included in Table 7.

Table 7. List of nuclides with the p-wave corrections.

S_1/S_0 - S_0 and S_1 values taken from RIPL3

[a] S_1 values estimated from Fig. 2.2 and DOM calculations in [BNL]

[b] No S_0 value available

p-wave - the estimated/calculated p-wave E1 contribution in M1 s-wave transitions at <En> = 2 KeV

[1] RACA calculations (BNL-ECN data base[),]

[2] boron estimate assumed with negligible p-wave contribution

[3] empirical estimate in this work from $E1_p/M1_s = 0.19S_1/S_0^{0.29}$

[4] estimated from DRC data

Nucleus	n-beam	S_1/S_0	p-wave E1in M1 s-wave estimate.	p-wave E1in M1 applied
As-76	Sc	0.96	0.19	0.19[3]
Zr-92	Sc	18.1	0.45	0.45[3] M1
Mo-96	Sc	14.66	0.43	0.66[1]
Mo-98	Sc	23.79	0.49	0.49 [3]
Ru-102	Sc	10.34	0.38	0.33[1]
Pd-106	B	10.27	0.36	0.33[4]
Pd-109	Sc	5.67	0.31	0[5] M1
Cd-114	Sc	9.68	0.37	0.24[1]
Te-124	Sc	1.90 [a]	0.23	0.23[3] M1
I-128	Sc	2.57	0.26	0.26[3]
Ba-135	Sc	1.77	0.23	0.23[3]
Ba-136	Sc	1.3	0.21	0.21[3]
Nd-146	B	1.10 [a]	0.20	0[2]
Sm-148	B	0.19	0.12	0[2]
Sm-150	B	0.06	0.08	0[2]
Sm-155	Sc	0.68 [a]	0.17	0.21[1]
Eu-154	Sc	2.20	0.24	0.24[3]
Gd-155	Sc	0.75 [a]	0.18	0.18[3]
Gd-156	B	1.68	0.23	0[2]
Gd-157	Sc	0.34	0.14	0.15[1]
Gd-158	B	1	0.19	0[2]
Gd-159	Sc	0.81	0.18	0.18[3]
Dy-162	Sc	0.71	0.17	0.13[1]
Dy-163	Sc	0.63	0.17	0.17[3]
Dy-164	Sc	0.58	0.16	0.18[1]
Dy-165	Sc	0.7	0.17	0.17[3]
Ho-166	B	0.54	0.25	0[2]
Er-168	B	0.52	0.16	0[2]
Tm-170	Sc	0.60 [a]	0.17	0.2[3]
Yb-172	Sc	0.63	0.17	0.09[1]
Yb-174	B	0.54	0.16	0.16[3]
Lu-176	Sc	0.27	0.13	0.15[1]
Hf-178	Sc	0.38	0.14	0.14[3]

Hf-180	B	0.48	0.15	0[2)]
Ta-182	Sc	0.38	0.14	0.14[3)]
W-184	B	0.38	0.14	0[2)]
W-185	Sc	0.23	0.12	0.12[3)]
W-187	Sc	0.17	0.11	0.11[3)]
Ta-182	Sc	0.35	0.14	0.14[3)]
Os-188	Sc	0.2	0.12	0.12[3)]
Os-189	Sc	0.13	0.10	0.10 [3)]
Os-191	Sc	[b)]		0.2[3)]
Os-193	Sc	[b)]		0.2[3)]
Ir-192	Sc	0.26 [a)]	0.13	0.13[3)]
Ir-194	Sc	0.38 [a)]	0.15	0.15[3)]
Pt-195	Sc	0.25 [a)]	0.13	0.31[1)]
Pt-196	Sc	0.28 [a)]	0.14	0.14[3)]
Pt-197	Sc	0.28 [a)]	0.14	0.14[3)]
Pt-199	Sc	0.36 [a)]	0.15	0.15[3)]
Au-198	Sc	0.84	0.18	0.18[3)]
Th-233	Sc	1.79	0.23	0.39[1)]
U-236	Sc	1.84	0.23	0.23[3)]
U-239	B	1.68	0.22	0[2)]
Np-238	Sc	1.96	0.23	No M1
Pu-240	Sc	1.55	0.22	0.22[3)]

All corrections from this section have been applied and led to the final version of *JUKOLIB-ARC-2017*.

3. PSF internal validation

3.1<f(M1)> comparison against DRC data

The M1 transitions were not used for f(L) normalization (except for two nuclides without E1 data), the reasons were discussed in Sect. 2.3). It may be therefore of interest to compare two independent sets of M1 data from DRC and ARC experiments. The results of the <f(M1)> comparison is shown in Fig. 5. The data in absolute units can be compared directly, because in both experiments similar energy regions have been used.

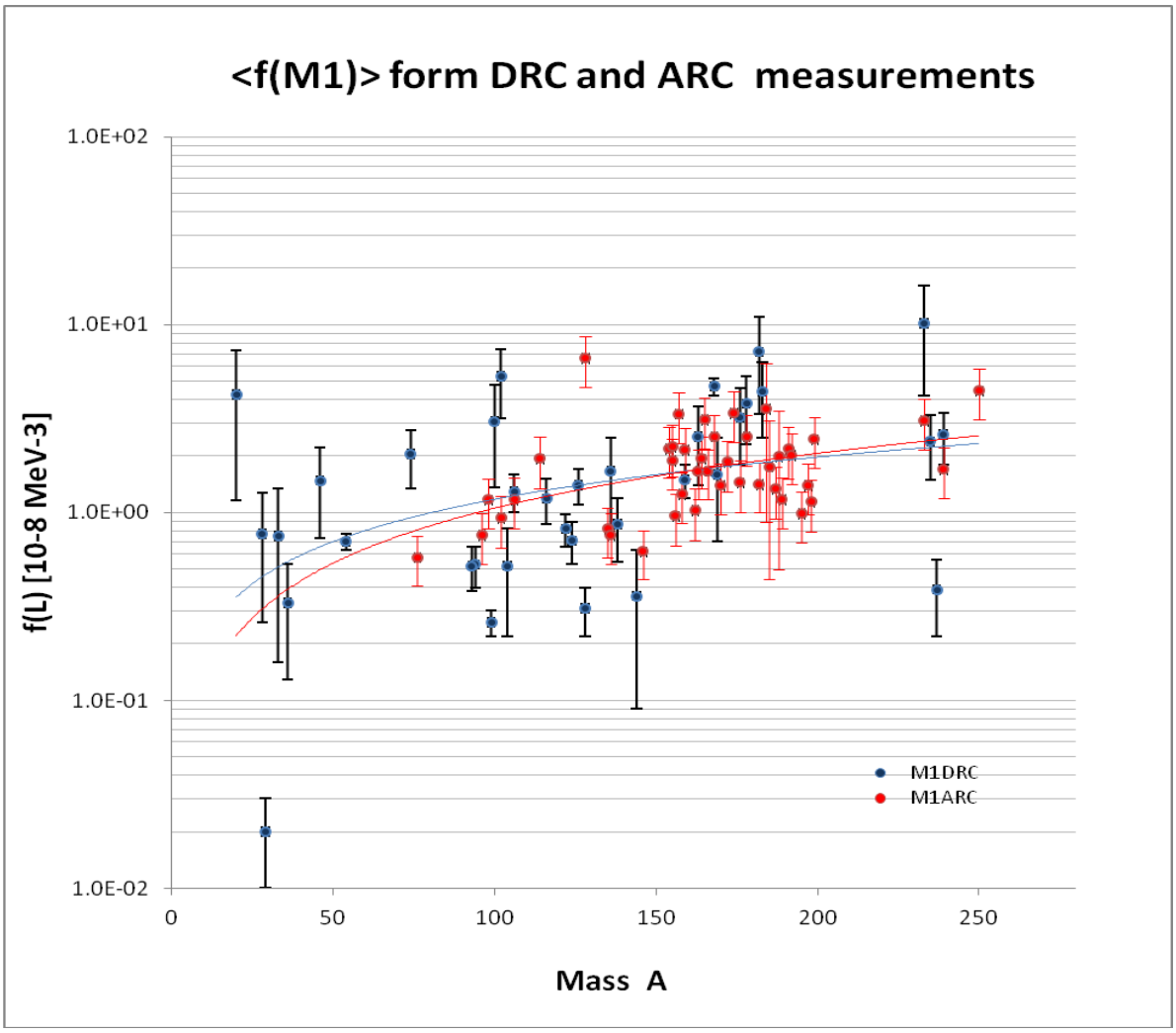

Fig. 5 Comparison of <f(M1)> values from DRC measurements [18] and recent ARC data taken from the present *JUKOLIB-2017*file.

Both data sets are in a very good agreement, which is also supported by two trend lines, which are close to each other. We may conclude that the adopted normalization procedure using exclusively E1 transitions gives good results for pure M1 strength.

3.2The E1/M1 ratio in ARC and DRC (comparison)

While both the E1 and M1 strengths are affected by uncertainties, as described in Sect. 2, the ratio of the E1 to M1 strengths remains independent of the conversion procedure from the intensities I_γ/E_γ^3 into PSF format, if the competing E1 contribution to M1 transitions for the p-wave capture is properly allowed for (see Sect. 2.5). We show in Fig. 6 the E1-to-M1 ratio as a function of the atomic mass A, both from the original ARC data at energies ranging between 3.6 and 7.2 MeV and after renormalizing the ARC data at the average reference energy of 6.2 ±0.25 MeV. The energy regions of E1 and M1 data (on average about 1 MeV wide) were identical in order to minimize the internal energy dependence between them. For the renormalization to the reference energy, an empirical factor, derived from the present ARC data, was applied. As can be seen in Fig. 6,

the original E1/M1 ratio is widely distributed between 1.5 and 7.8. However, this ratio is obtained at different energies and for nuclei that can be either spherical or deformed.

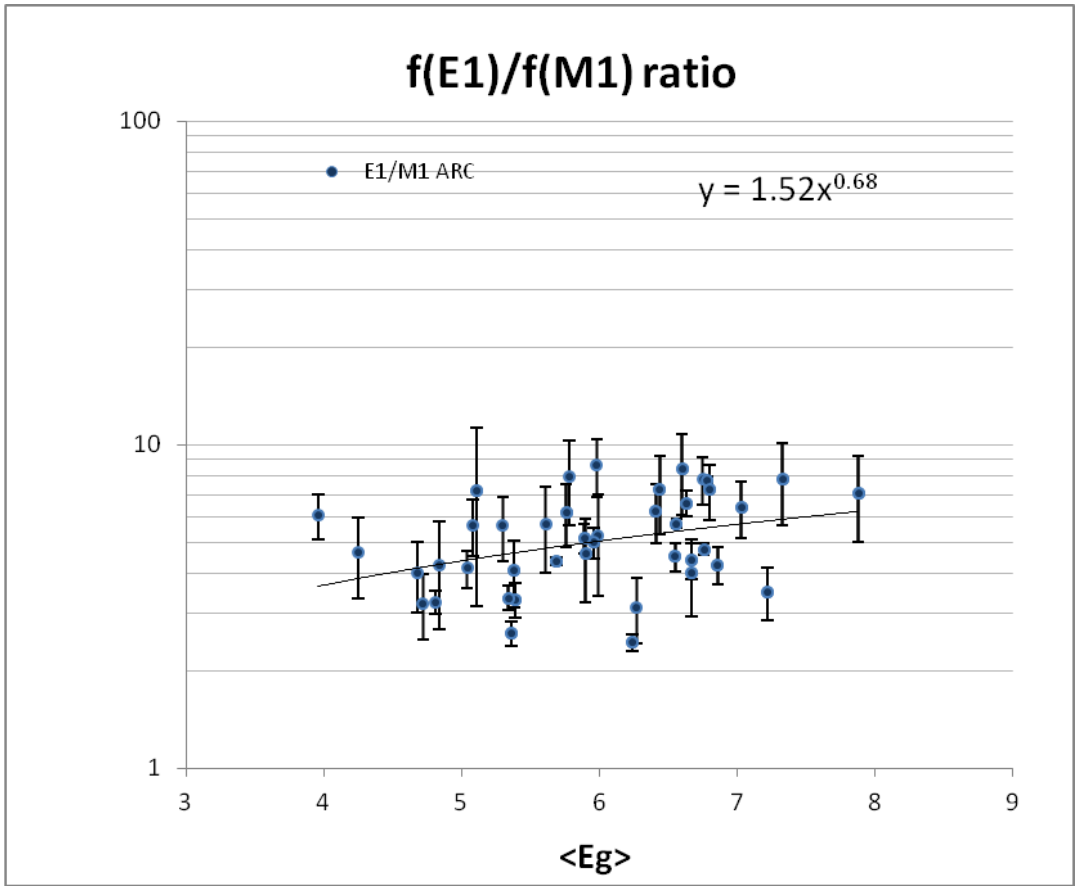

Fig. 6 The energy dependence of <f(E1)>/<f(M1)> ratio as a function of the mean transition energy $<E_\gamma>$, taken from the present ARC data.

It is therefore not recommended to extract a systematics from such data. Previous analyse of ARC data [22,23] led to some systematics at the reference energy of 6.2 MeV; more precisely it was proposed to consider the $f(E1)/f(M1) = 0.059\ A^{0.87}$ trend. This expression is the one recommended by the RIPL-3 library at the reference energy of 7 MeV [20]. With the additional data available now, we can further test and improve this systematics. As shown in Fig. 7, at the reference energy of 6.2 MeV, an average ratio $f(E1)/f(M1) = 0.35A^{0.53}$ can explain the general trend. This agreement supports the compatibility of DRC and ARC measurements. However, a large dispersion around such a systematics is also found, so that it remains hazardous to use such expressions for single events rather than as a general trend only. This dispersion is partly due to the difference in the mean energy of <f(E1)> and <f(M1)> regions used for averaging and also to the variety of M1 excitation modes as a function of A.

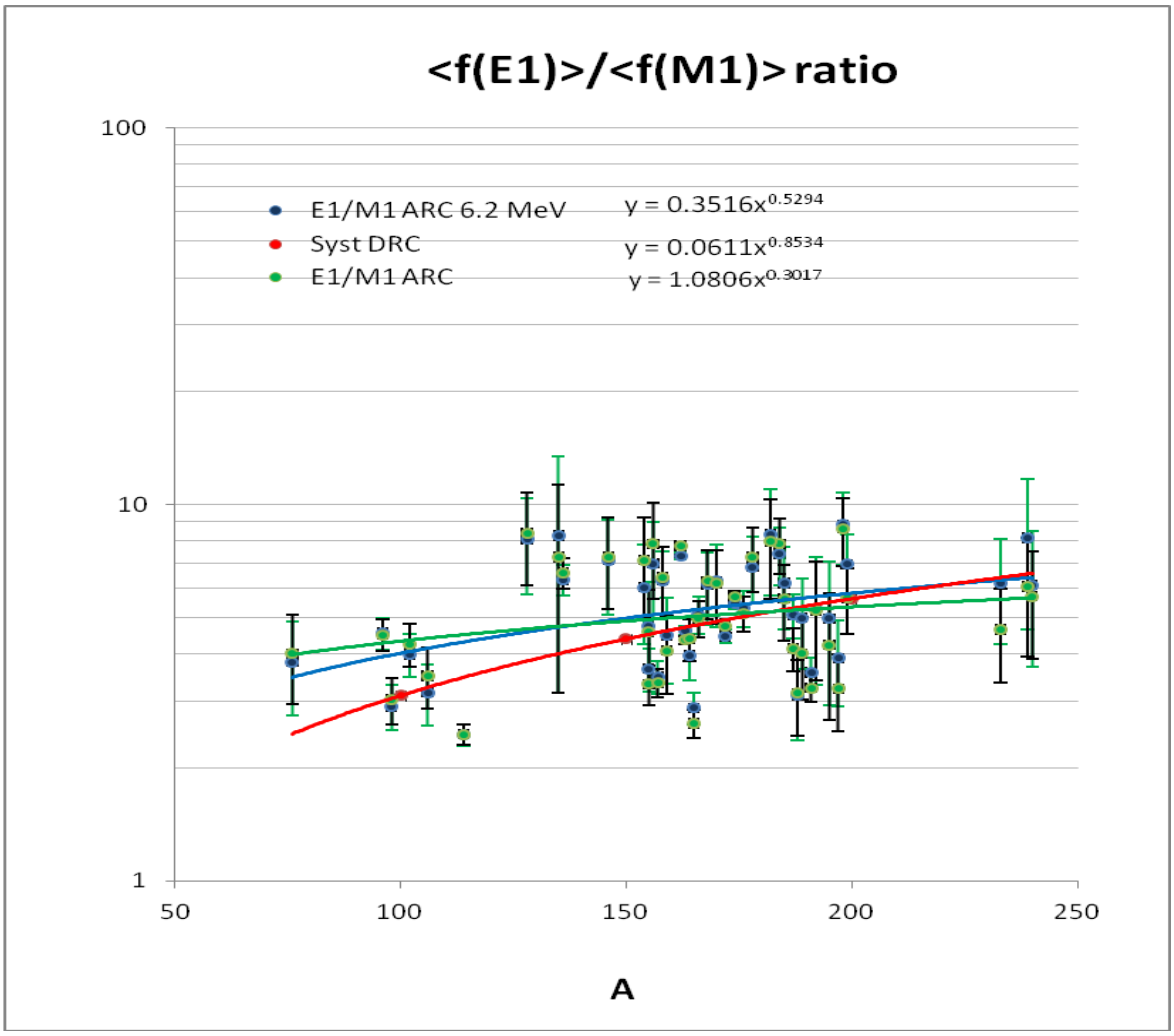

Fig. 7 The E1 to M 1 strengths ratio extracted from ARC data as a function of the atomic mass *A*. The green squares correspond to the ratio at the measured average energy and the blue squares renormalized at 6.2 MeV. The solid blue line is the newly proposed systematics of $(E1)/f(M1) = 0.35A^{0.53}$ at 6.2 MeV. The red line is the widely used the RIPL-3 systematics $f(E1)/f(M1) = 0.06A^{0.85}$ [20,23].

3.3 The comparison with PSF models

The recent the D1M+QRPA approach [24,25] has been chosen for the comparison of the final ARC data against the model predictions. Most of the nuclei for which ARC data are available correspond to deformed nuclei, except for light nuclei like ^{76}As, ^{92}Zr, ^{96,98}Mo, ^{146}Nd or ^{135,136}Ba, as seen by the M1 strength pattern from QRPA predictions (see an example in Fig. 8). All results for E1 and M1 strength are shown in Figs. 9and 10.

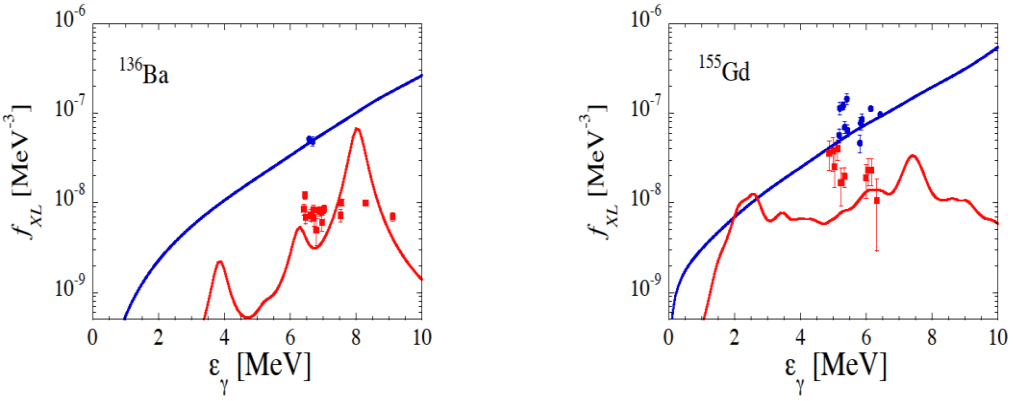

Fig 8. A typical distribution of the M1 strength for a spherical and deformed nuclide from QRPA calculations.

Indeed, for deformed nuclei QRPA calculations give an additional low-energy M1 component corresponding to the scissors mode, which is absent in spherical nuclei, where the spin-flip resonance dominates around 8 MeV [25].

In general, the agreement between D 1M+QRPA and ARC data is rather satisfactory, despite some outliers for both E1 and M1 strength, including ^{155}Sm, ^{156,157,159}Gd and ^{165}Dy, where D1M+QRPA underestimate the ARC data. Some of this disagreement may be due to the uncertain conversion between I_γ/E^3 into PSF format, which may involve uncertainties of DRC evaluations, which is supported by the fact that both E1 and M1 strengths are underestimated together. For these nuclides (except ^{157}Gd) the systematic equation was used for the normalization, and they belong to the mass region in which is the conflict between DRC measurement and deduced systematic trend line is seen (see Fig.3). The ^{157}Gd DEC measurement seems to exceed the neighbouring data very strongly.

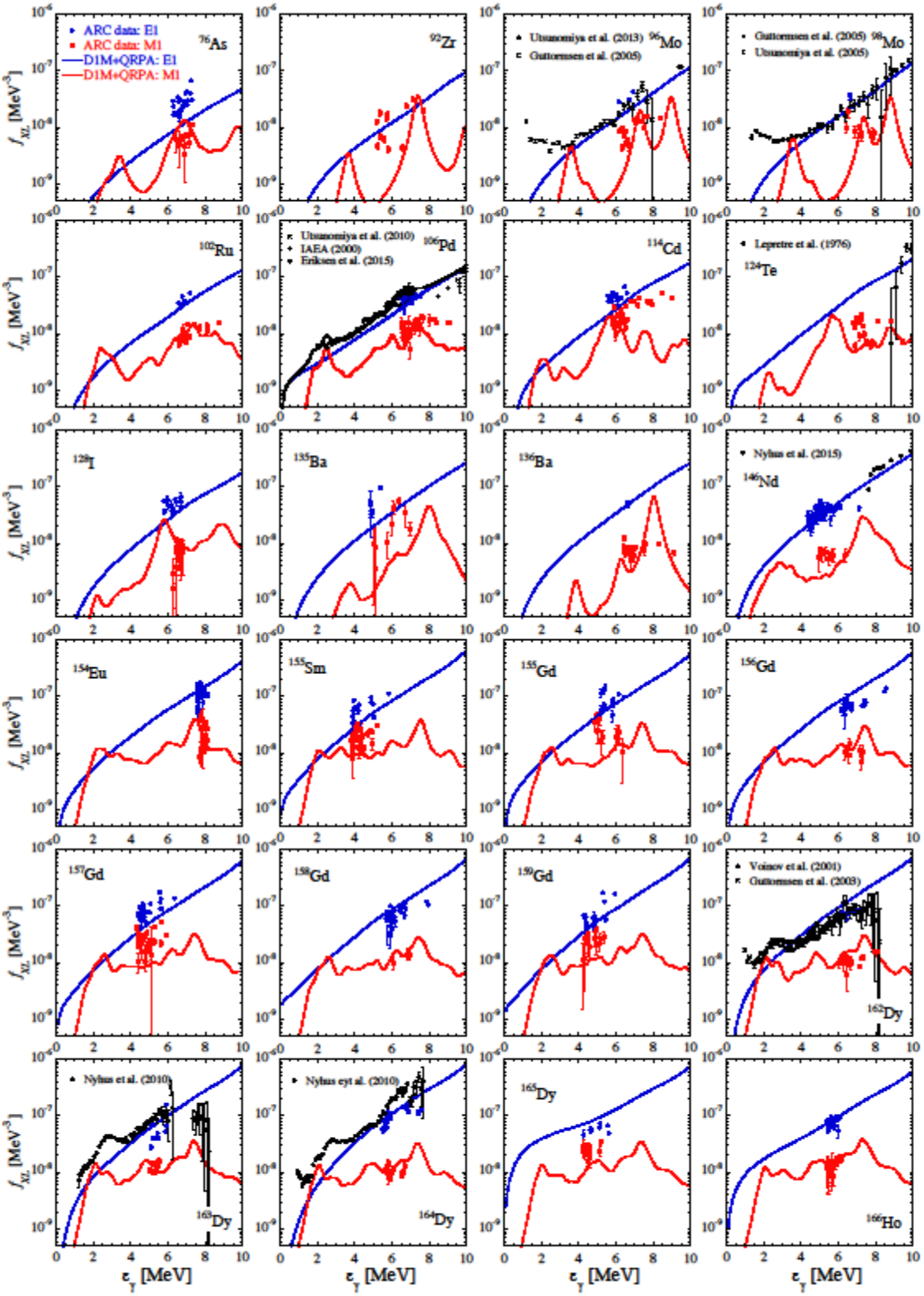
ARC data: E1
ARC data: M1
D1M+QRPA: E1
D1M+QRPA: M1
^{76}As
^{92}Zr
Utsunomiya et al. (2013)
Guttormsen et al. (2005)
^{96}Mo
Guttormsen et al. (2005)
Utsunomiya et al. (2005)
^{98}Mo
^{102}Ru
Utsunomiya et al. (2010)
IAEA (2000)
Eriksen et al. (2015)
^{106}Pd
^{114}Cd
Lepretre et al. (1976)
^{124}Te
^{128}I
^{135}Ba
^{136}Ba
Nyhus et al. (2015)
^{146}Nd
^{154}Eu
^{155}Sm
^{155}Gd
^{156}Gd
^{157}Gd
^{158}Gd
^{159}Gd
Voinov et al. (2001)
Guttormsen et al. (2003)
^{162}Dy
Nyhus et al. (2010)
^{163}Dy
Nyhus eyt al. (2010)
^{164}Dy
^{165}Dy
^{166}Ho
f_{XL} [MeV^{-3}]
ε_γ [MeV]

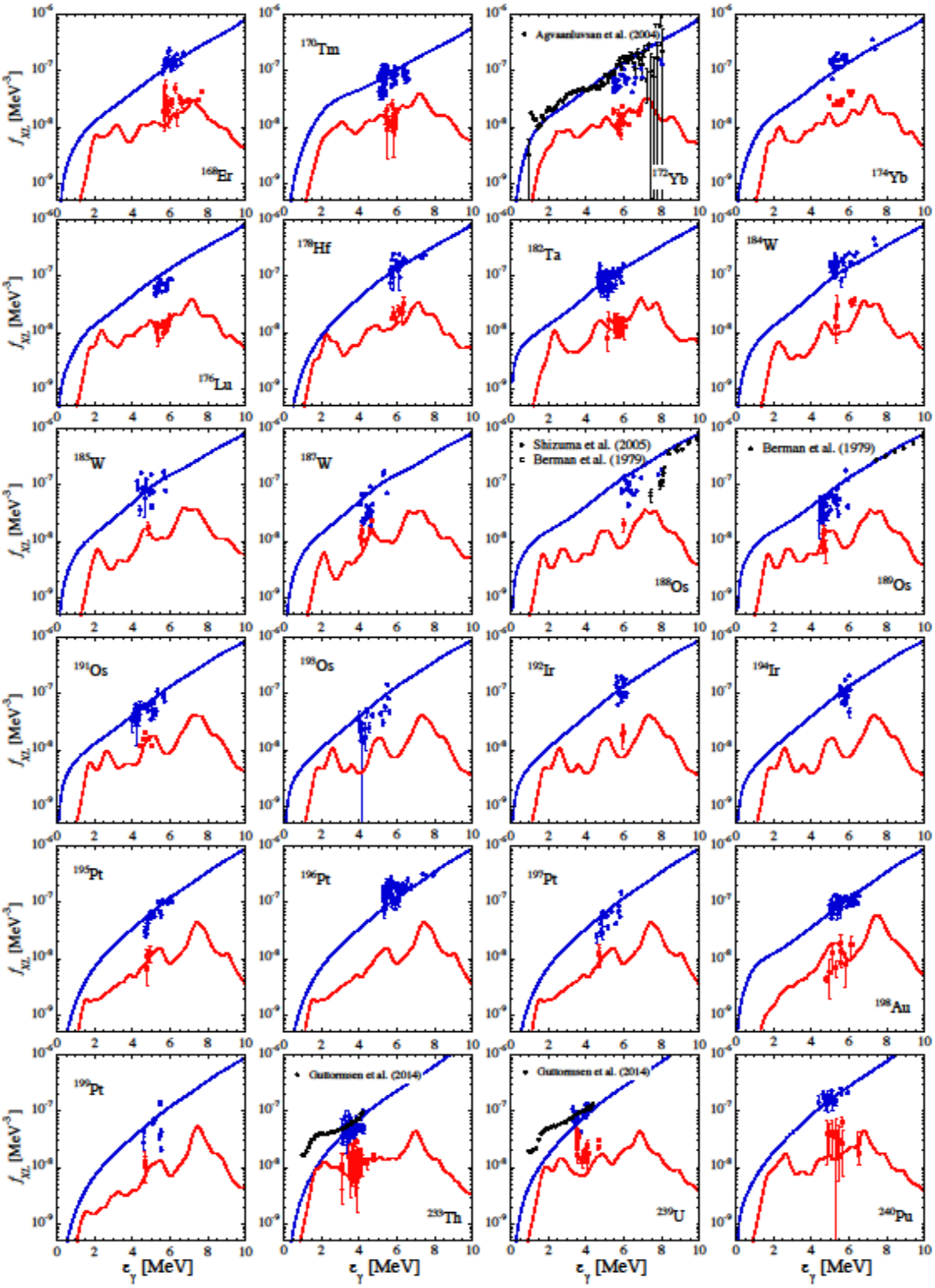

Figs 9-10. Comparison between E1 and M1 strength functions derived from ARC data and D1M+QRPA calculations [24,25] and private communication from S. Goriely. Also shown are the total strength functions extracted from other measurements, in particular (γ,n) cross section or transfer reaction through the Oslo method.

4. Conclusions

ARC data measured at different filter beam facilities have been re-analyzed. They include all measurements made at ANL, INEL and BNL between 1970 and 1990, but until now only partially exploited. This is the first time that a comprehensive re-evaluation of all measured data was completed and applied for a systematic comparison with estimated PSF in the mass range 70 < A < 240. Updated spectroscopic information on the states of interest is used to extract the E1 and M1 transition groups in the PSF. This re-evaluation provides new experimental information on the E1 and M1 strength function around the neutron binding energy and also provides new constraints for existing γ-ray strength models used in statistical reaction codes. The direct measurement of capture primary transitions is a model independent method to derive the gamma-ray strength function (PSF), contrary to model dependent two step reactions, such as TSC or (n,xγ) cases.

Globally, the revised data agree rather well with the total strength function extracted from photonuclear data or from transfer or inelastic reactions by the so-called Oslo method. The ARC data also show that the recent QRPA calculations based on the D1M Gogny force give rather satisfactory predictions, both for the E1 and M1 strengths. The ratio of the E1 to M 1 strength functions is found to remain within the small range of 1.5 and 7.8 but not to follow any clear systematics, as expected from microscopic predictions of different excitation modes for M1 radiation (see Fig. 11). The ARC E1-to-M1 strength ratio represents a new stringent test for the future elaboration of theoretical models for the dipole strength function.

The *JUKOLIB-ARC-2017 library* is available from the author on request.

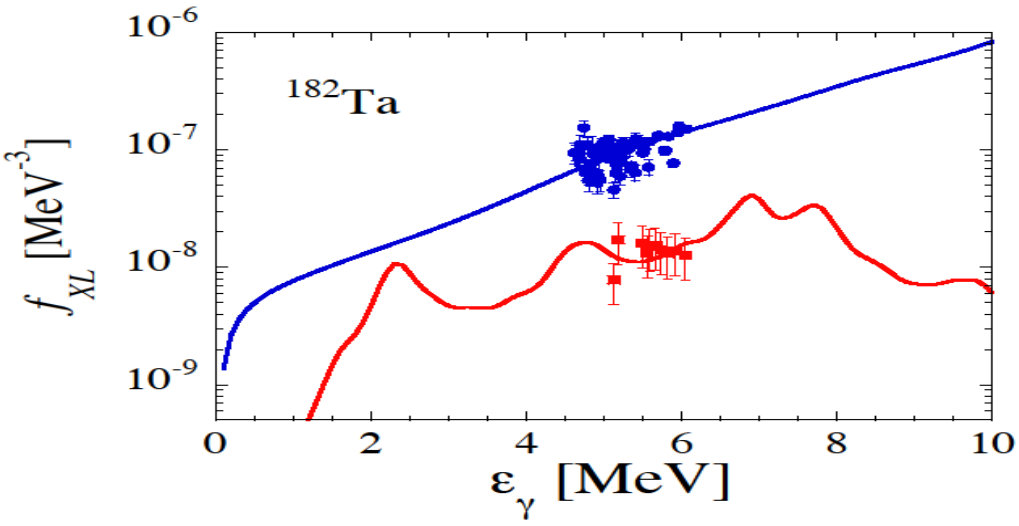

Fig 11. Note the complexity of different M1 excitation modes below the spin-flip resonance, strongly influencing the E1/M1 ratio as a function of Eγ.

Acknowledgment

JK acknowledges the long and fruitful collaboration with the late R.E. Chrien. JK also acknowledges the inspiration and continues support by S. Goriely. F. Becvar has contributed with many fruitful discussions and awarding access to old data.

References

[1] L.M. Bollinger and G.E. Thomas, Phys.Rev. C2 (1970) 1951 and L.M. Bollinger, "*Photonuclear Reactions and Applications"* Pacific Grove, California (1973) 783

[2] R.B. Schwartz et al., *Proc, Int. Symposium on Neutron Capture Gamma-rays Spectroscopy and related Topics*, Petten (NH) (1974) 346

[3] G.A. Bartholomew et al., Adv.Nucl.Phys. 7 (1973) 229.

[4] M.A. Lone, "*Neutron Gamma Ray Spectroscopy and Related Topics"*, Plenum New York, 1979, 161

[5] R. Greenwood and C. Reich, Nucl.Phys. A **223**, (1974) 66

[6] R. Greenwood and R. Chrien, Nucl.Instr.Meth. **138** (1976) 125

[7] M.L. Stelts, "*Nuclear Cross Sections for Technology"* (Knoxwille Conf.) Nat.Bur. of Stds.Sp.Publ.594, (1980) 936

[8] R.E. Chrien, "*Neutron-Capture Gamma-Ray Spectroscopy and related Topics, Physics Conf. Seriers No 62"*, (The Inst. of Phys., Bristol and London) 1982, 342

[9] J. Kopecky, "*Neutron Gamma Ray Spectroscopy and Related Topics"* Knowville, (Tennessee) (1984) 318

[10] R.E. Chrien, *"Fourth Int. Symposium on Neutron Induced Reactions"*, Smolenice (CZ) (1985) 200

[11] R.E. Chrien, "*5rd Int. School on Neutron Physics"*, Alushta (USSR) CONF-8610176—2 October 1986 and BNL-38900 report

[12] A. F. Gamalii *et al.*, Sov. J. Nucl. Phys **15**, 1 (1972)

[13] A.V. Murzin et al.,Proc. 40th *Ann. Conf. Nucl. Structure At. Nuclei*, (Leningrad 1990) 86

[14] H. Ottmar et al., *Proc, Int. Symposium on Neutron Capture Gamma-rays Spectroscoy and related Topics*, Petten (NH) (1974) 658

[15] R. Chrien, J. Kopecky, H. Liou, O. Wasson, J. Garg, and M. Dritsa, Nucl. Phys. A436 (1985) 205

[16] J. Kopecky and R. Chrien, Nucl. Phys. A **468**, (1987) 285

[17] J. Kopecky and M. Uhl, Phys. Rev. C **41**, (1990) 1941

[18] J. Kopecky, M.Uhl and R.E.Chrien, Phys.Rev. C47 (1983) 312

[19] J. Kopecky et al., Phys.Rev.C CW10472 (2017)

[20] R. Capote et al., Nuclear Data Sheets **110**, 3107 (2009)

[21] U. Mayerhofer et al., Nucl.Phys. A492(1989) 1

[22] J. Kopecky, INDC(NED)-013 (September 2016)

[23] J. Kopecky, *ECN-RX-92-011*, Tech. Rep. 011, ECN (1992)

[24] M. Martini et al. Phys.Rev.C**94** 0143 04(2016)

[25] S. Goriely et al., Phys.Rev. **C94** 044306 (2016)

APPENDIX

Table 1. List of recovered ARC measurements with neutron filtered beams (B and Sc) selected for the final PSF data base. Selected ARC data for the PSF data base are denoted with red x.

[Ref] BNL/ECN stands for the data from quoted references processed in to the BNL/ECN data base.

Product nuclide	**B**	**Sc**	**Final *ATLAS f(L)***	**Excluded mesurements**
Ti-49		x	[1]	Poor averaging
Co-60			[2]	24 keV only
Cu-64		x	[3]	Poor averaging
Cu-66		x	[4]	Poor averaging
As-76		x	[5]	
Zr-92		x	[6]	
Mo-96		x	[7] BNL/ECN	
Mo-98		x	[7]	
Ru-102		x	[8] BNL/ECN	
Pd-106	x	x	[9] BNL/ECN	[10][11][12] BNL/ECN
Pd-109		x	[13]	
Ag-108		x	[14]	No Iγ data
Cd-114		x	[15] BNL/ECN	
Te-124		x	[16]	
I-128		x	[12]	
Ba-135		x	[17]	
Ba-136		x	[18]	
Ce-137		x	[19]	No Iγ data
Nd-146	x	x	[20]	[21]
Sm-148	x		[22]	
Sm-150	x		[22]	
Sm-155		x	[23] BNL/ECN	
Eu-154		x	[24]	
Gd-155		x	[25]	[26] [27]
Gd-156	x	x	[9] BNL/ECN	[28] [29]
Gd-157		x	[26] BNL/ECN	[27]
Gd-158	x	x	[9]	[14] [30]
Gd-159		x	[31]	
Gd-161		x	[27]	
Dy-162		x	[32] BNL/ECN	

Dy-163		x	[33]	
Dy-164		x	[32] BNL/ECN	
Dy-165		x	[34]	
Ho-166	x		[9]	
Er-168	x	x	[9] BNL/ECN	[35]
Tm-170		x	[36]	
Yb-172		x	[37] [BNL/ECN	
Yb-174		x	[38]	[39]
Lu-176		x	[40] BNL/ECN	
Hf-178		x	[41]	
Hf-180	x		[42]	
Ta-182		x	[43]	
W-184	x	x	[44]	[45]
W-185		x	[46]	
W-187		x	[46]	
Os-188		x	[47]	
Os-189		x	[48]	
Os-191		x	[49]	
Os-193		x	[50]	
Ir-192		x	[51]	
Ir-194		x	[52]	
Pt-195		x	[53] BNL/ECN	
Pt-196		x	[54]	
Pt-197		x	[55]	
Pt-199		x	[55]	
Au-198		x	[56]	
Th-233		x	[57] BNL/ECN	
U-236		x	[58]	
U-239	x	x	[59] BNL/ECN	[60] BNL/ECN
Np-238		x	[61]	
Pu-240		x	[62]	

Filtered beams ARC data:

[1] A.F. Gamalii et al., Sov.J.Nucl.Phys. 15(1972) 1 *Ti-49, Mo-96,98*

[2] J. Kopecky et al., Nucl. Phys.A427 (1984) 413 *Co-60*

[3] M.G. Delfini et al., Nucl. Phys. A404 (1983) 225 *Cu-64*

[4] M.G. Delfini et al., Nucl.Phys. A404 (1983) 250 *Cu-66*

[5] F. Hoyler at al., Nucl.Phys. A512 (1990) 189 *As-76*

[6] M.J. Kenny at al., *Proceedings of Neutron Gamma Ray Capture Spectroscopy and related topics, BNL*, (Upton 1978) 676 and BNL- 24698 *Zr-92,93,95*

[7] K. Rimavi and R.E. Chrien, Phys.Rev. C15 (1977) 1271 *Mo-93,95,97,99*

[8] BNL/ECN database (unpublished BNL data) *Mo-96, Ru-102, Pd-106*

[9] L.M. Bollinger and G.E. Thomas, Phys.Rev. C2 (1970) 1951 *Pd-106, Gd-156,158, Ho-166, Er-168*
[10] J. Kopecky and R.E. Chrien, Nucl.Phys. A468 (1987) 285 *Pd-106*
[11] B. Fogelberg et al., Nucl.Phys. A475 (1987) 301 *Pd-106*
[12] C. McCullagh, Univ. Stony Brook Thesis, (1978) *Pd-106, I-128*
[13] R.F. Casten et al., Phys.Rev. C21 (1990) 65 *Pd-109*
[14] T.D. MacMahon et al., J.Phys. G11 (1985) 1231 *Ag-108, Gd-158*
[15] A. Meemeed et al., NP A412 (1984) 113 *Cd-114*
[16] R.F. Casten et al., Phys.Rev. C44 (1991) 523 *Te-124*
[17] R.E. Chrien et al., Phys.Rev. C48 (1973) 109 *Ba-135*
[18] K. Schreckenbach et al., *Capture Gamma-Ray Conf. Proc*., 1981) 200 *Ba-136*
[19] B.K. Koene et al., priv. com. 1981 *Ce-136*
[20] D.L. Bushnell et al., Phys.Rev. C14 (1975) 75 *Nd-146*
[21] S. Raman et al., J.Phys. G9 (1983) L137 *Nd-146*
[22] D.J. Buss et al., Phys.Rev. C2 (1970) 1513 *Sm-148,150*
[23] K. Schreckenbach et al. Nucl.Phys. A376 (1982) 149 *Sm-155*
[24] M.A. Balodis et al., Nucl.Phys. A572 (1987) 445 *Eu-154*
[25] H.H. Schmidt et al., J.Phys. (London) G12 (1986) 411*Gd-155*
[26] R.C. Greenwood et al., *Proceedings of Neutron Gamma Ray Capture Spectroscopy and related topics*, RCN Petten (September 1974) *Gd-155,157*
[27] R.G. Greenwood and R.E. Chrien, Bull. Am. Phys. Soc. 22 No.8 ED9 (1977) 1032 *Gd-155,157,159,161*
[28] A. Backlin et al., Nucl.Phys. A380(1982) 189 *Gd-156*
[29] J. Kopecky et al., Phys.Rev. C47(1993) 312 *Gd-156*
[30] R.C. Greenwood et al., Nucl.Phys. A304 (1978) 327 *Gd-158*
[31] C. Granja et al., Nucl.Phys. A279 (2003) 679 *Gd-159*
[32] D.D. Warner et al., Phys.Rev. C27(1983) 2292 *Dy-162,164*
[33] H.H. Schmidt, et al., Nucl. Phys. A504 (1989) 1 *Dy-163*
[34] E. Kaerts et al., Nucl.Phys. A514 (1990) 173 *Dy-165*
[35] W. Davidson et al., J.Phys. G7 (1981) 843 *Er-168*
[36] R.W. Hoff et al., Phys. Rev. C (1996) 78 *Tm-170*
[37] R. C. Greenwood et al., Nucl.Phys. A252(1975) 260 *Yb-172*
[38] C. Granja et al., Nucl.Phys. A757(2005) 287 *Yb-174*
[39] R.C. Greenwood et al., Phys.Rev. C23(1981) 153 *Yb-174*
[40] R.W. Hoff et al., Nucl.Phys. A437 (1985) 285 *Lu-176*
[41] A. Hague et al., Nucl.Phys. A455 (1986) 231*Hf-178*
[42] D.L. Bushnell et al., Phys.Rev. C10 (1974) 2483 *Hf-180*
[43] R.G. Helmers et al., Nucl.Phys, A168 (1971) 449 *Ta-182*
[44] R.C. Greenwood et al., Nucl.Phys. A223 (1974) 66 *W-184*
[45] D.L. Buschnell et al., Phys. Rev. C11 (1975) 1401 *W-184*
[46] A.M. Bruce et al., Nucl. Phys. A465 (1987) 221 *W-185,187*
[47] A.V.Murzin et al., Proc. 40th *Ann. Conf. Nucl. Structure At. Nuclei*, (Leningrad 1990) *86 Os-188*
[48] A.M. Bruce et al., Nucl. Phys. A452 (1992) 1 *Os-189*
[49] R.F. Casten et al., Nucl. Phys. A285 (1977) 235 *Os-191*
[50] D. D. Warner et al., Nucl.Phys. A316 (1979) 13 *Os-193*
[51] J. Kern et al., Nucl. Phys. A534 (1991) 77 *Ir-192*
[52] M. Balodis et al., Nucl. Phys. A641 (1998) 133 *Ir-194*
[53] D.D.Warner et al., Phys.Rev. C26 (1982) 1921 *Pt-195*
[54] J. Cizewski et al., Nucl. Phys. A323 (1979) 349 *Pt-196*
[55] R.F. Casten et al., Phys. Rev. C 27(1983) 1310 *Pt-197, 199*
[56] U. Mayerhofer et al., Nucl.Phys. A492(1989) 1 *Au-198*
[57] P. Jeuch et al., Nucl.Phys. A317 (1979) 363 *Th-233*

[58] H. Ottmar et al., *Proc, Int. Symposium on Neutron Capture Gamma-rays Spectroscopy and related Topics*, Petten (NH) (1974) 658 *U-236*
[59] L.M. Bollinger and G.E. Thomas, Phys.Rev. C6(1972) 1322 *U-239*
[60] R.E. Chrien and J. Kopecky, Nucl. Phys. A414 (1984) 281 *U-239*
[61] R.W. Hoff et bal., Phys.Rev. C41 (1990) 484 *Np-238*
[62] R.E. Chrien et al., Nucl.Phys. A436 (1985) 205 *Pu-240*

TEST OF p-WAVES INFLUENCE FOR BORON ARC DATA

The assumption of a negligible influence of p-wave capture at boron filtered neutron beam energies has been tested. The RACA calculations indicated that the main factor for this effect is the ration of neutron strength functions S1 and S0. The calculation has shown that if the S1/S0 ratio is close to 10, the p-wave component has to be considered.

In the scanned figures (Fig. A1) from BNL resonance book is seen that the mass region between 75 < A 130 can give ratios close to ten and the adopted boron data should be tested against the disturbing p-wave capture.

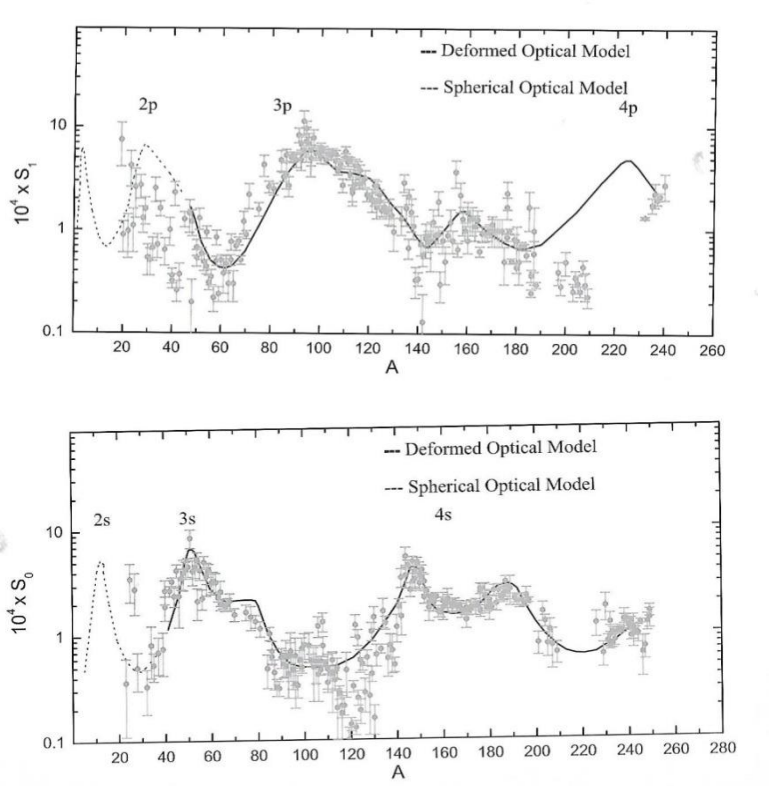

Fig. A1 Ratio of S1/S0 strength functions from the latest BNL resonance book

Firstly we looked at regions where S1/S0 is about 1, where no p-wave is expected. For this test we have made the use of a comparison of available B, Sc and DRC data. In such a case the DRC data serve a pure information on E1 and M1 strength, because of well defined initial states, namely the discrete resonances. Such comparison for a typical target from the S1/S0 region Er-168 is shown in the Fig. A2.

The excellent agreement between M1 data points from all three different measurements confirms the assumption of a negligible influence of p-waves in the capture process. The same result was found also for remaining nuclides with S1/S0 ratio around one, such as ^{146}Nd, $^{156, 158}$Gd, ^{166}Ho, ^{184}W and ^{239}U.

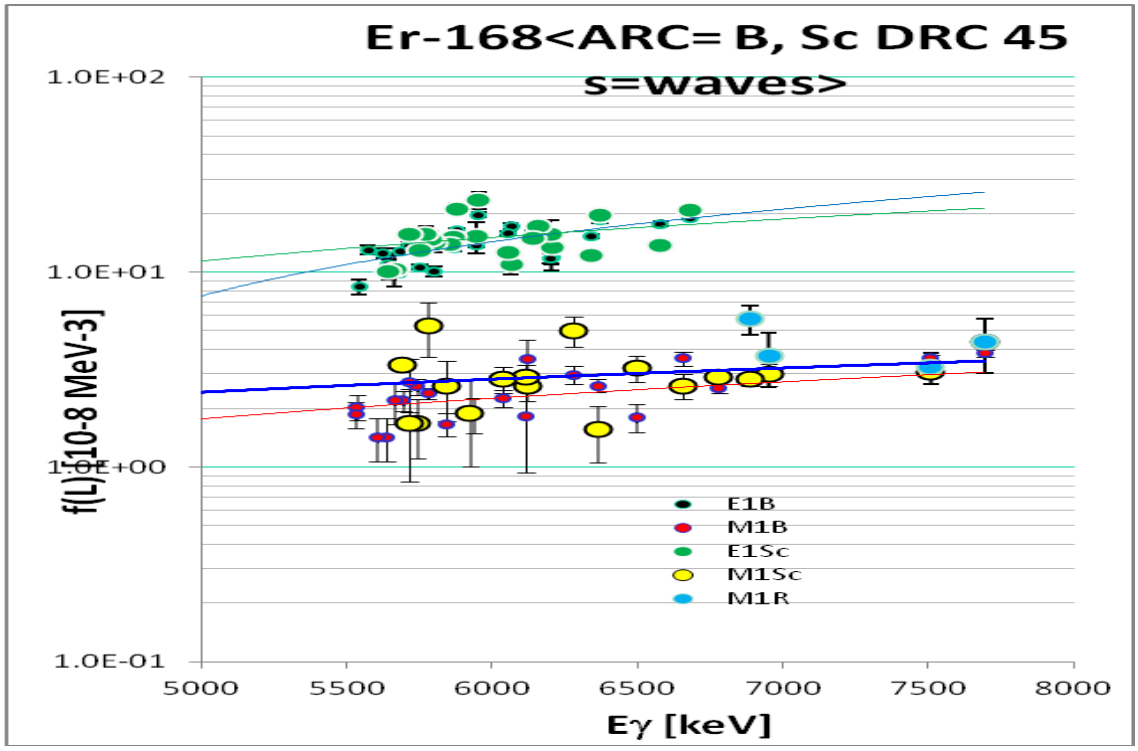

Fig. A2 All available ARC data for ^{168}Er (B, Sc and DRC) are plotted. Mind the agreement of M1 data points from two measurements, DRC and B data..

For the next step, to test nuclides with S1/S0 ~ 10, the well established ARC data for ^{106}Pd were used and are shown in Fig. A3. M1 data are here plotted from 4 independent measurements, M1 B = boron data, M1 Sc = BNL/ECN collaboration processed with the RACA code, M1 CMc = Sc measurement in McCullagh thesis [12] and finally M1R = data from DRC measurement.

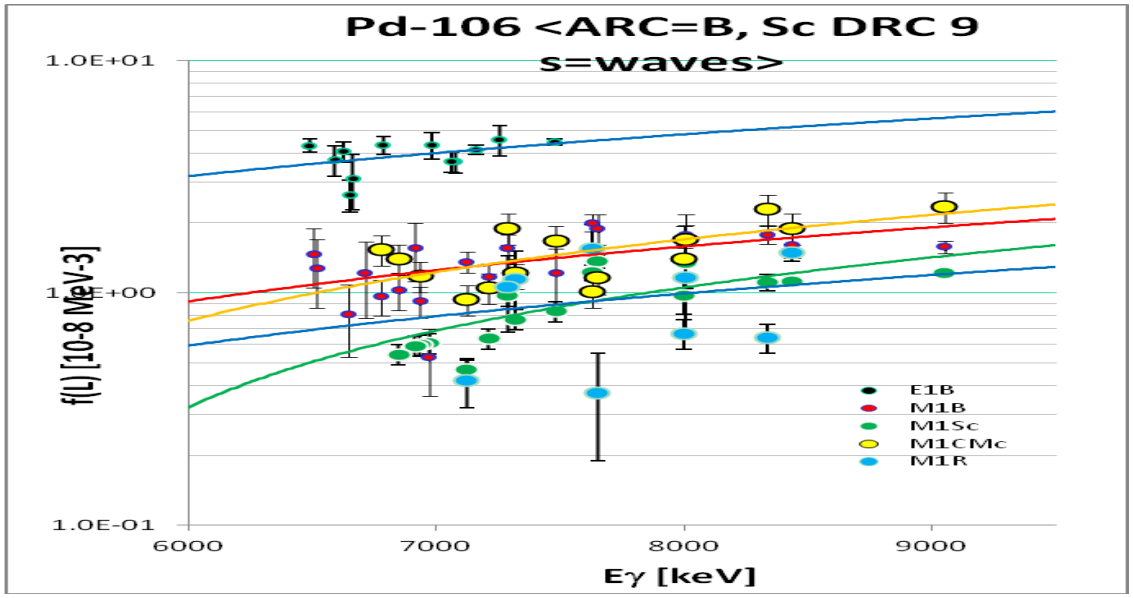

Fig. A3 A combined plot of all ^{106}Pd measurements with in order to compare M1 strength

There is a clear distinction between two pairs of measurements. The DRC and by RACA corrected Sc data points nicely agree and are lower compared to B and Sc (uncorrected) data, which indicates the contribution of E1 strength from the p-wave capture . The conclusion is obvious, the M1 strength for nuclides with S1/S0 ratio about 10 is by the p-wave capture. The corrected B data are shown in the next figure A4.

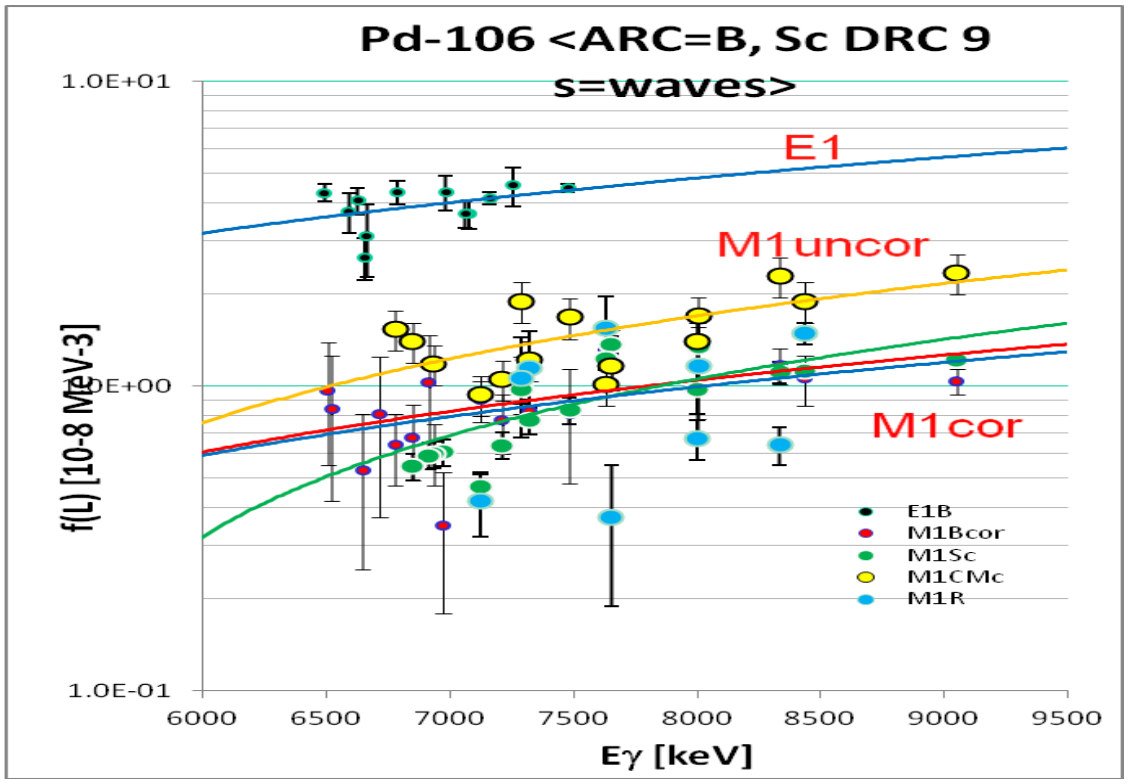

Fig. A4 The corrected boron data for ^{106}Pd using the estimated value of 0.33 (see Table 7).

DATA BASE

The data base of *JUKOLIB-ARC-2017* in EXCEL format is available by the author and can be requsted via juko@planet.nl mail address.

DATA BASE PLOTS

Plots of all nuclides are shown, the trend curves serves as an indication of the mean value fitted with the trend curve option of EXCEL. **This curve does not represent any of PSF models.**

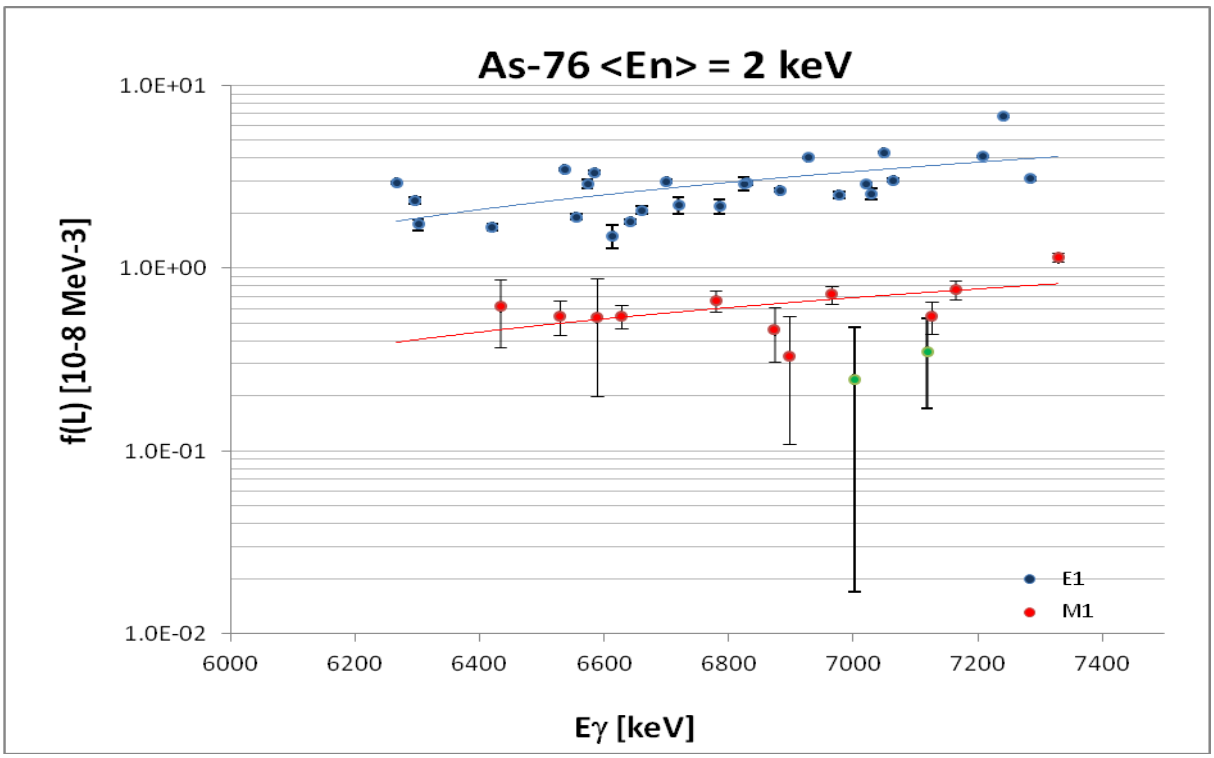
As-76 <En> = 2 keV
1.0E+01
1.0E+00
1.0E-01
1.0E-02
f(L) [10-8 MeV-3]
6000
6200
6400
6600
6800
7000
7200
7400
Eγ [keV]
E1
M1

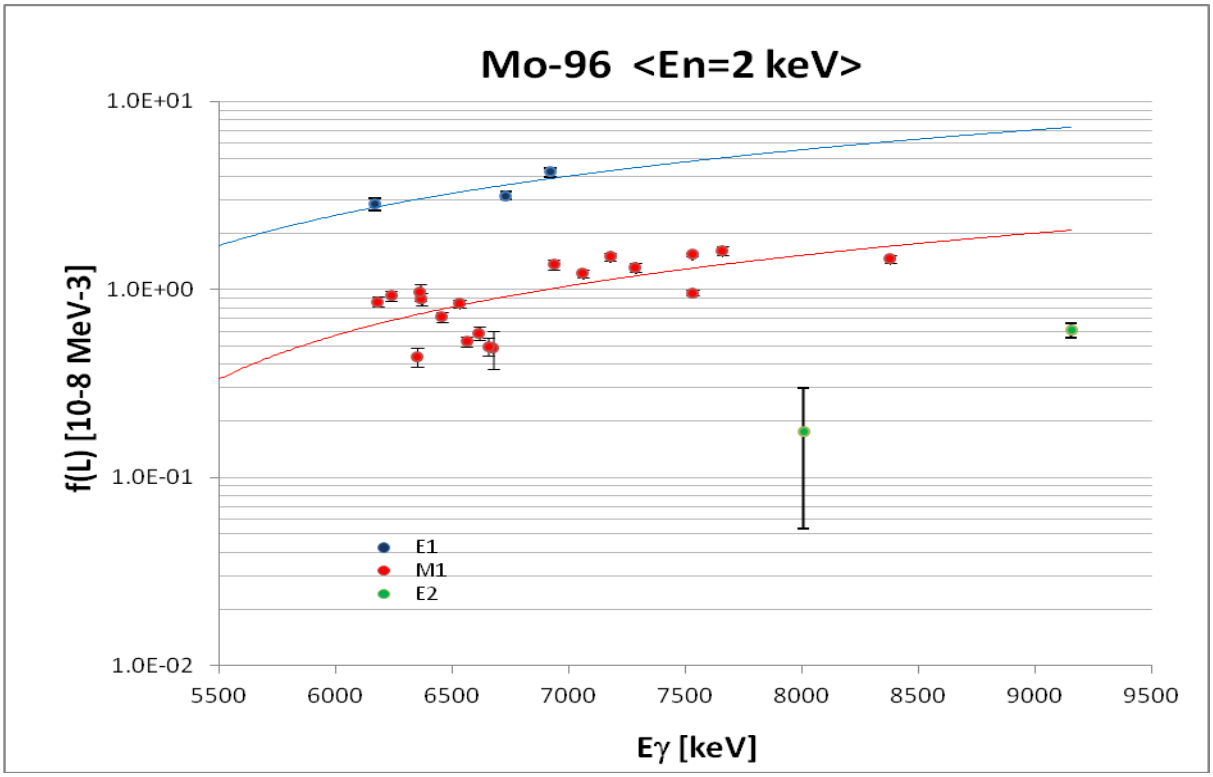
Mo-96 <En=2 keV>
1.0E+01
1.0E+00
1.0E-01
1.0E-02
f(L) [10-8 MeV-3]
5500
6000
6500
7000
7500
8000
8500
9000
9500
Eγ [keV]
E1
M1
E2

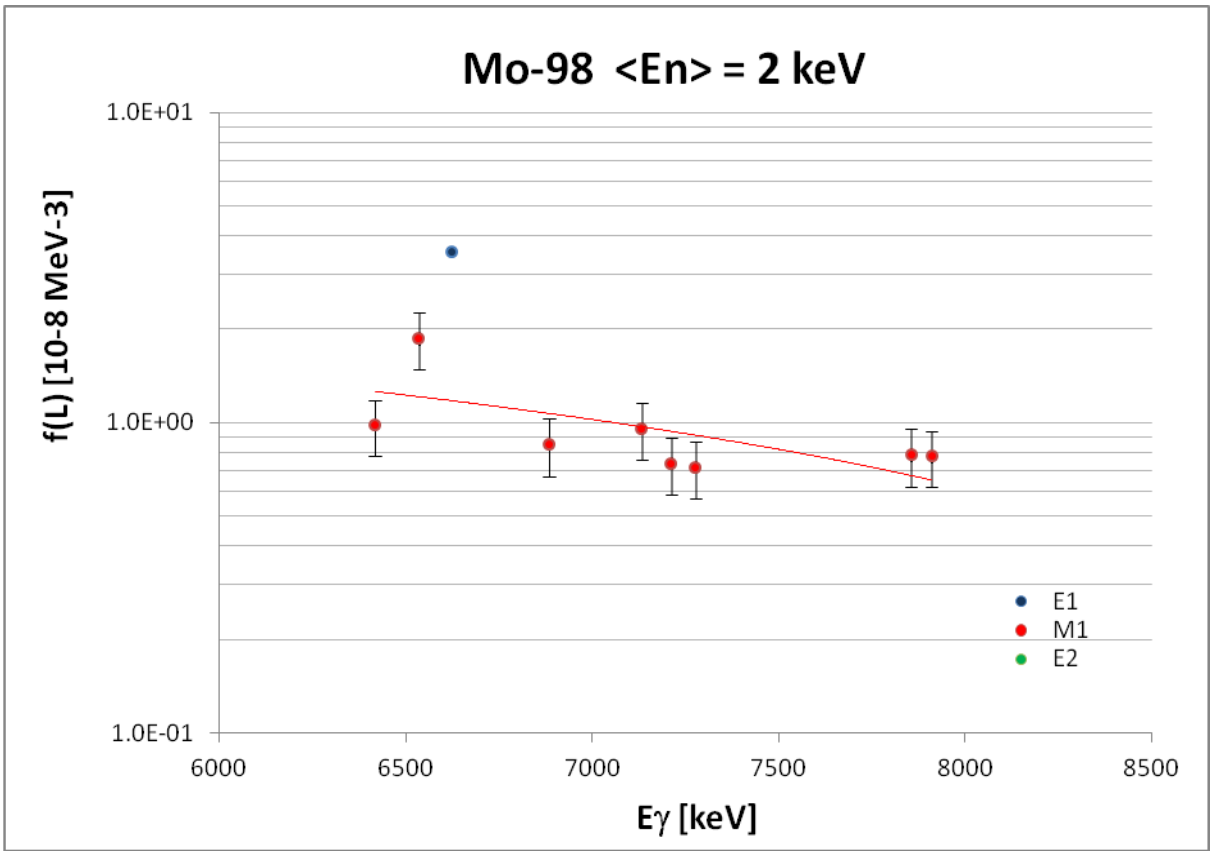
Mo-98 <En> = 2 keV
f(L) [10-8 MeV-3]
1.0E+01
1.0E+00
1.0E-01
6000
6500
7000
7500
8000
8500
Eγ [keV]
E1
M1
E2

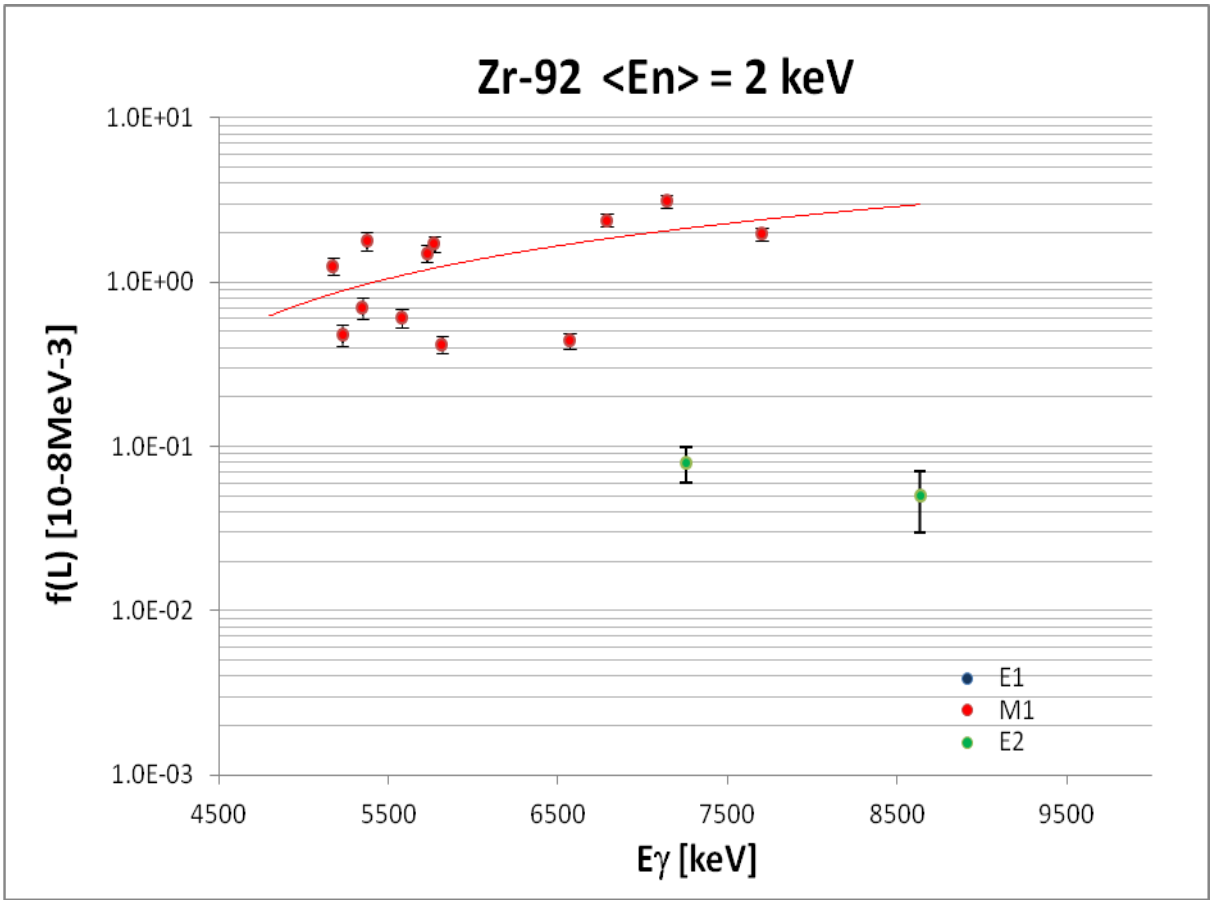
Zr-92 <En> = 2 keV
f(L) [10-8MeV-3]
1.0E+01
1.0E+00
1.0E-01
1.0E-02
1.0E-03
4500
5500
6500
7500
8500
9500
Eγ [keV]
E1
M1
E2

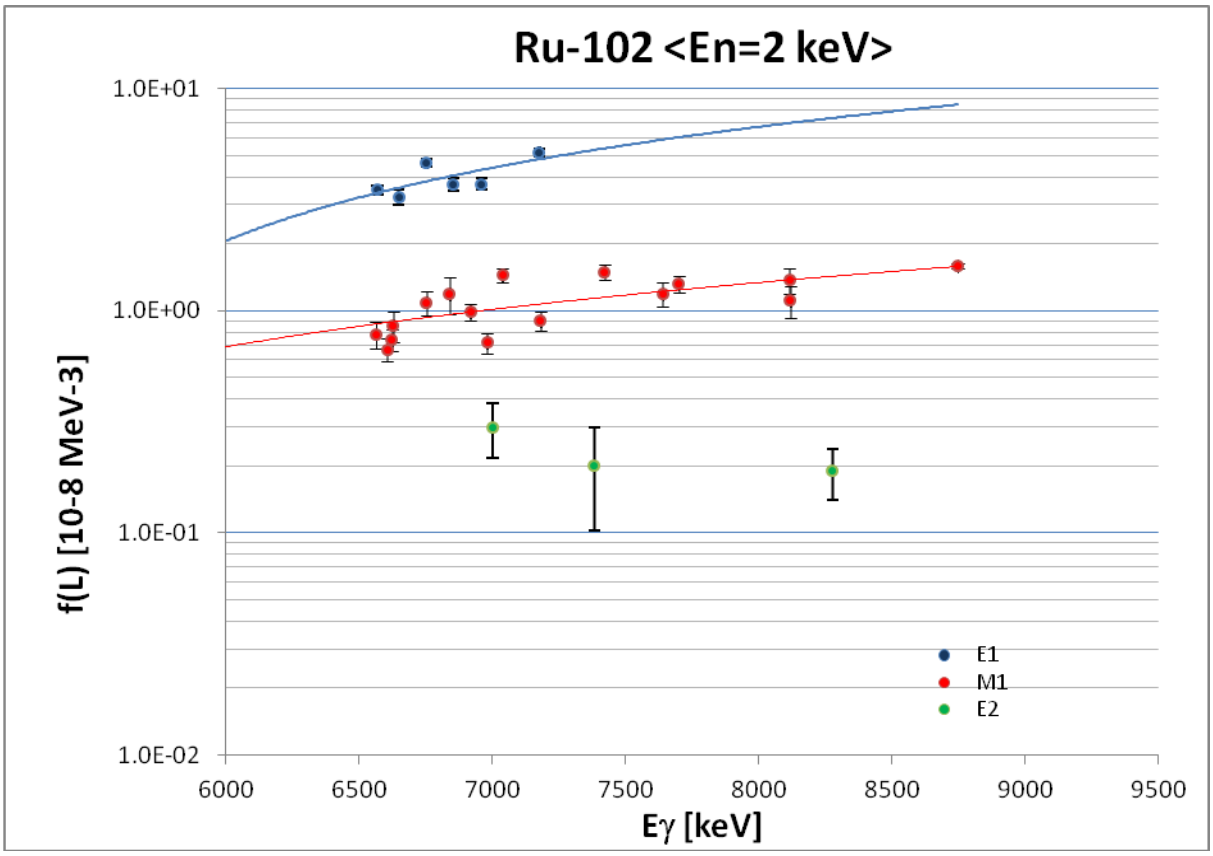
Ru-102 <En=2 keV>
1.0E+01
1.0E+00
1.0E-01
1.0E-02
f(L) [10-8 MeV-3]
6000
6500
7000
7500
8000
8500
9000
9500
Eγ [keV]
E1
M1
E2

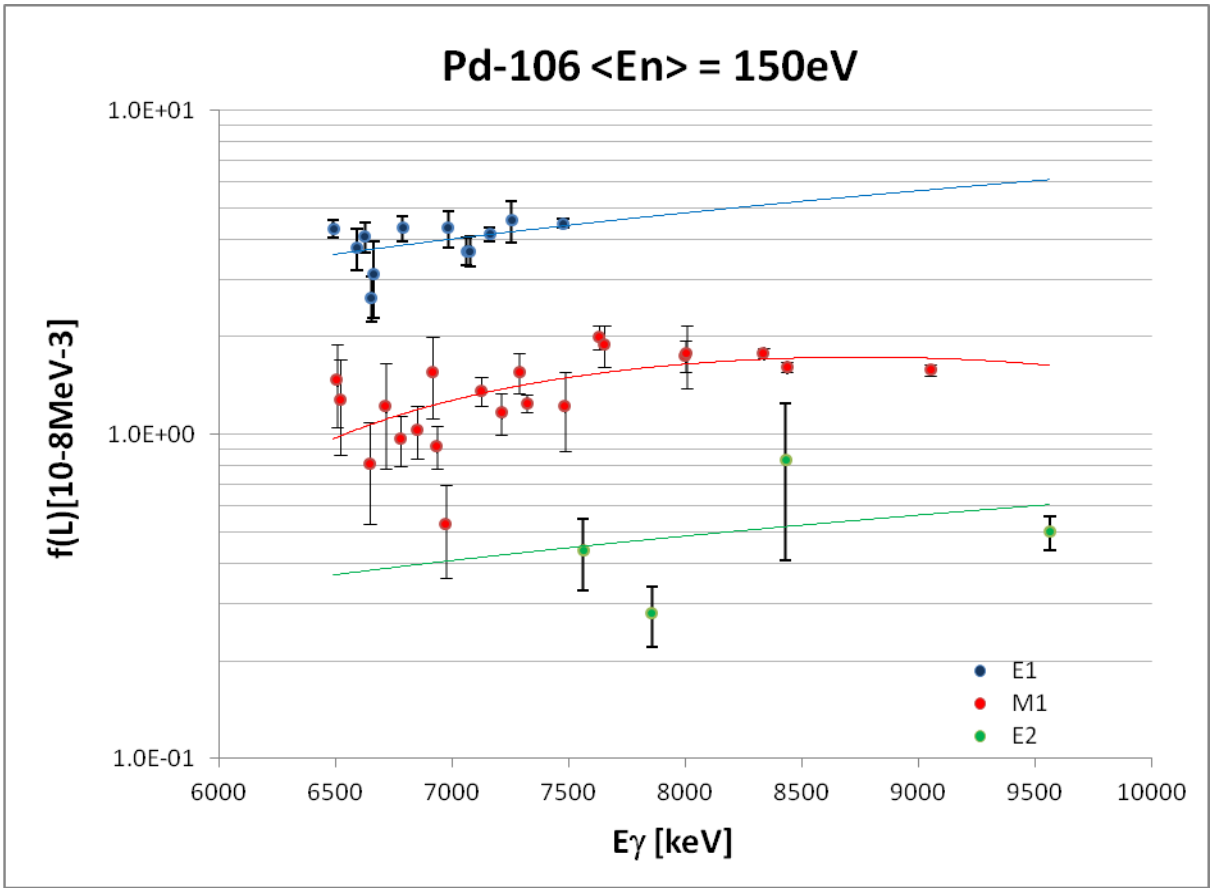
Pd-106 <En> = 150eV
1.0E+01
1.0E+00
1.0E-01
f(L)[10-8MeV-3]
6000
6500
7000
7500
8000
8500
9000
9500
10000
Eγ [keV]
E1
M1
E2

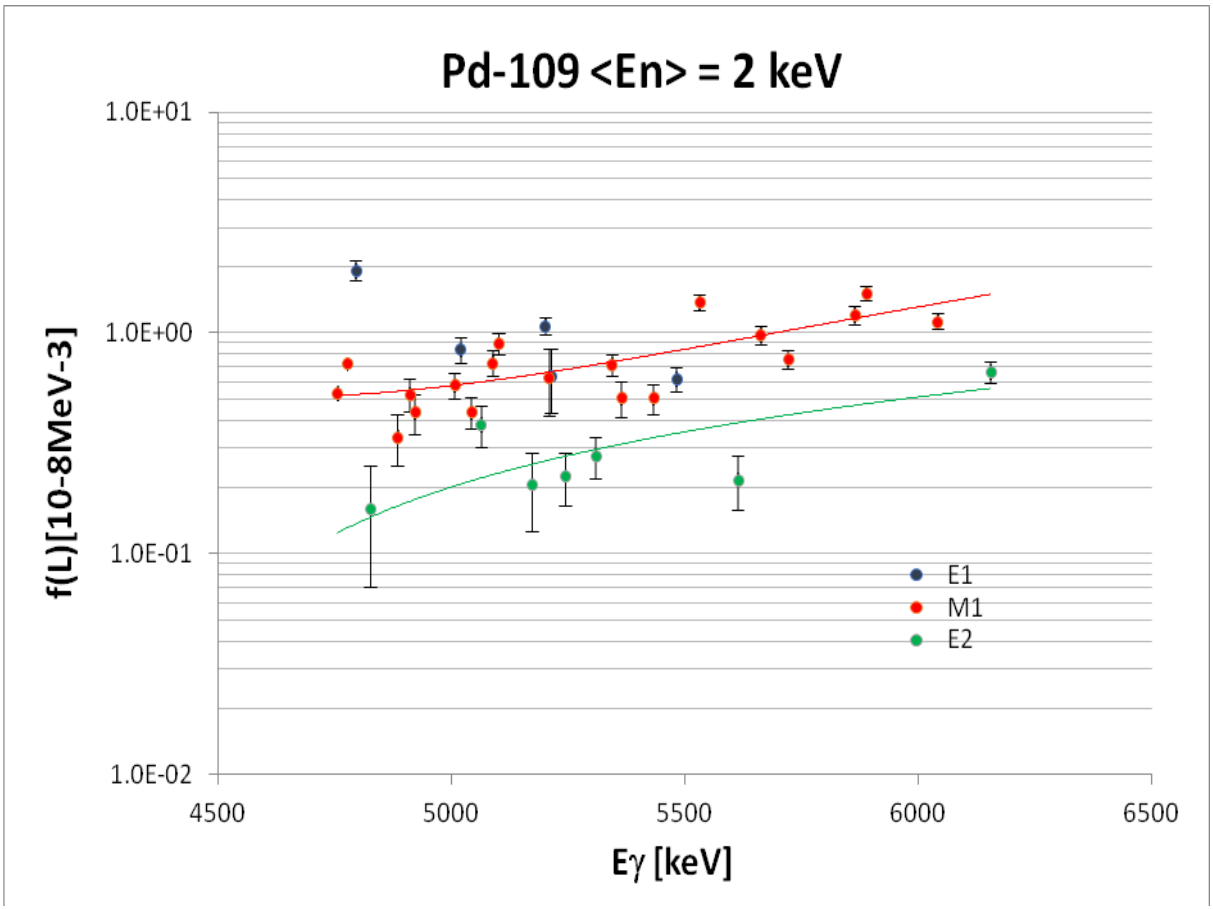
Pd-109 <En> = 2 keV
1.0E+01
1.0E+00
1.0E-01
1.0E-02
f(L)[10-8MeV-3]
4500
5000
5500
6000
6500
Eγ [keV]
E1
M1
E2

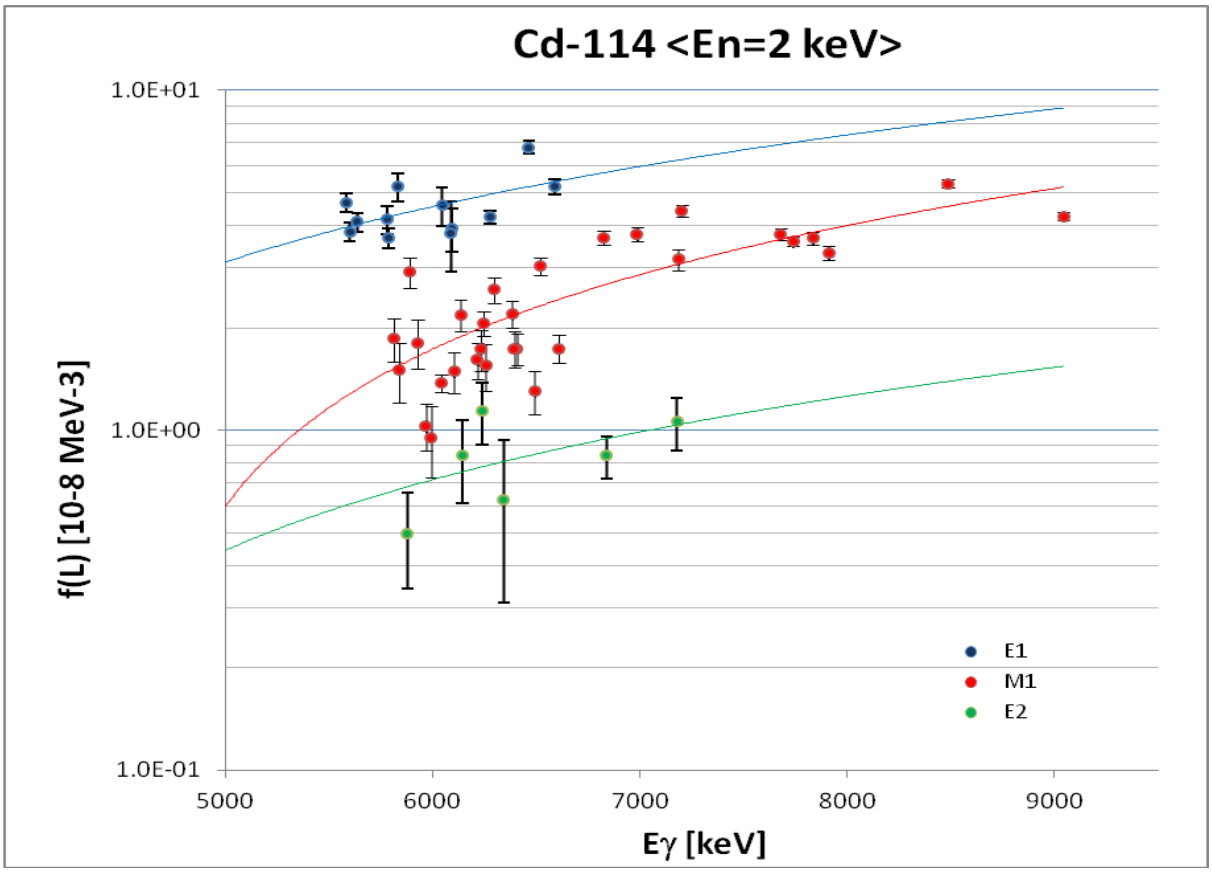
Cd-114 <En=2 keV>
1.0E+01
1.0E+00
1.0E-01
f(L) [10-8 MeV-3]
5000
6000
7000
8000
9000
Eγ [keV]
E1
M1
E2

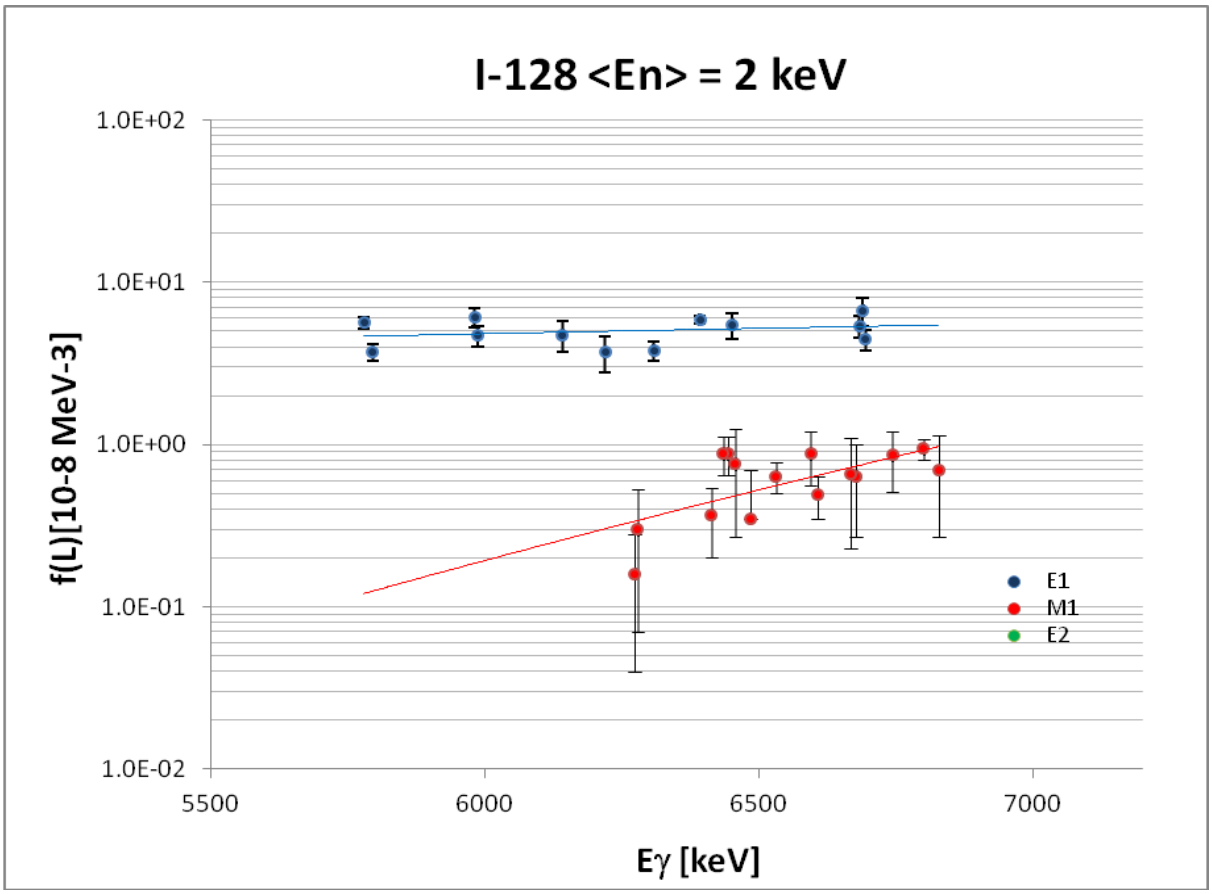
I-128 <En> = 2 keV
1.0E+02
1.0E+01
1.0E+00
1.0E-01
1.0E-02
f(L)[10-8 MeV-3]
5500
6000
6500
7000
Eγ [keV]
E1
M1
E2

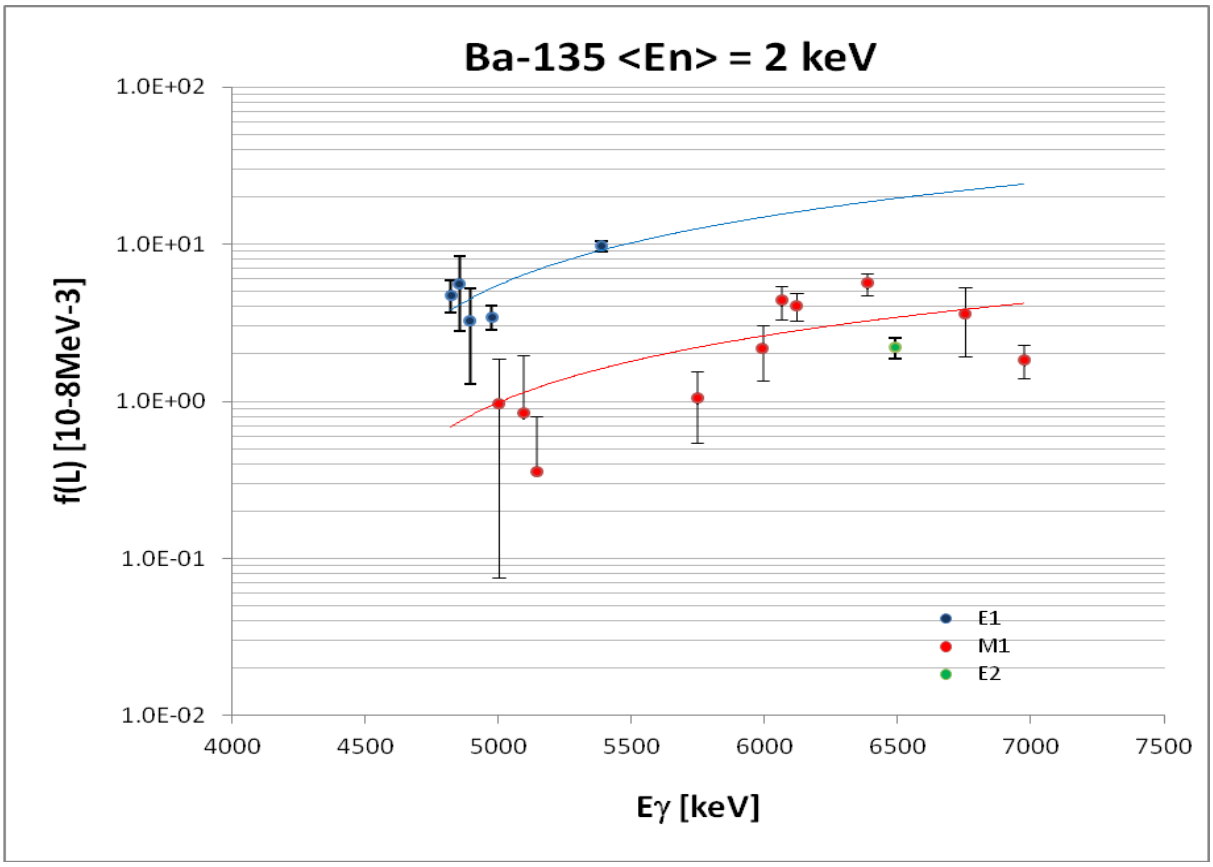
Ba-135 <En> = 2 keV
1.0E+02
1.0E+01
1.0E+00
1.0E-01
1.0E-02
f(L) [10-8MeV-3]
4000
4500
5000
5500
6000
6500
7000
7500
Eγ [keV]
E1
M1
E2

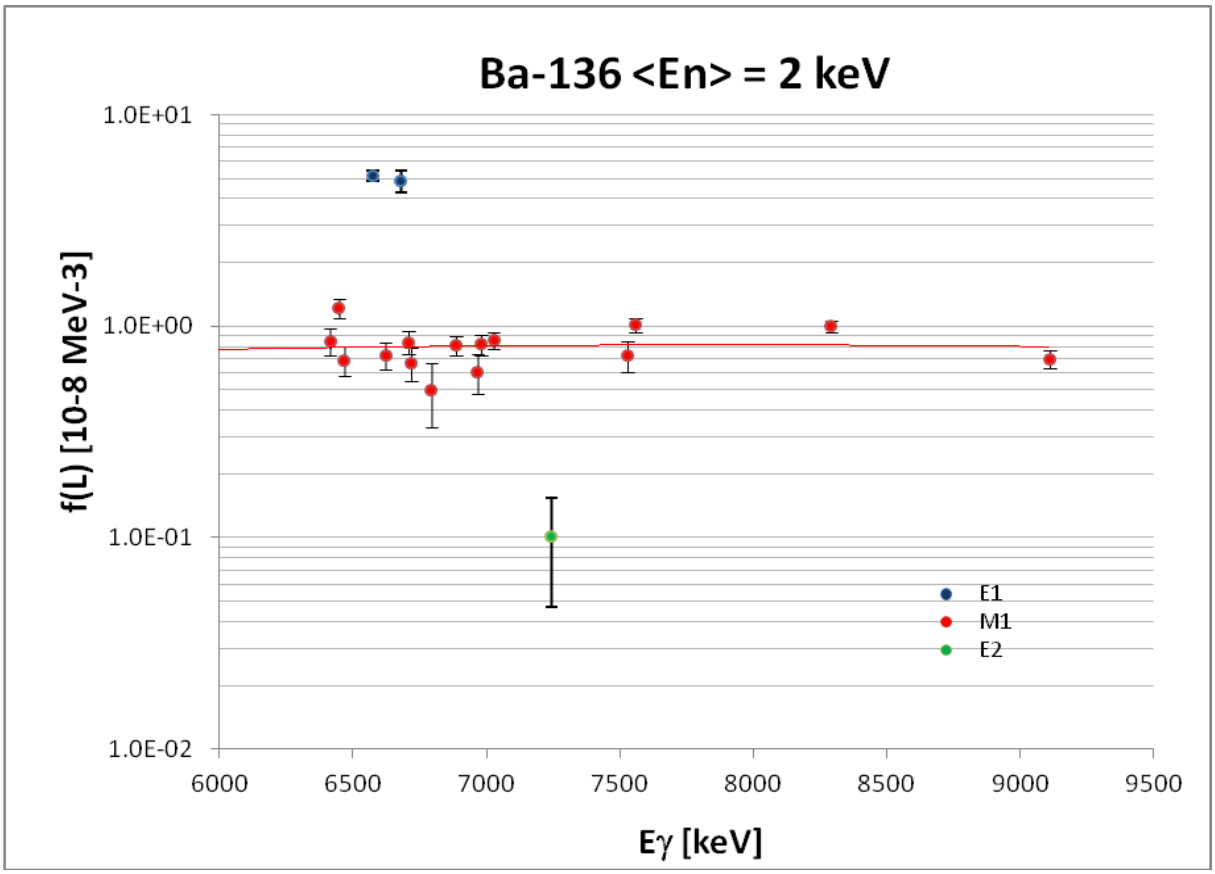
Ba-136 <En> = 2 keV
f(L) [10-8 MeV-3]
1.0E+01
1.0E+00
1.0E-01
1.0E-02
6000
6500
7000
7500
8000
8500
9000
9500
Eγ [keV]
E1
M1
E2

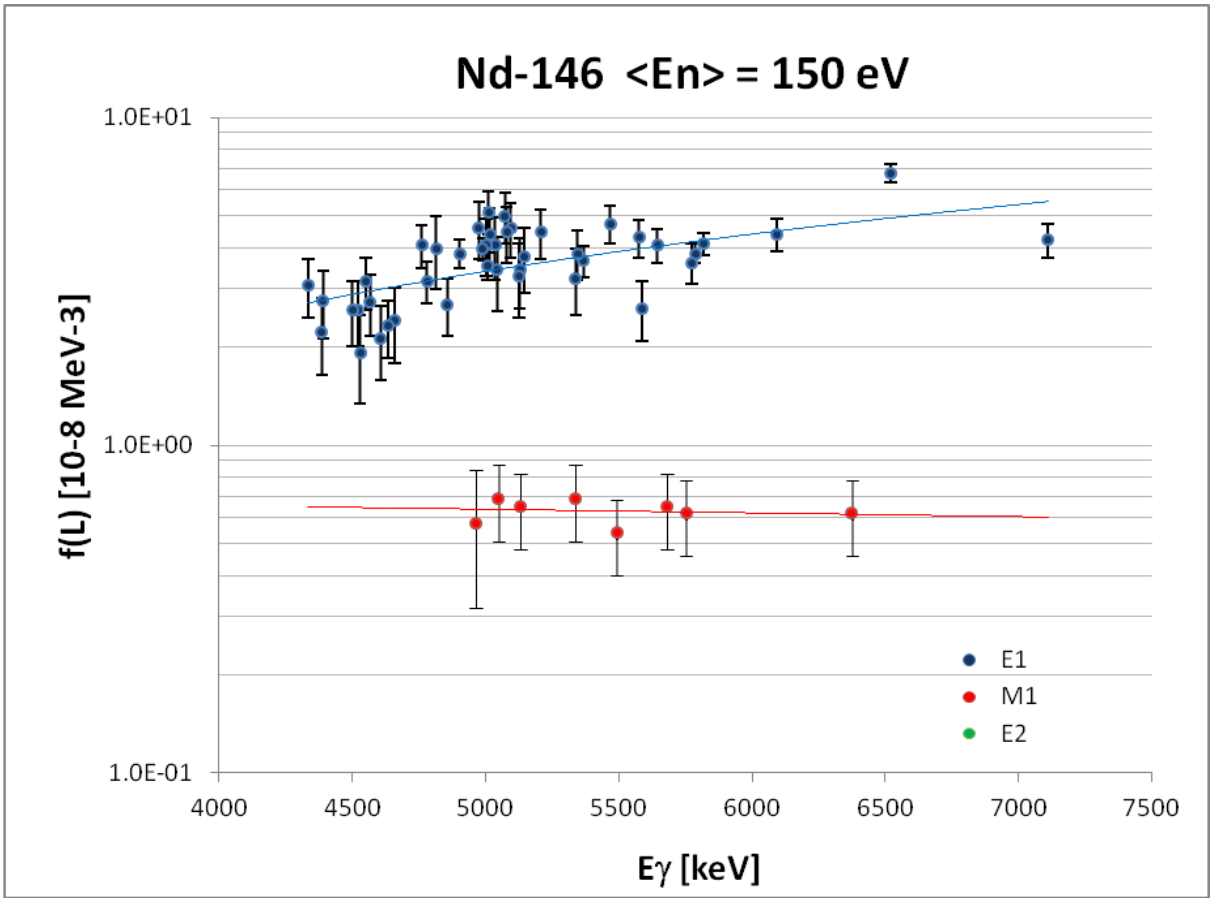
Nd-146 <En> = 150 eV
f(L) [10-8 MeV-3]
1.0E+01
1.0E+00
1.0E-01
4000
4500
5000
5500
6000
6500
7000
7500
Eγ [keV]
E1
M1
E2

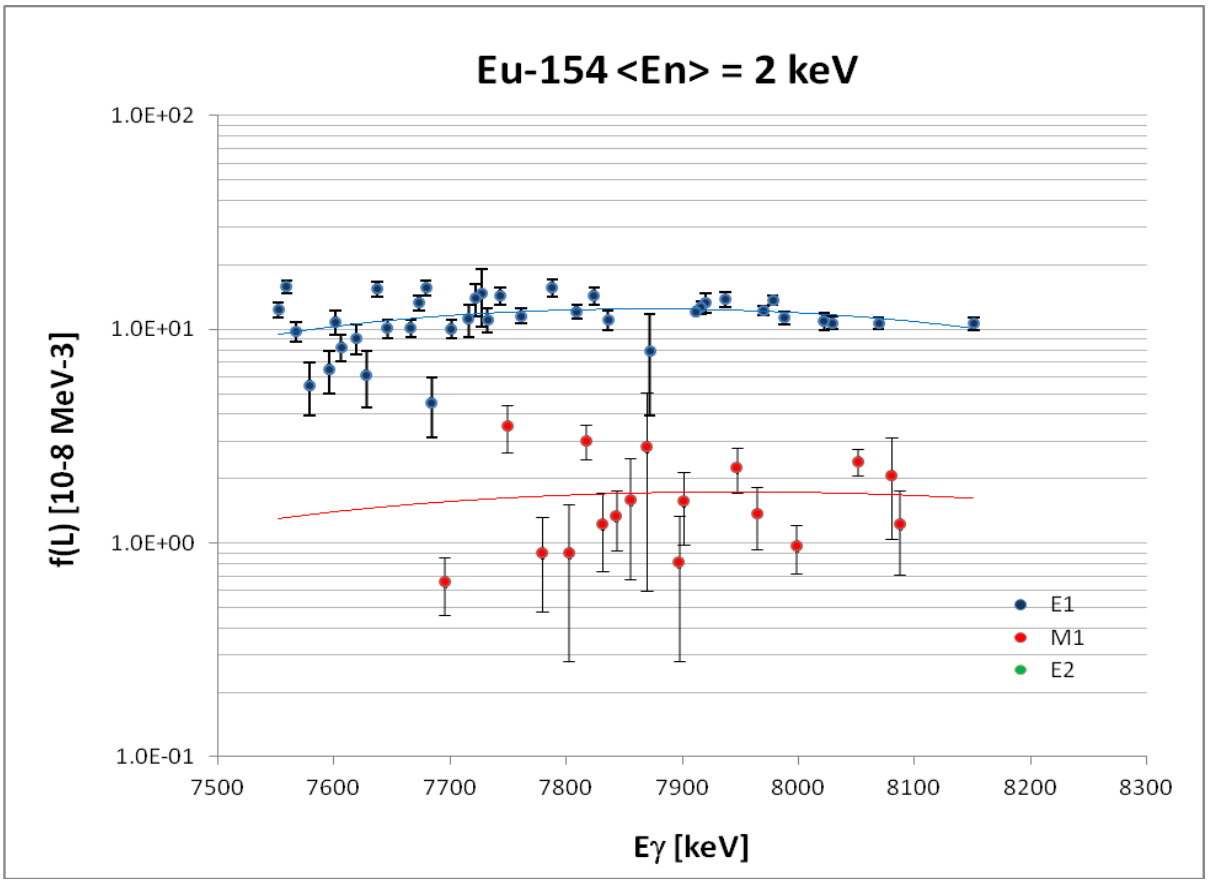
Eu-154 <En> = 2 keV
1.0E+02
1.0E+01
1.0E+00
1.0E-01
f(L) [10-8 MeV-3]
7500
7600
7700
7800
7900
8000
8100
8200
8300
Eγ [keV]
E1
M1
E2

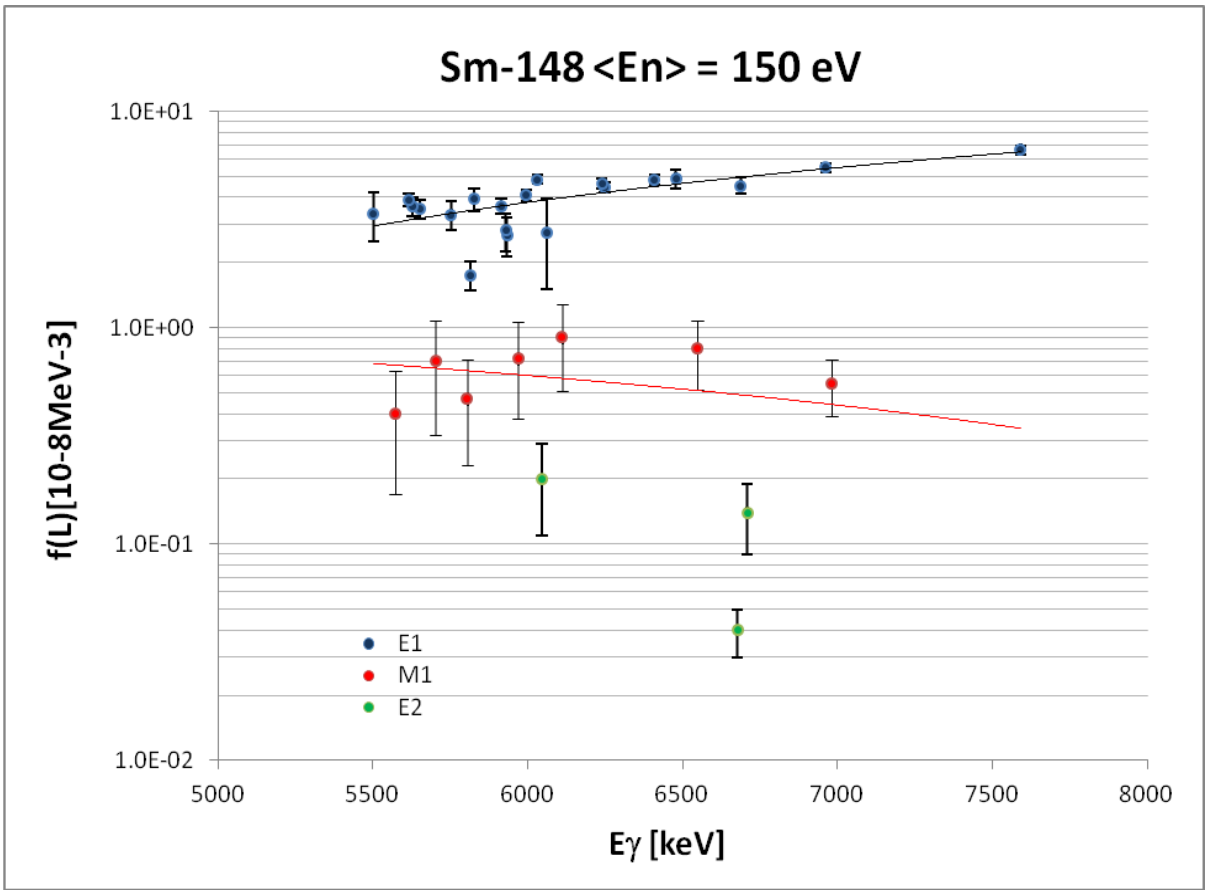
Sm-148 <En> = 150 eV
1.0E+01
1.0E+00
1.0E-01
1.0E-02
f(L)[10-8MeV-3]
5000
5500
6000
6500
7000
7500
8000
Eγ [keV]
E1
M1
E2

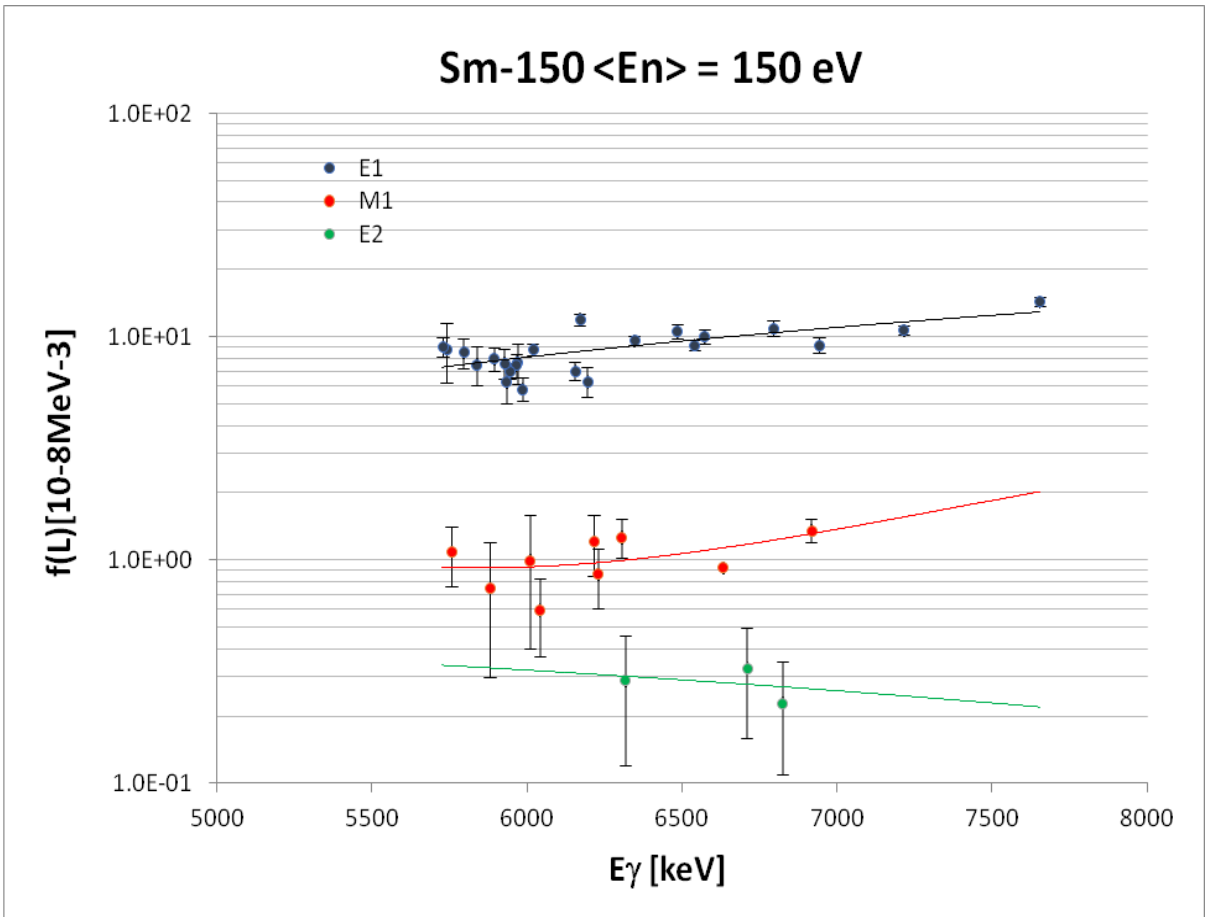
Sm-150 <En> = 150 eV
1.0E+02
1.0E+01
1.0E+00
1.0E-01
f(L)[10-8MeV-3]
E1
M1
E2
5000
5500
6000
6500
7000
7500
8000
Eγ [keV]

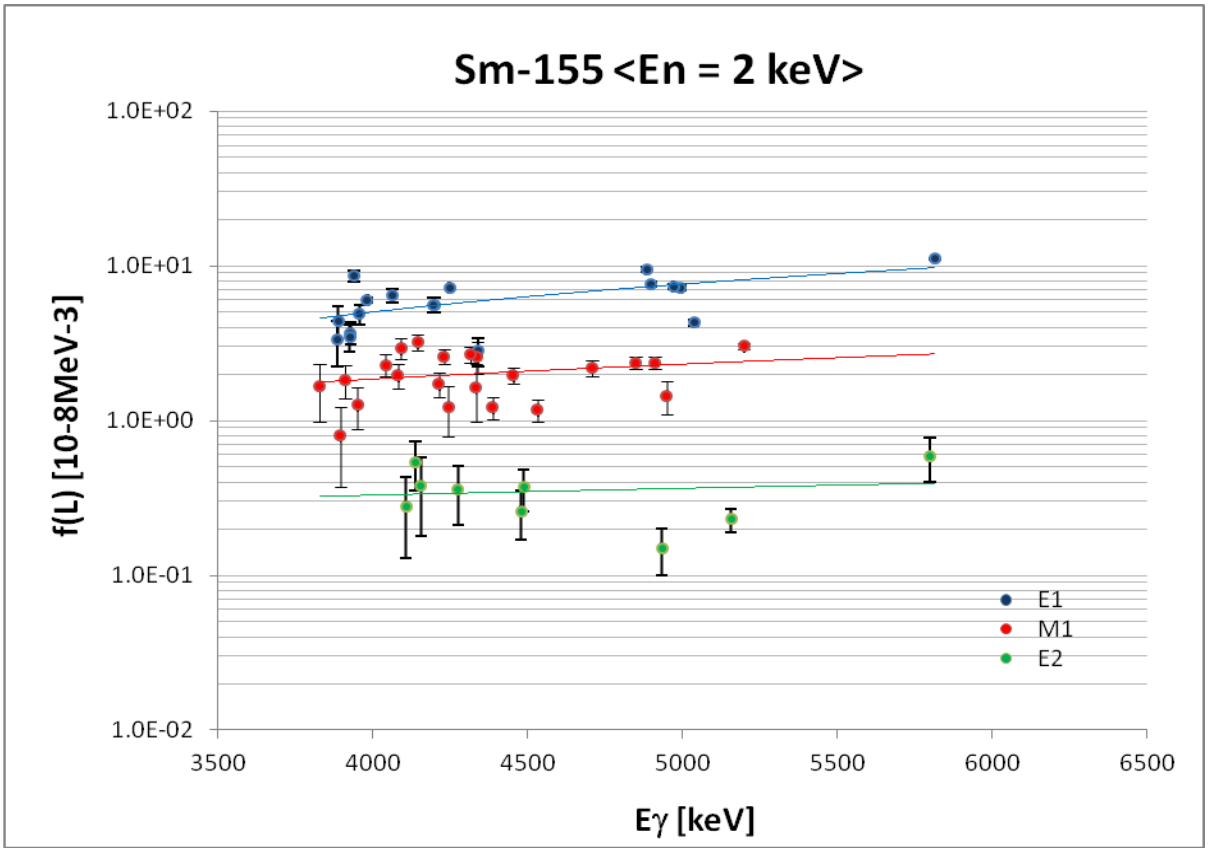
Sm-155 <En = 2 keV>
1.0E+02
1.0E+01
1.0E+00
1.0E-01
1.0E-02
f(L) [10-8MeV-3]
E1
M1
E2
3500
4000
4500
5000
5500
6000
6500
Eγ [keV]

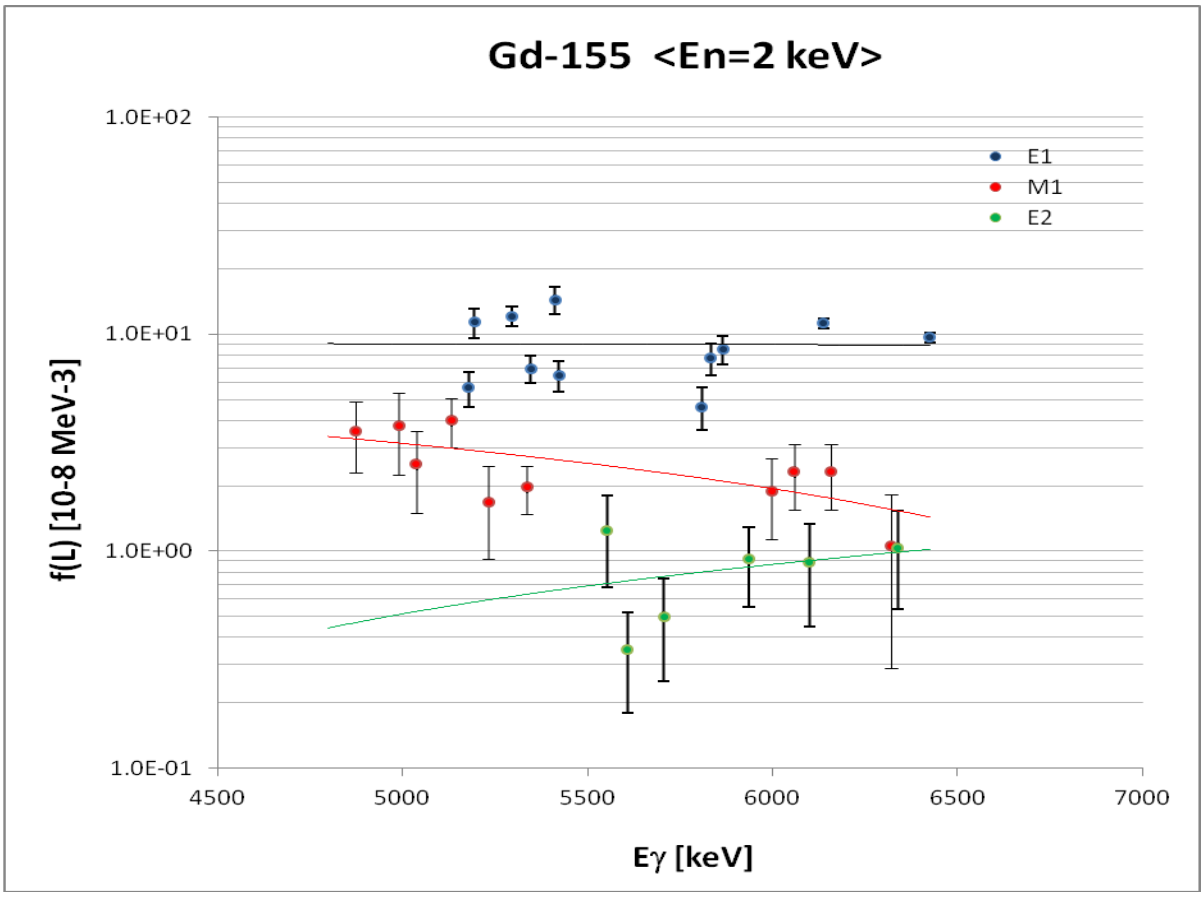
Gd-155 <En=2 keV>
1.0E+02
1.0E+01
1.0E+00
1.0E-01
f(L) [10-8 MeV-3]
4500
5000
5500
6000
6500
7000
Eγ [keV]
E1
M1
E2

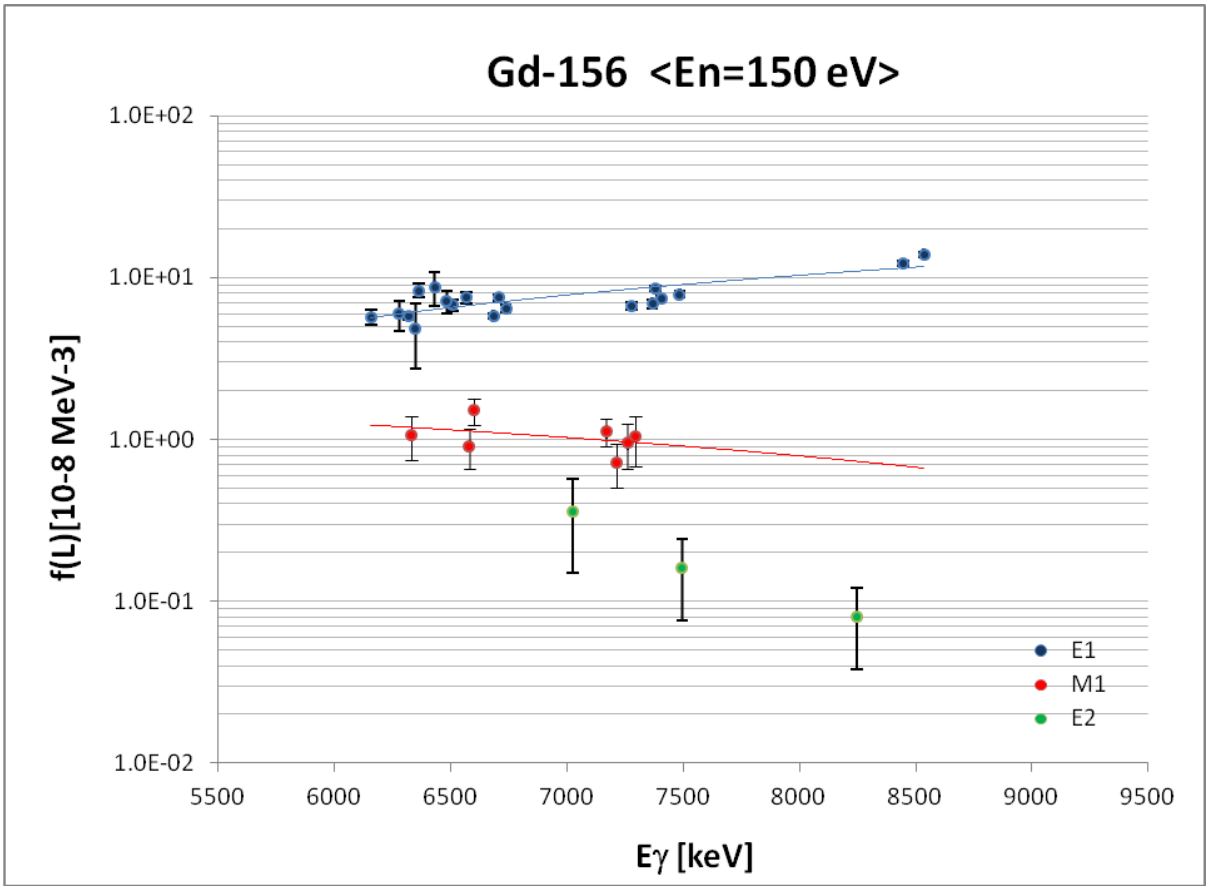
Gd-156 <En=150 eV>
1.0E+02
1.0E+01
1.0E+00
1.0E-01
1.0E-02
f(L)[10-8 MeV-3]
5500
6000
6500
7000
7500
8000
8500
9000
9500
Eγ [keV]
E1
M1
E2

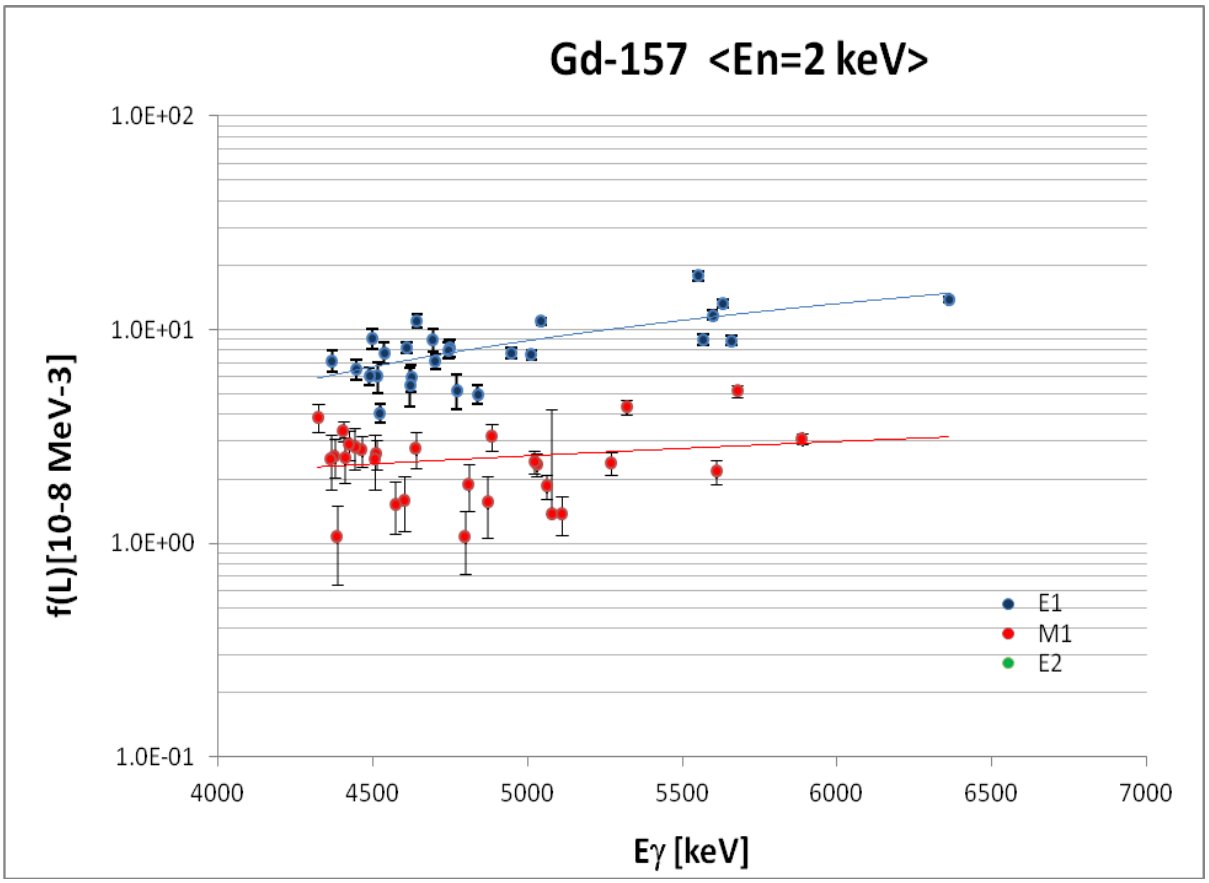
Gd-157 <En=2 keV>
1.0E+02
1.0E+01
1.0E+00
1.0E-01
f(L)[10-8 MeV-3]
4000
4500
5000
5500
6000
6500
7000
Eγ [keV]
E1
M1
E2

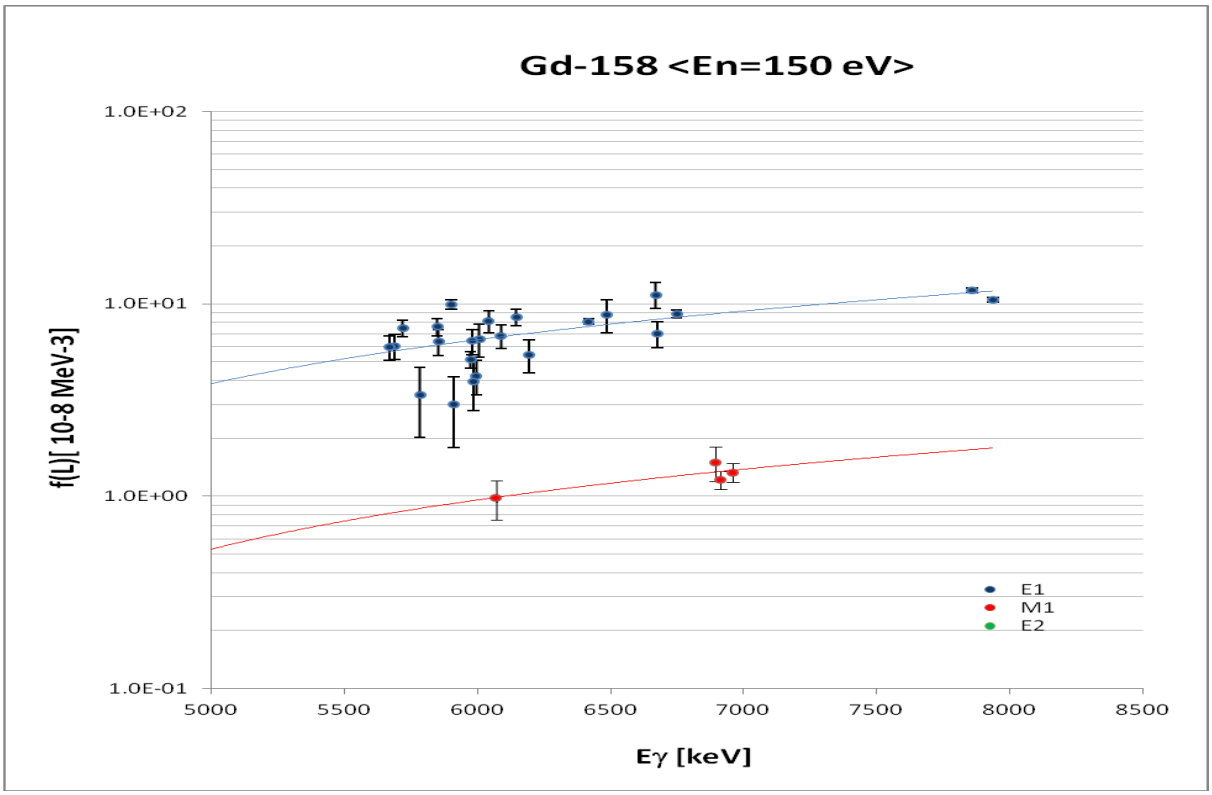
Gd-158 <En=150 eV>
1.0E+02
1.0E+01
1.0E+00
1.0E-01
f(L)[10-8 MeV-3]
5000
5500
6000
6500
7000
7500
8000
8500
Eγ [keV]
E1
M1
E2

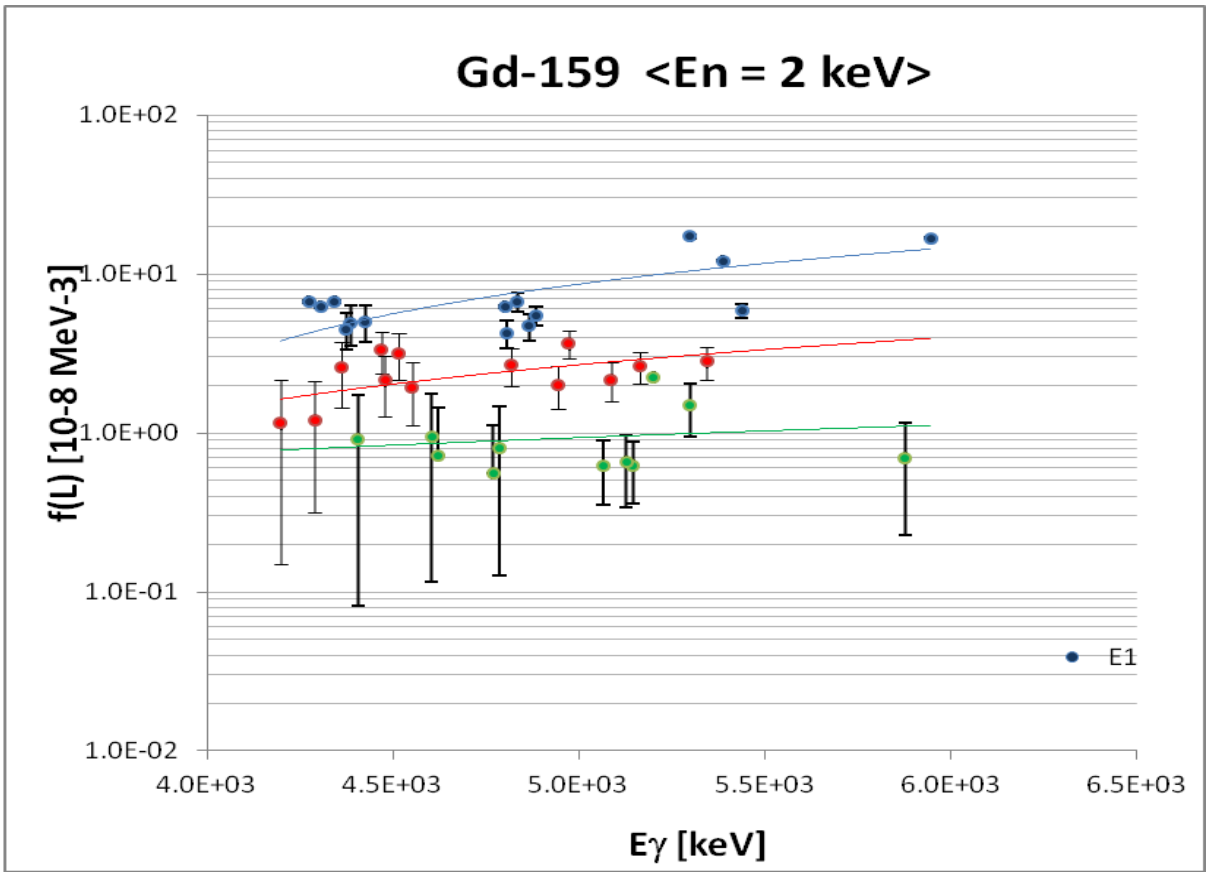
Gd-159 <En = 2 keV>
1.0E+02
1.0E+01
1.0E+00
1.0E-01
1.0E-02
f(L) [10-8 MeV-3]
4.0E+03
4.5E+03
5.0E+03
5.5E+03
6.0E+03
6.5E+03
Eγ [keV]
E1

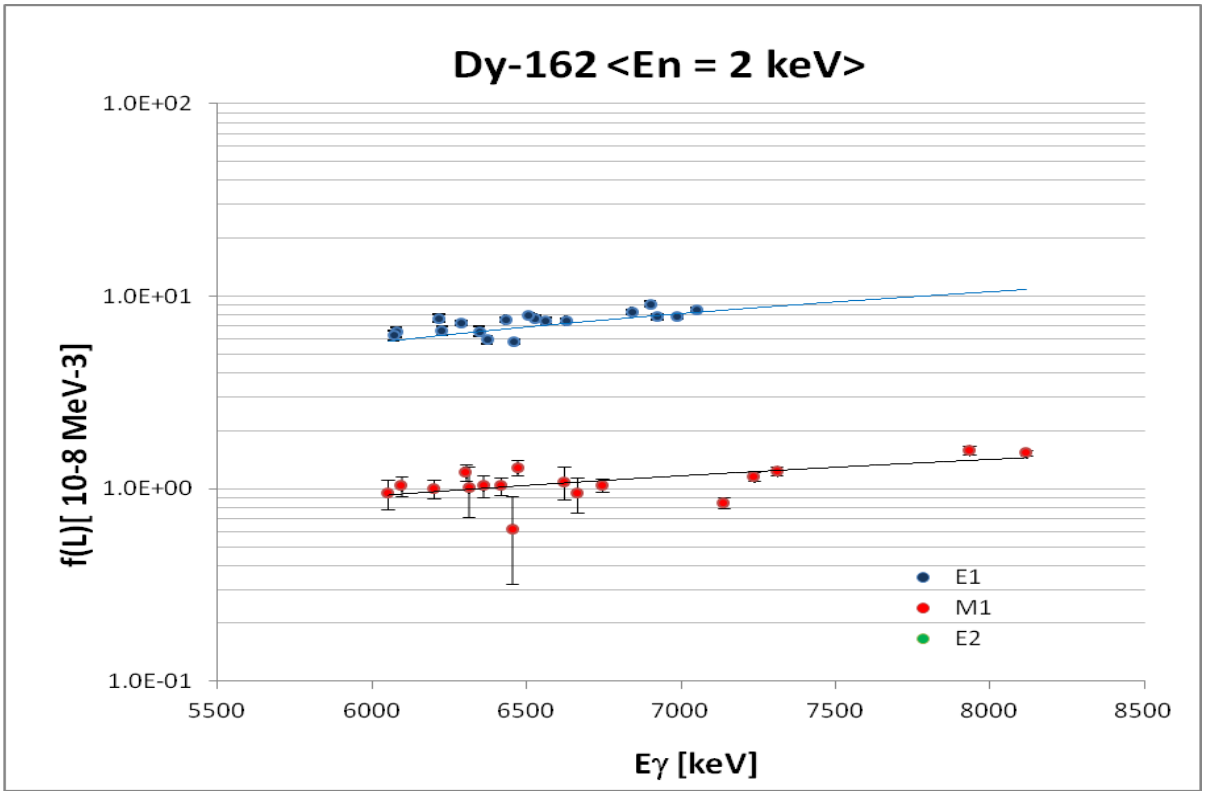
Dy-162 <En = 2 keV>
1.0E+02
1.0E+01
1.0E+00
1.0E-01
f(L)[10-8 MeV-3]
5500
6000
6500
7000
7500
8000
8500
Eγ [keV]
E1
M1
E2

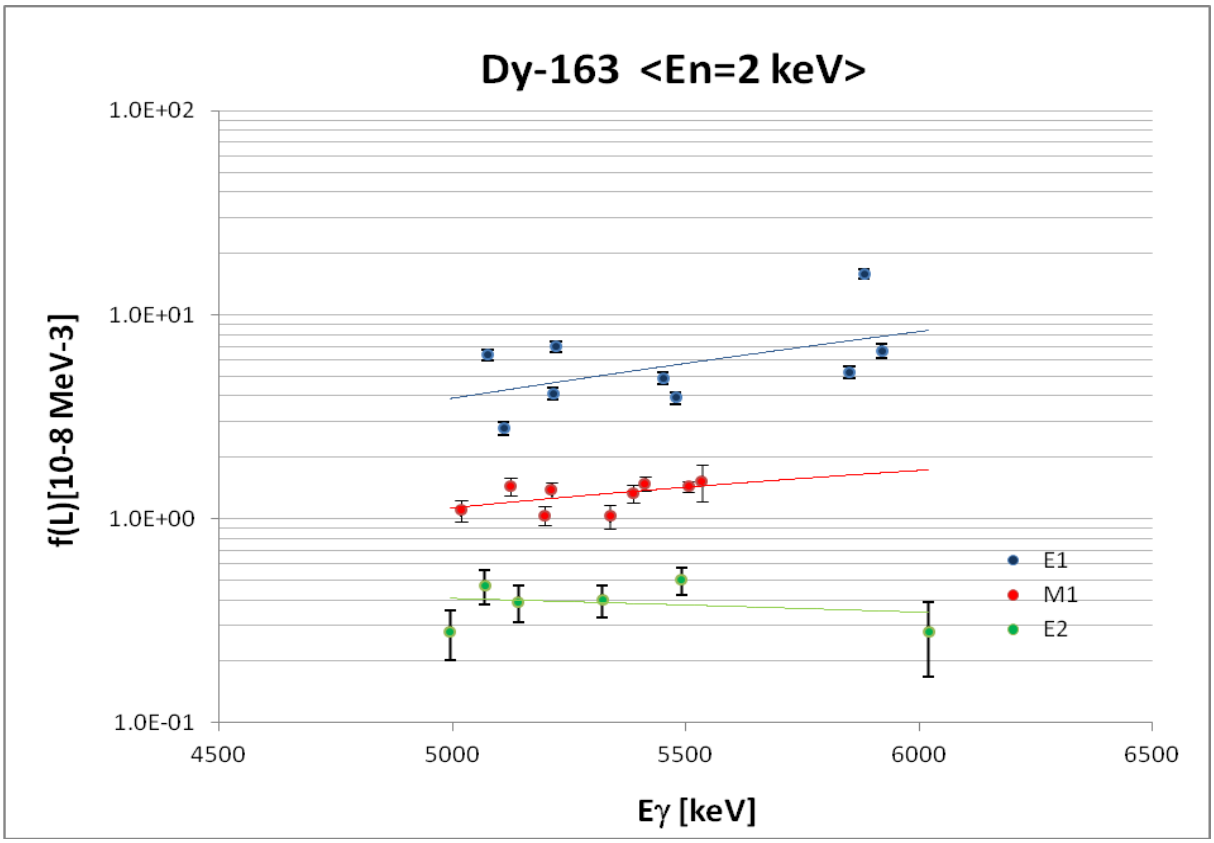
Dy-163 <En=2 keV>
1.0E+02
1.0E+01
1.0E+00
1.0E-01
f(L)[10-8 MeV-3]
4500
5000
5500
6000
6500
Eγ [keV]
E1
M1
E2

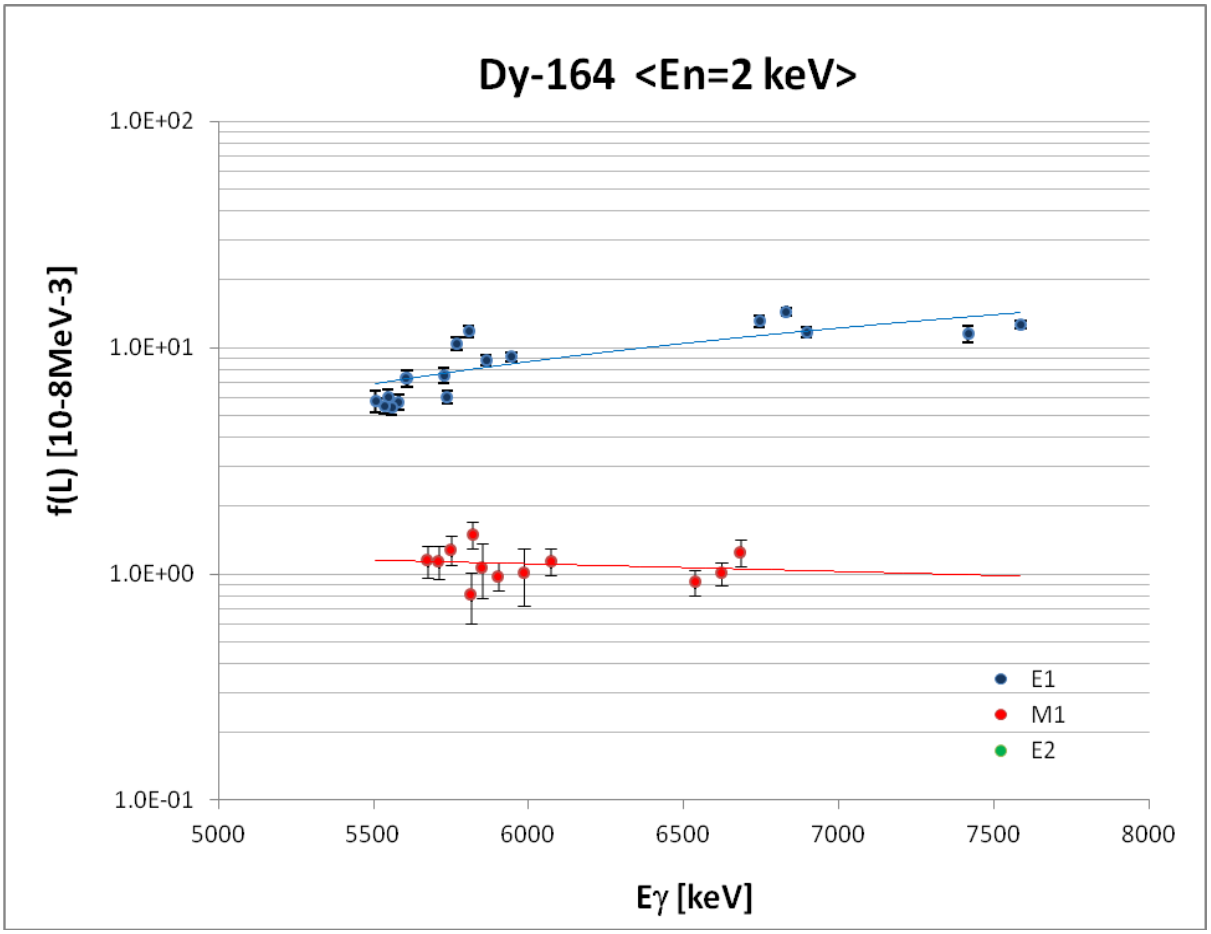
Dy-164 <En=2 keV>
1.0E+02
1.0E+01
1.0E+00
1.0E-01
f(L) [10-8MeV-3]
5000
5500
6000
6500
7000
7500
8000
Eγ [keV]
E1
M1
E2

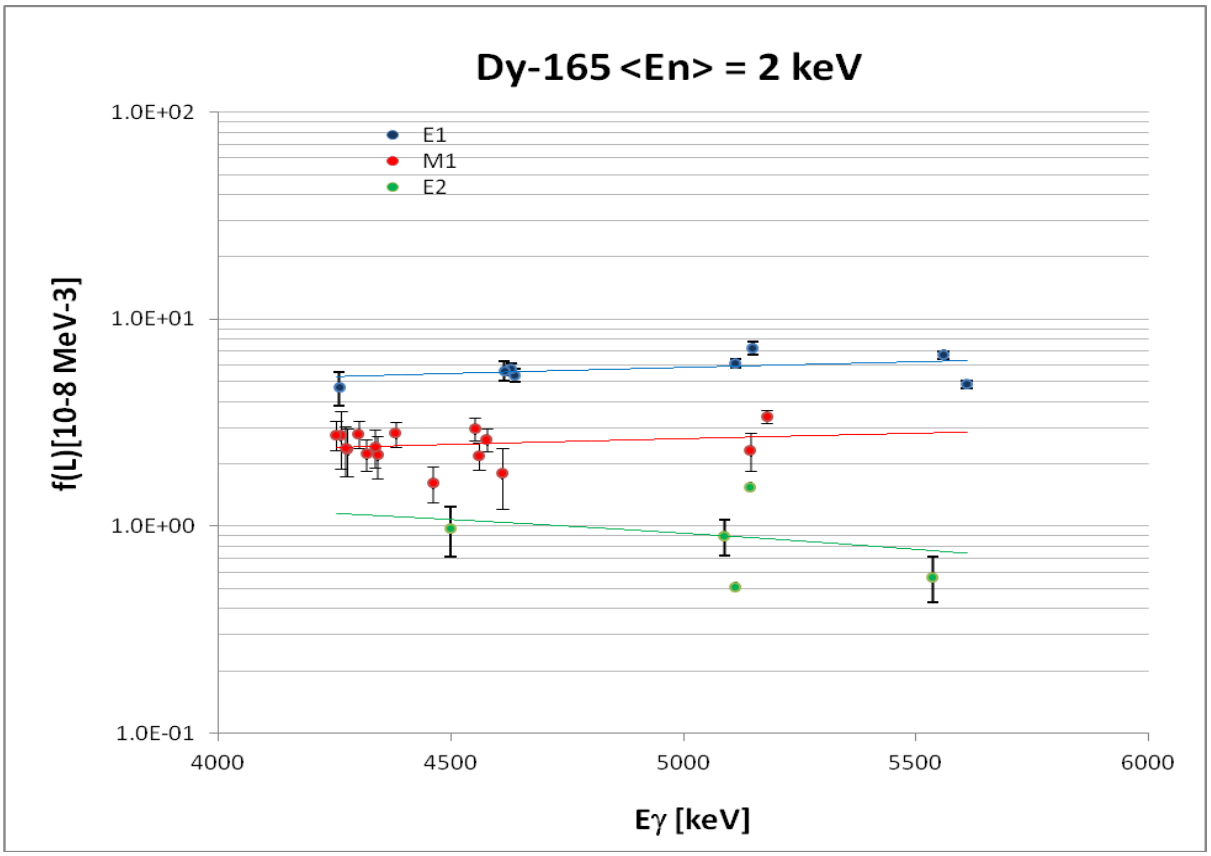
Dy-165 <En> = 2 keV
1.0E+02
1.0E+01
1.0E+00
1.0E-01
f(L)[10-8 MeV-3]
E1
M1
E2
4000
4500
5000
5500
6000
Eγ [keV]

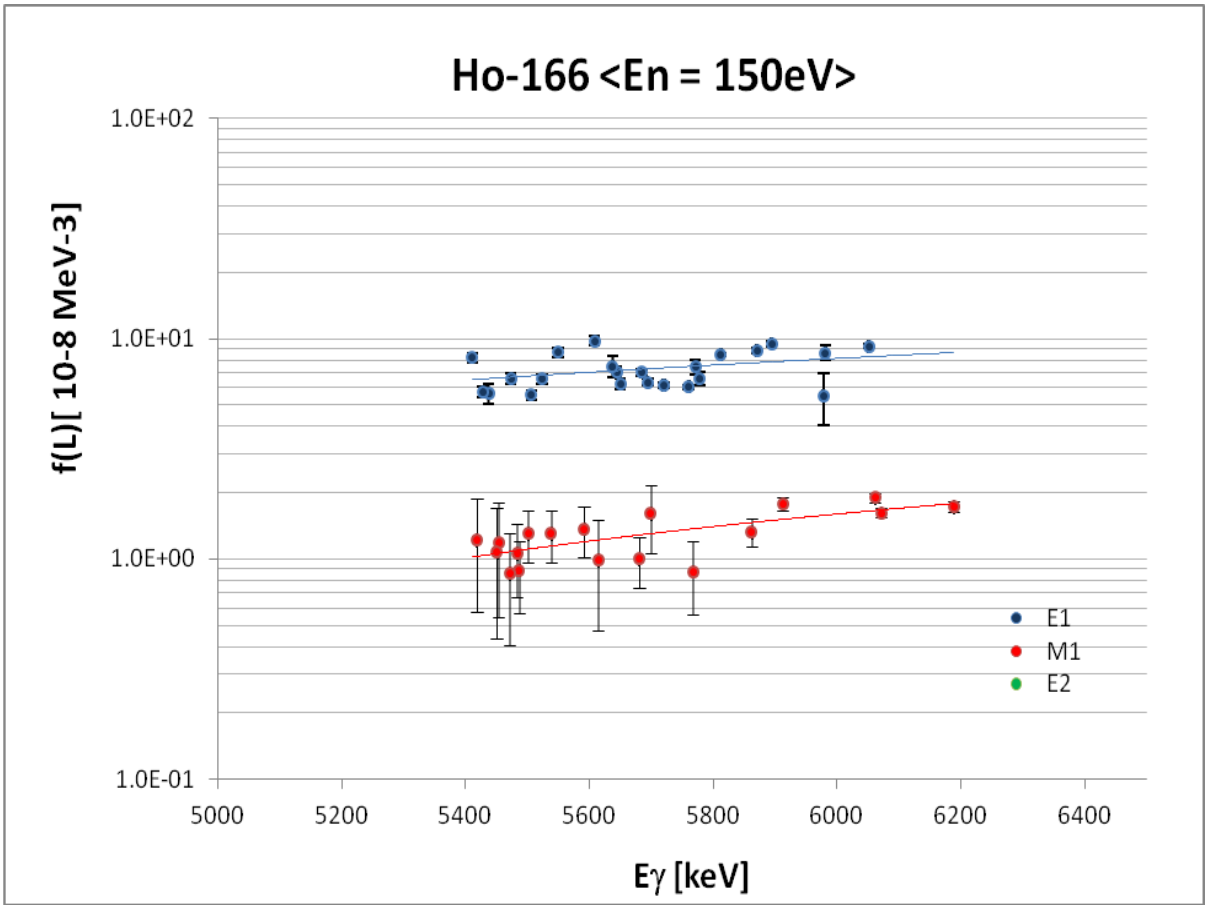
Ho-166 <En = 150eV>
1.0E+02
1.0E+01
1.0E+00
1.0E-01
f(L)[10-8 MeV-3]
E1
M1
E2
5000
5200
5400
5600
5800
6000
6200
6400
Eγ [keV]

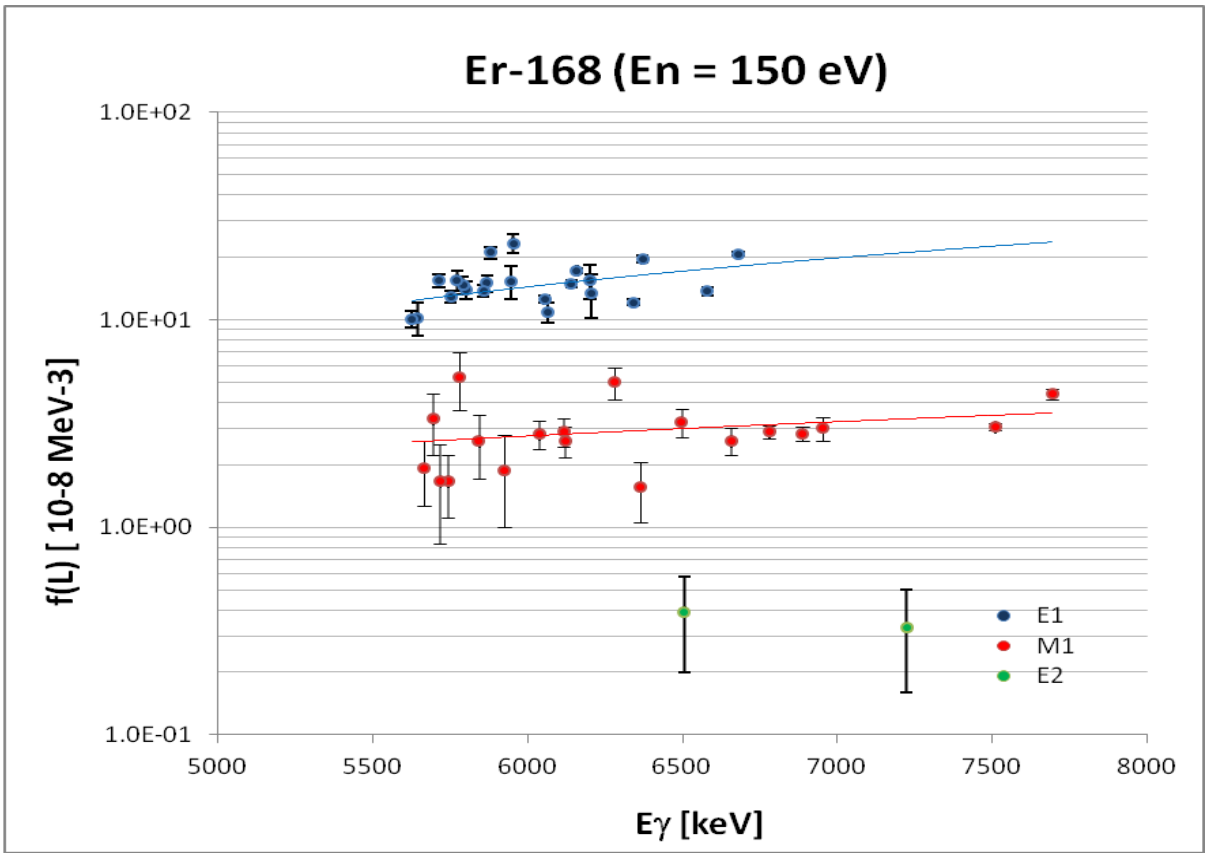
Er-168 (En = 150 eV)
1.0E+02
1.0E+01
1.0E+00
1.0E-01
f(L) [10-8 MeV-3]
5000
5500
6000
6500
7000
7500
8000
Eγ [keV]
E1
M1
E2

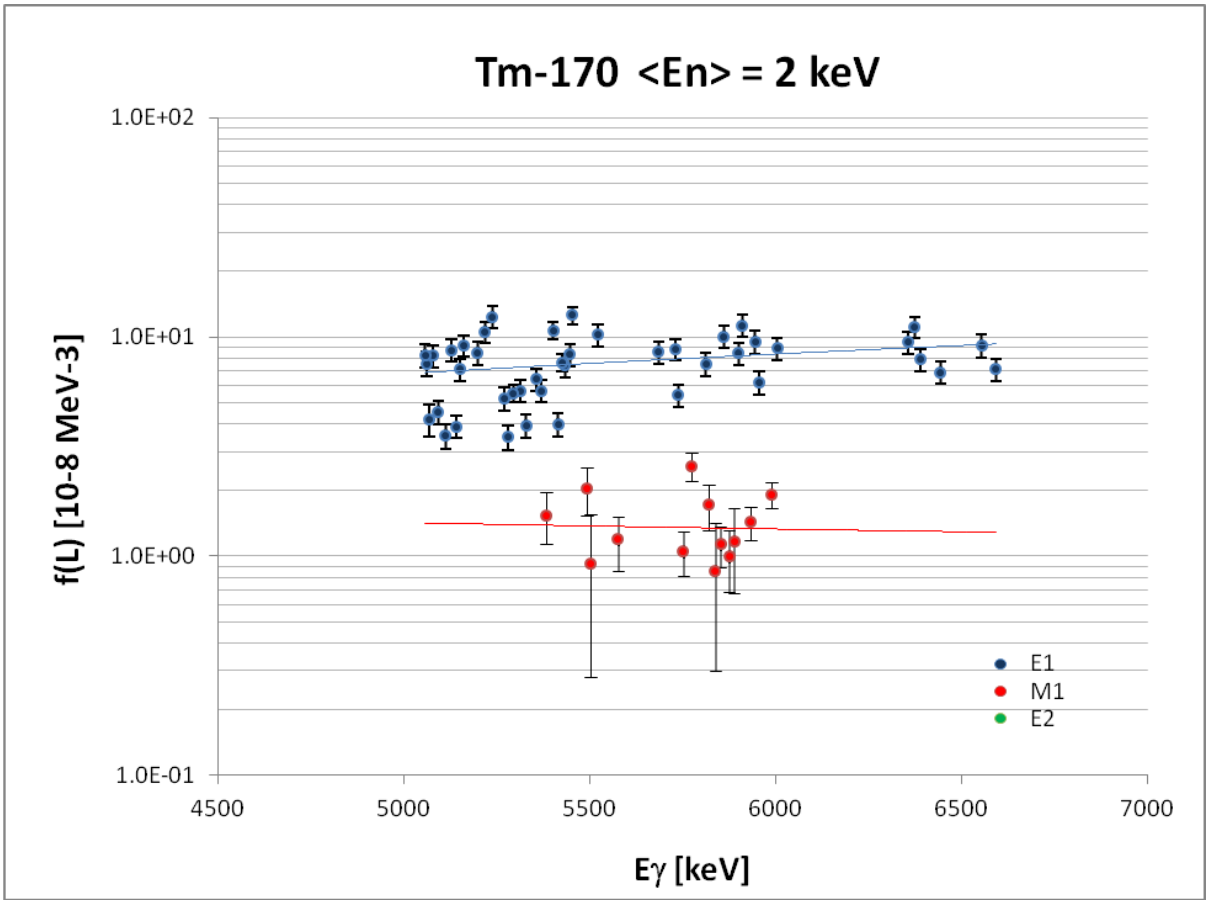
Tm-170 <En> = 2 keV
1.0E+02
1.0E+01
1.0E+00
1.0E-01
f(L) [10-8 MeV-3]
4500
5000
5500
6000
6500
7000
Eγ [keV]
E1
M1
E2

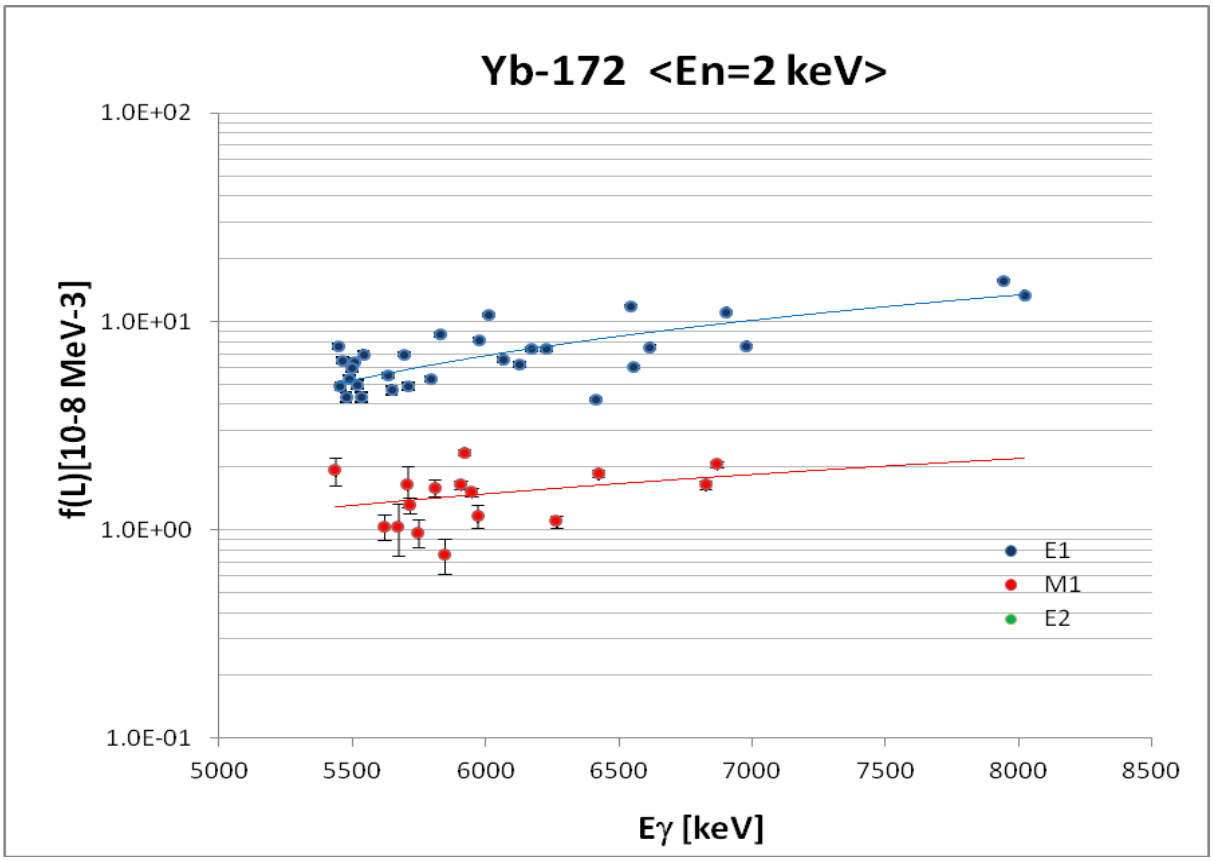
Yb-172 <En=2 keV>
f(L)[10-8 MeV-3]
1.0E+02
1.0E+01
1.0E+00
1.0E-01
5000
5500
6000
6500
7000
7500
8000
8500
Eγ [keV]
E1
M1
E2

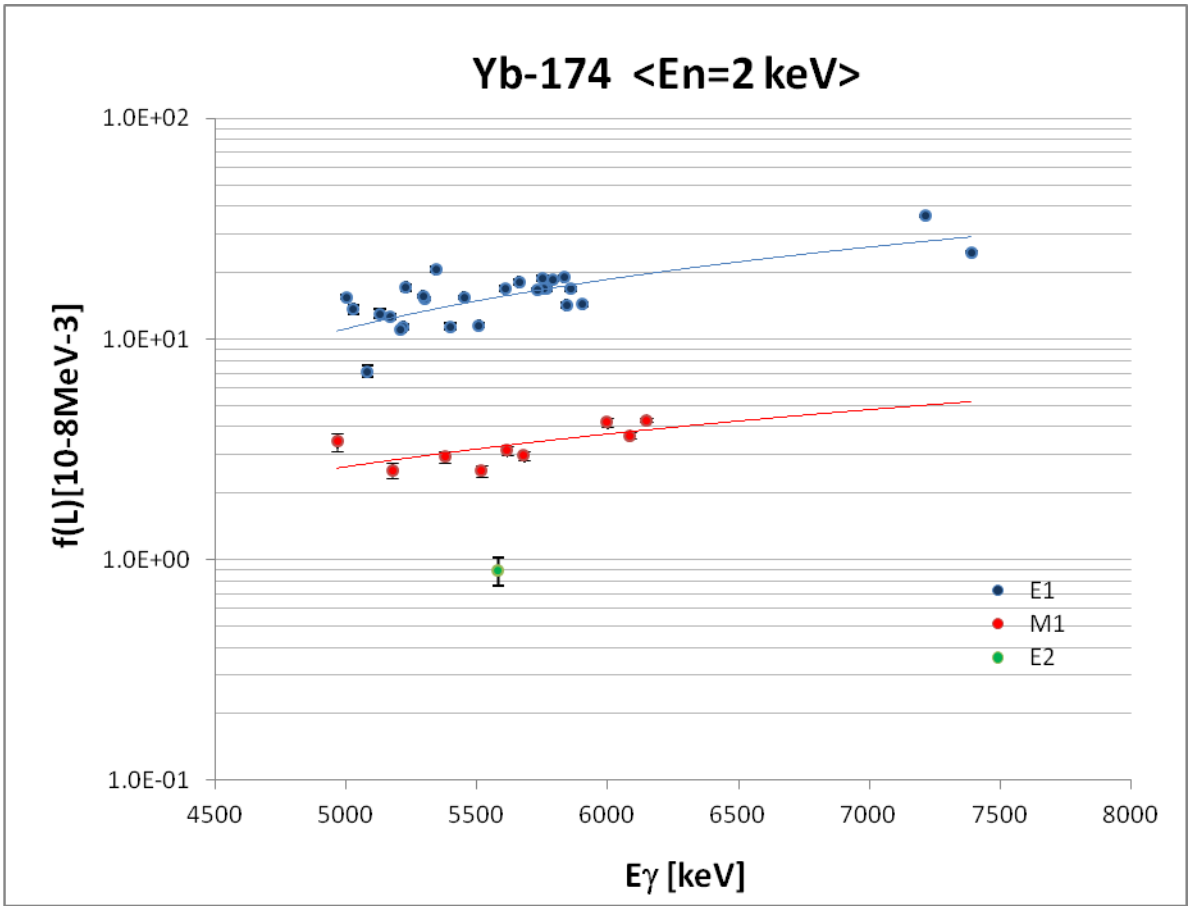
Yb-174 <En=2 keV>
f(L)[10-8MeV-3]
1.0E+02
1.0E+01
1.0E+00
1.0E-01
4500
5000
5500
6000
6500
7000
7500
8000
Eγ [keV]
E1
M1
E2

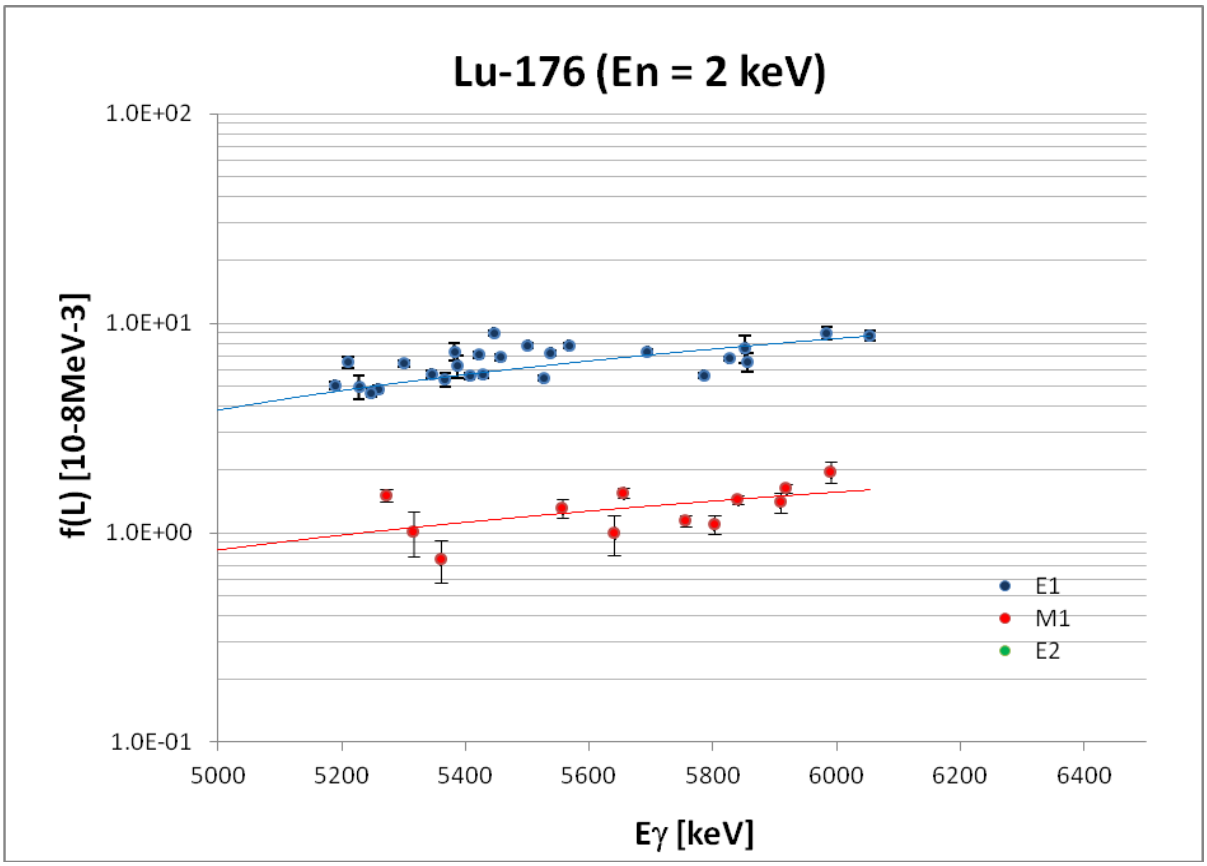
Lu-176 (En = 2 keV)
1.0E+02
1.0E+01
1.0E+00
1.0E-01
f(L) [10-8MeV-3]
5000
5200
5400
5600
5800
6000
6200
6400
Eγ [keV]
E1
M1
E2

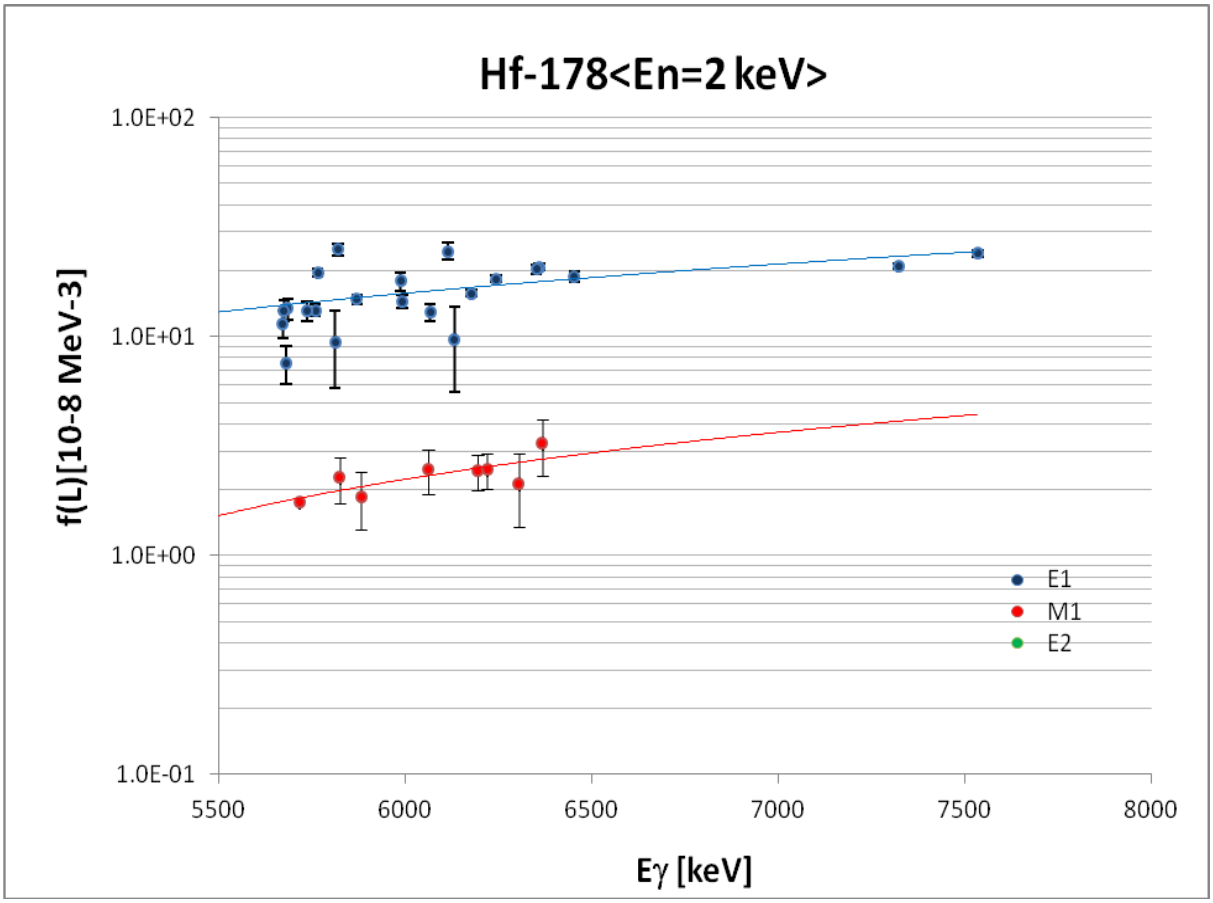
Hf-178<En=2 keV>
1.0E+02
1.0E+01
1.0E+00
1.0E-01
f(L)[10-8 MeV-3]
5500
6000
6500
7000
7500
8000
Eγ [keV]
E1
M1
E2

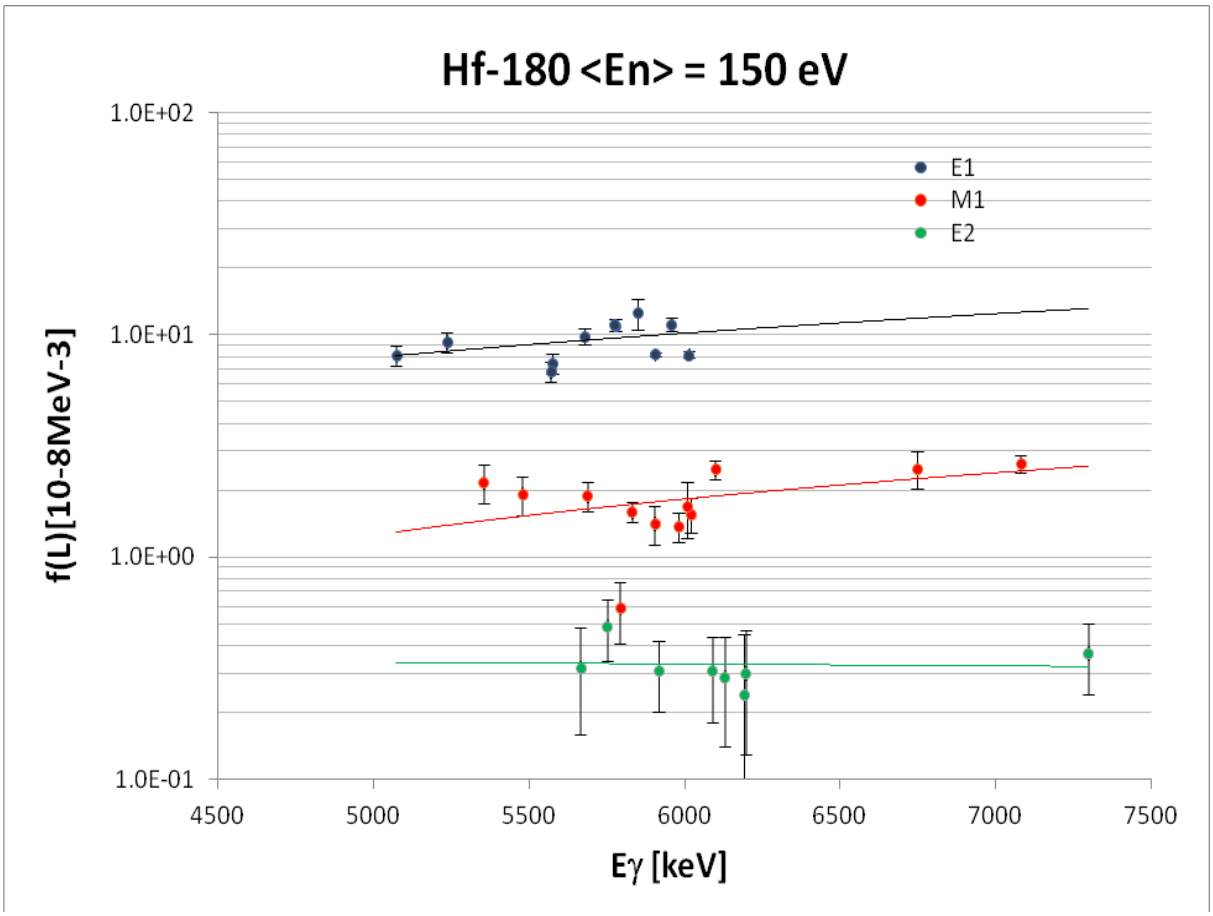
Hf-180 <En> = 150 eV
1.0E+02
1.0E+01
1.0E+00
1.0E-01
f(L)[10-8MeV-3]
4500
5000
5500
6000
6500
7000
7500
Eγ [keV]
E1
M1
E2

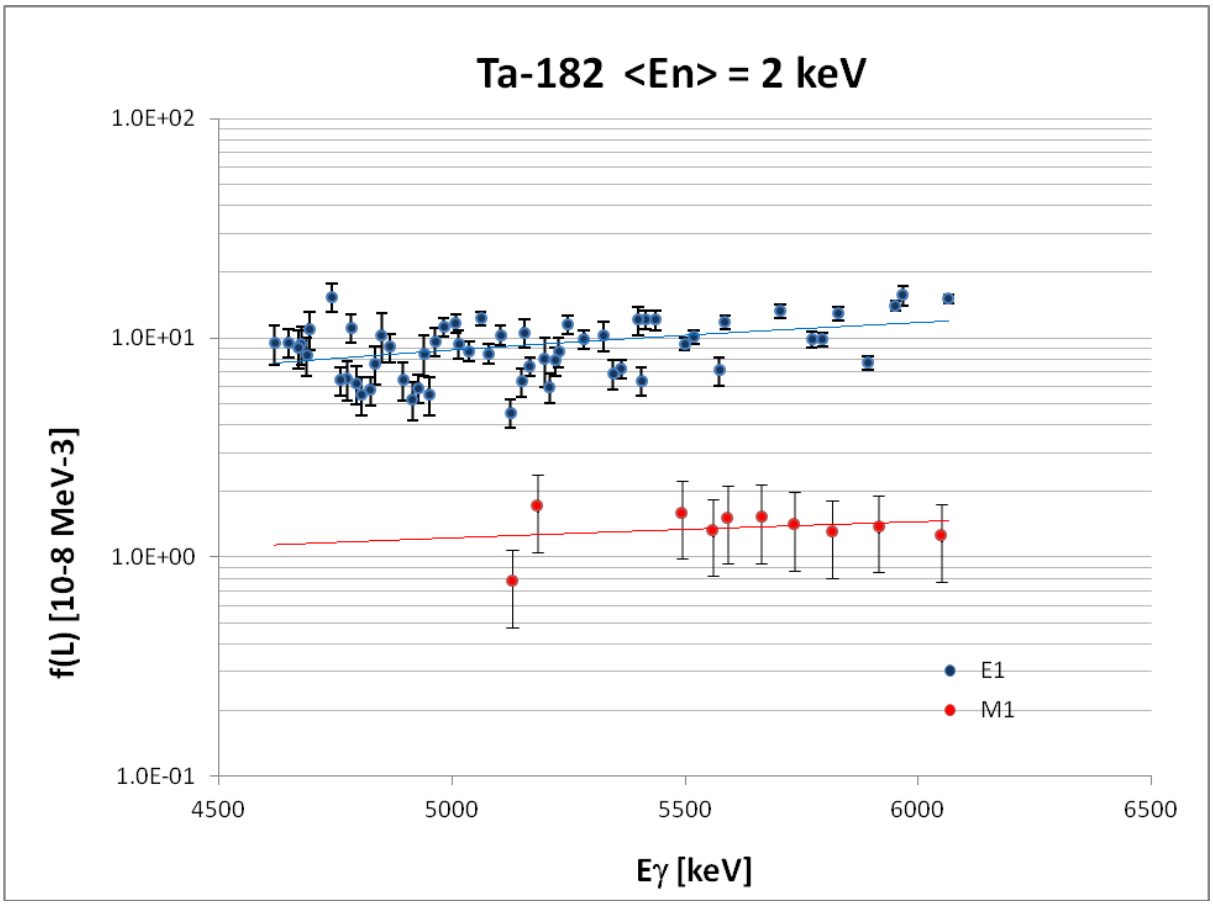
Ta-182 <En> = 2 keV
1.0E+02
1.0E+01
1.0E+00
1.0E-01
f(L) [10-8 MeV-3]
4500
5000
5500
6000
6500
Eγ [keV]
E1
M1

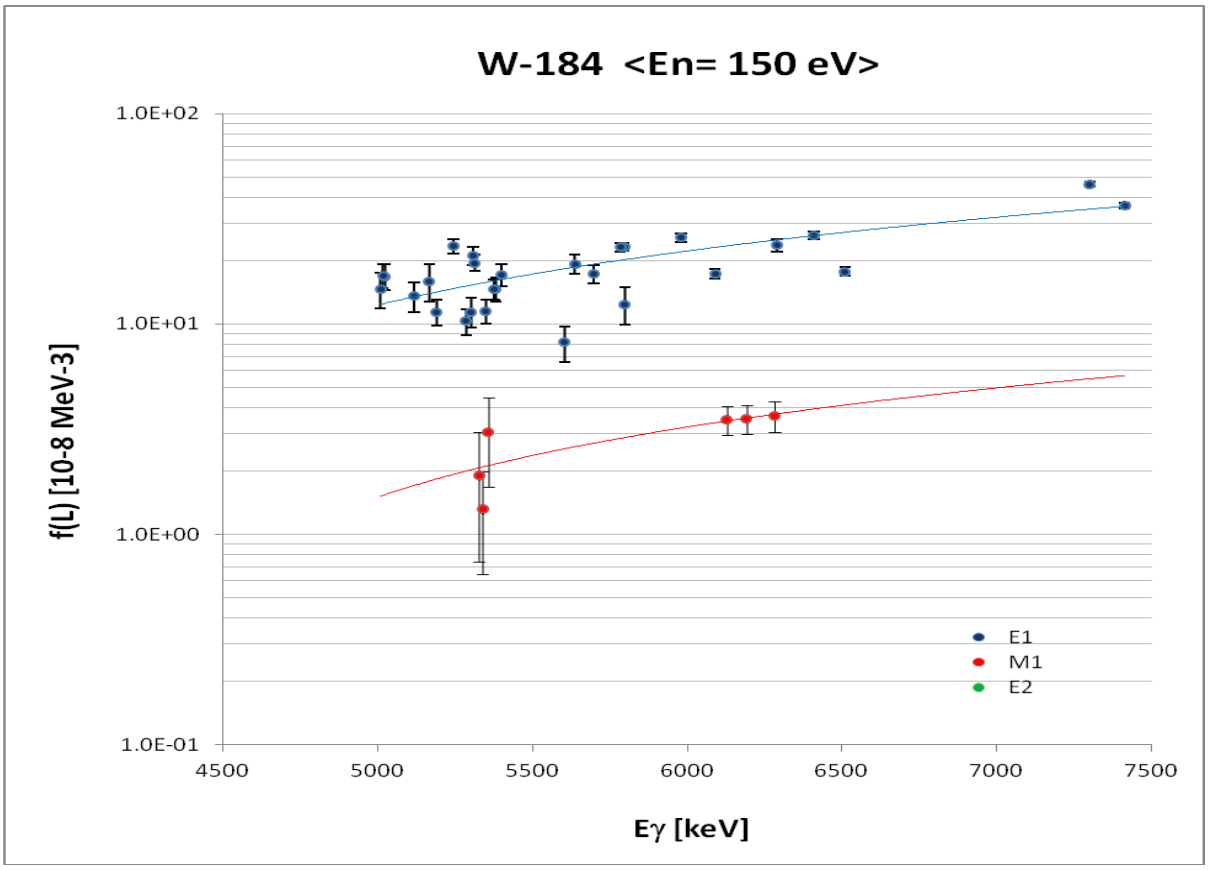
W-184 <En= 150 eV>
1.0E+02
1.0E+01
1.0E+00
1.0E-01
f(L) [10-8 MeV-3]
4500
5000
5500
6000
6500
7000
7500
Eγ [keV]
E1
M1
E2

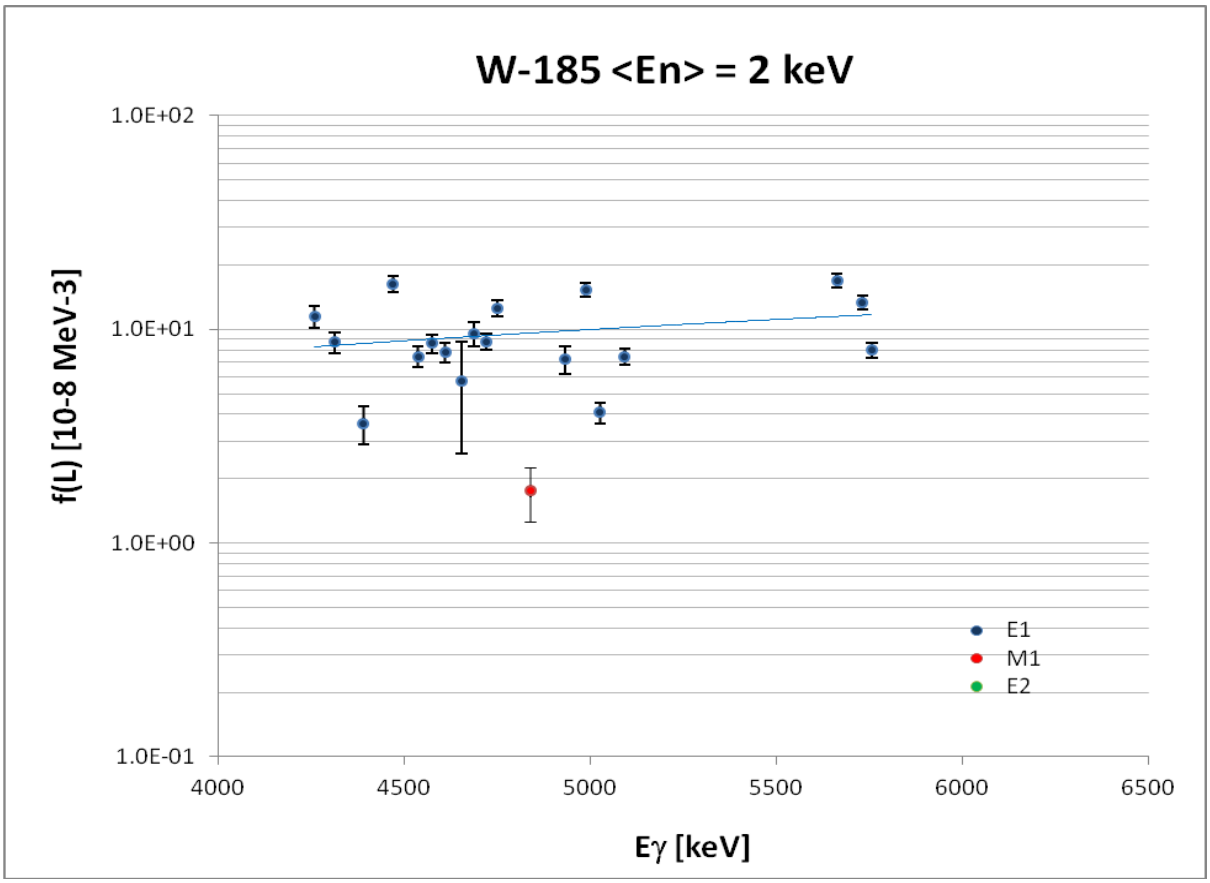
W-185 <En> = 2 keV
1.0E+02
1.0E+01
1.0E+00
1.0E-01
f(L) [10-8 MeV-3]
4000
4500
5000
5500
6000
6500
Eγ [keV]
E1
M1
E2

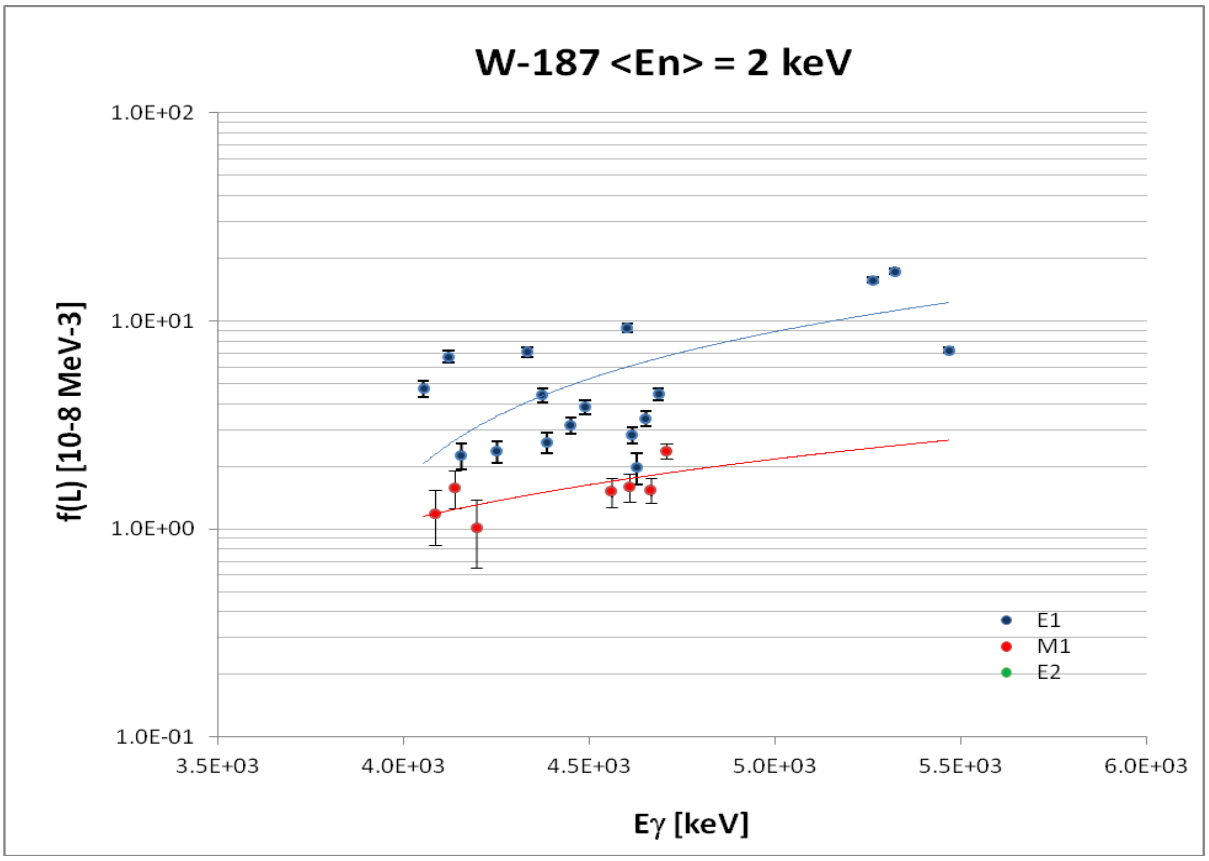
W-187 <En> = 2 keV
f(L) [10-8 MeV-3]
1.0E+02
1.0E+01
1.0E+00
1.0E-01
3.5E+03
4.0E+03
4.5E+03
5.0E+03
5.5E+03
6.0E+03
Eγ [keV]
E1
M1
E2

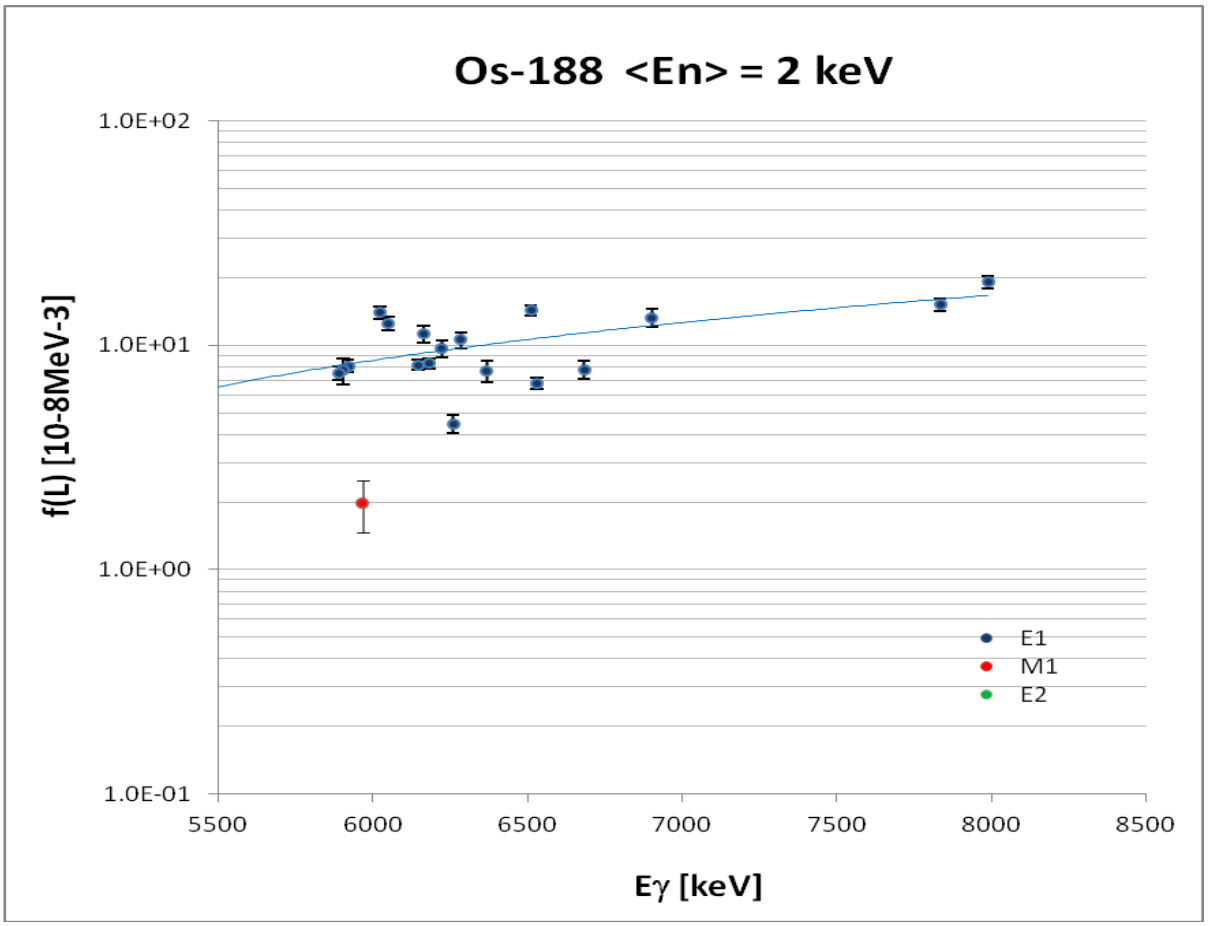
Os-188 <En> = 2 keV
f(L) [10-8MeV-3]
1.0E+02
1.0E+01
1.0E+00
1.0E-01
5500
6000
6500
7000
7500
8000
8500
Eγ [keV]
E1
M1
E2

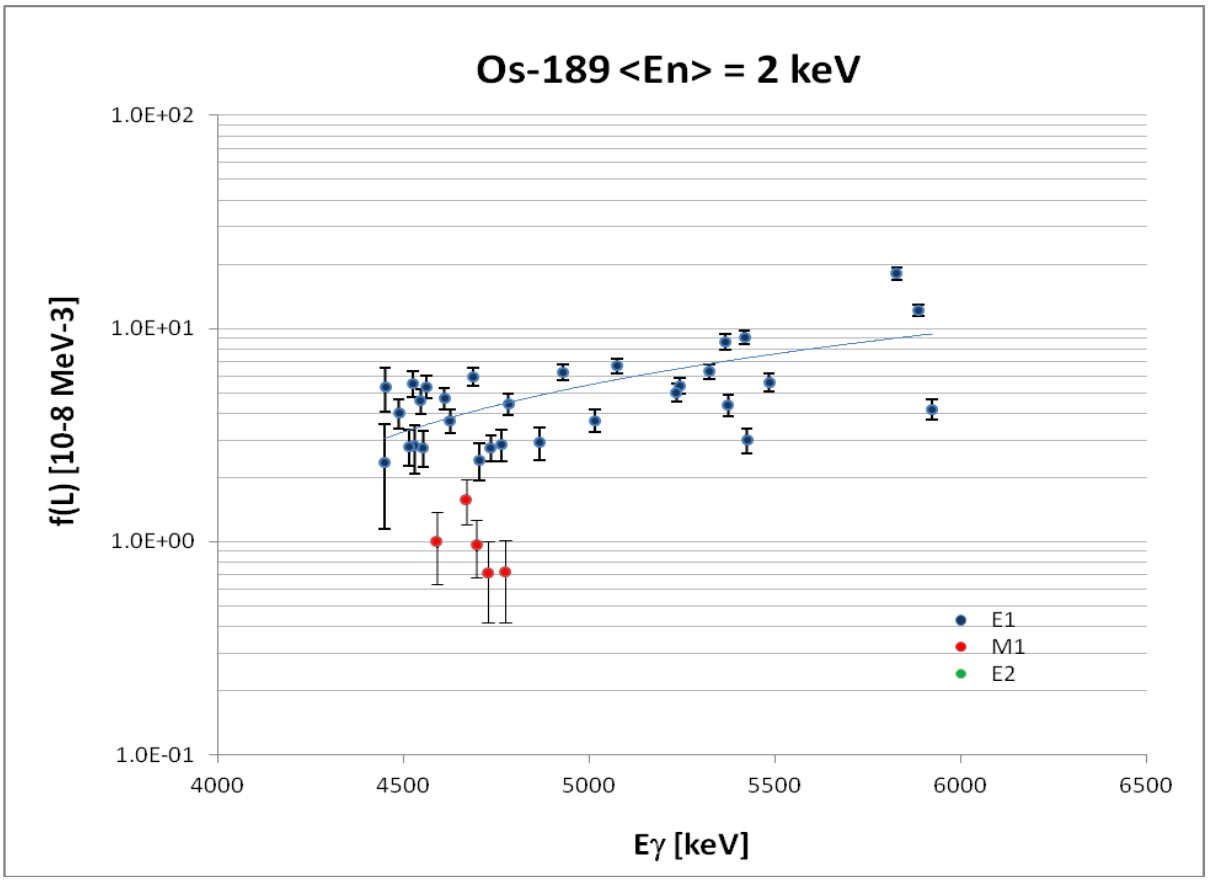
Os-189 <En> = 2 keV
1.0E+02
1.0E+01
1.0E+00
1.0E-01
f(L) [10-8 MeV-3]
4000
4500
5000
5500
6000
6500
Eγ [keV]
E1
M1
E2

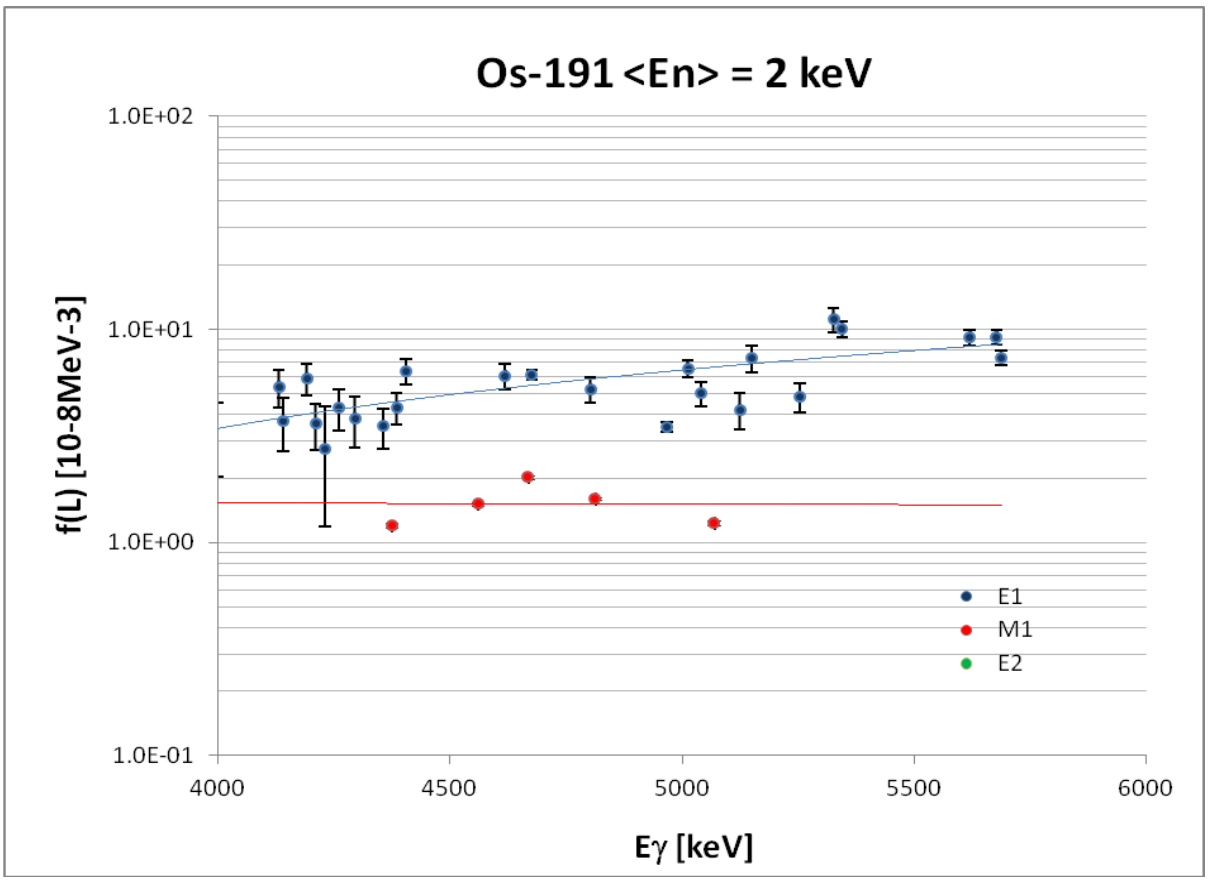
Os-191 <En> = 2 keV
1.0E+02
1.0E+01
1.0E+00
1.0E-01
f(L) [10-8MeV-3]
4000
4500
5000
5500
6000
Eγ [keV]
E1
M1
E2

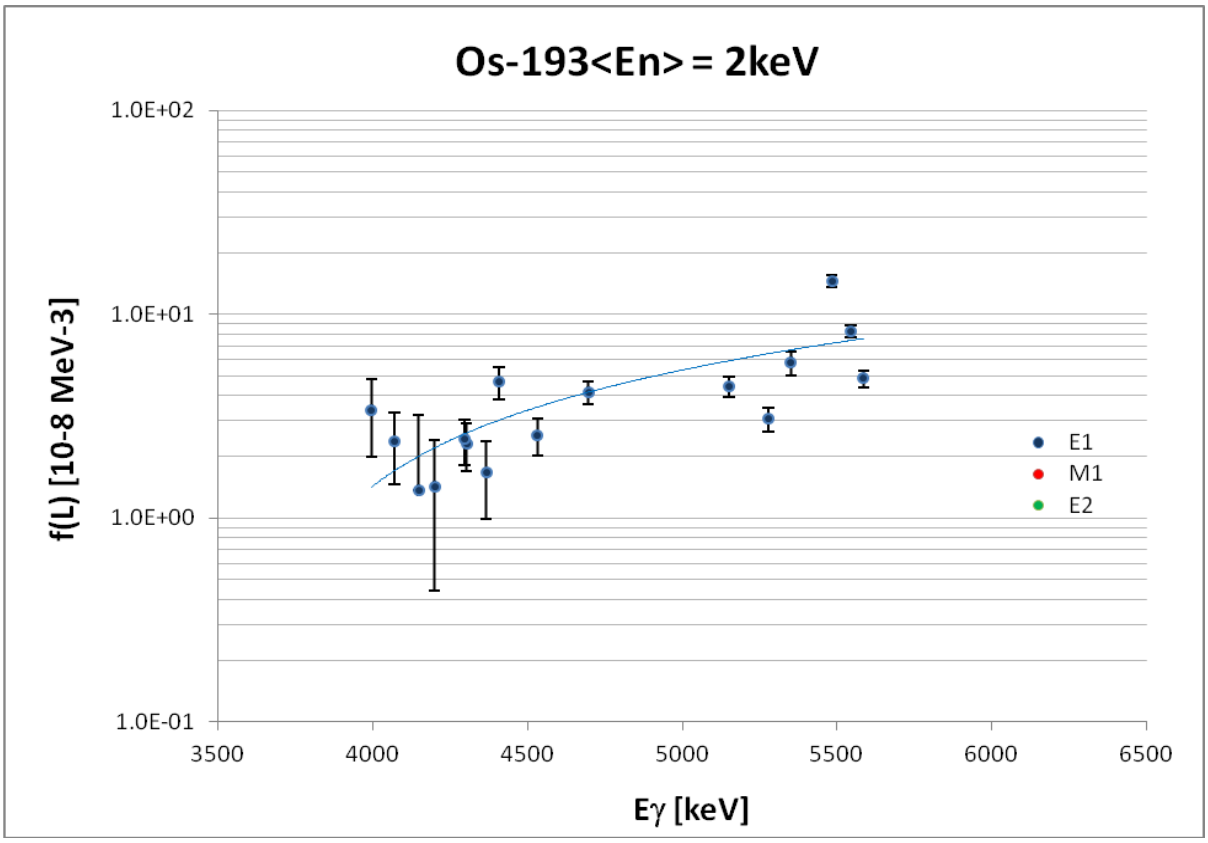
Os-193<En> = 2keV
1.0E+02
1.0E+01
1.0E+00
1.0E-01
f(L) [10-8 MeV-3]
3500
4000
4500
5000
5500
6000
6500
Eγ [keV]
E1
M1
E2

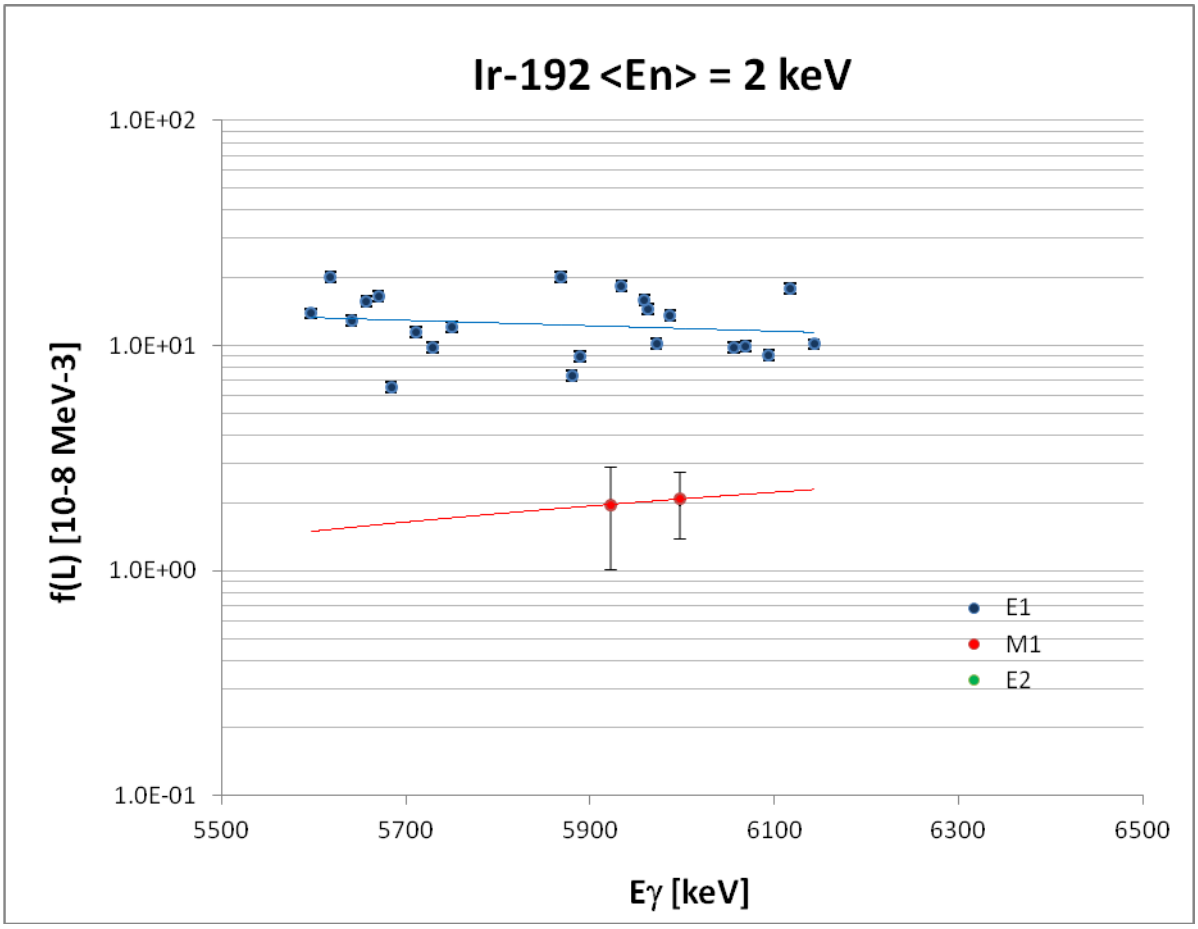
Ir-192 <En> = 2 keV
1.0E+02
1.0E+01
1.0E+00
1.0E-01
f(L) [10-8 MeV-3]
5500
5700
5900
6100
6300
6500
Eγ [keV]
E1
M1
E2

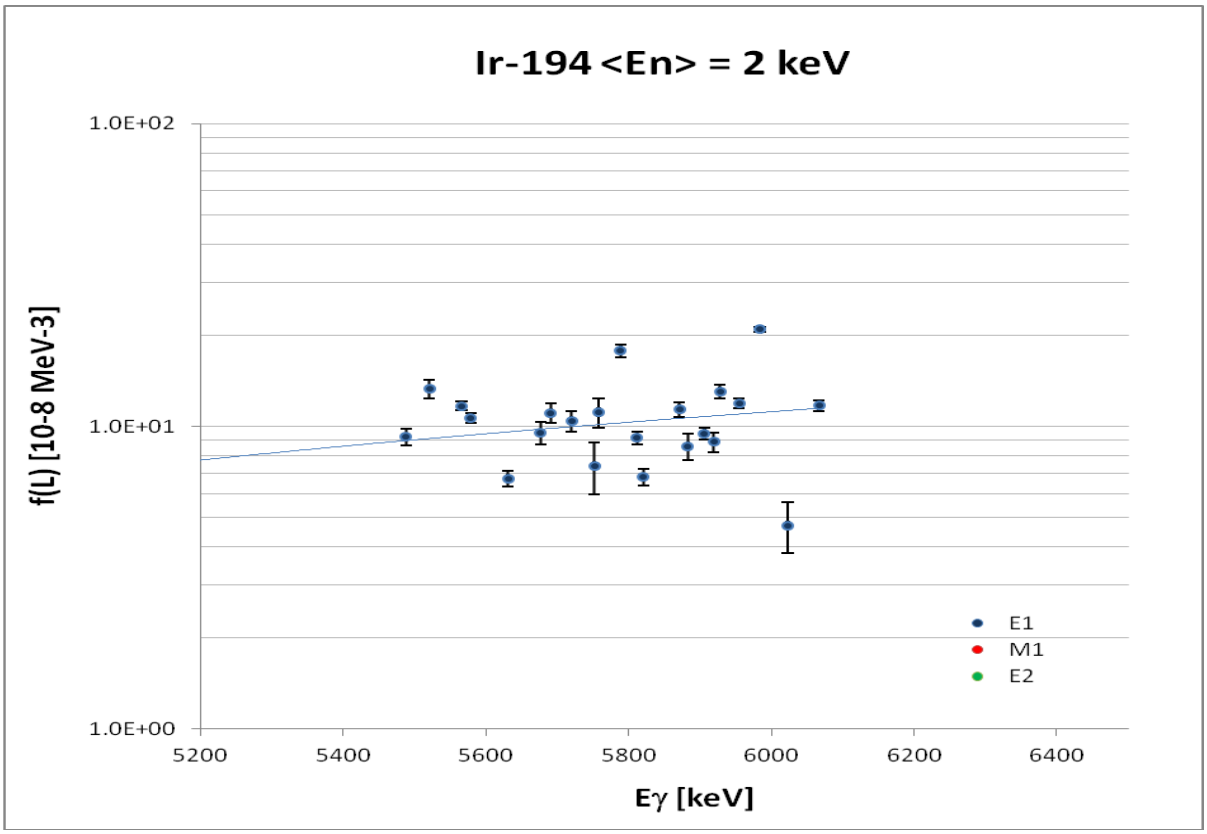
Ir-194 <En> = 2 keV
1.0E+02
1.0E+01
1.0E+00
f(L) [10-8 MeV-3]
5200
5400
5600
5800
6000
6200
6400
Eγ [keV]
E1
M1
E2

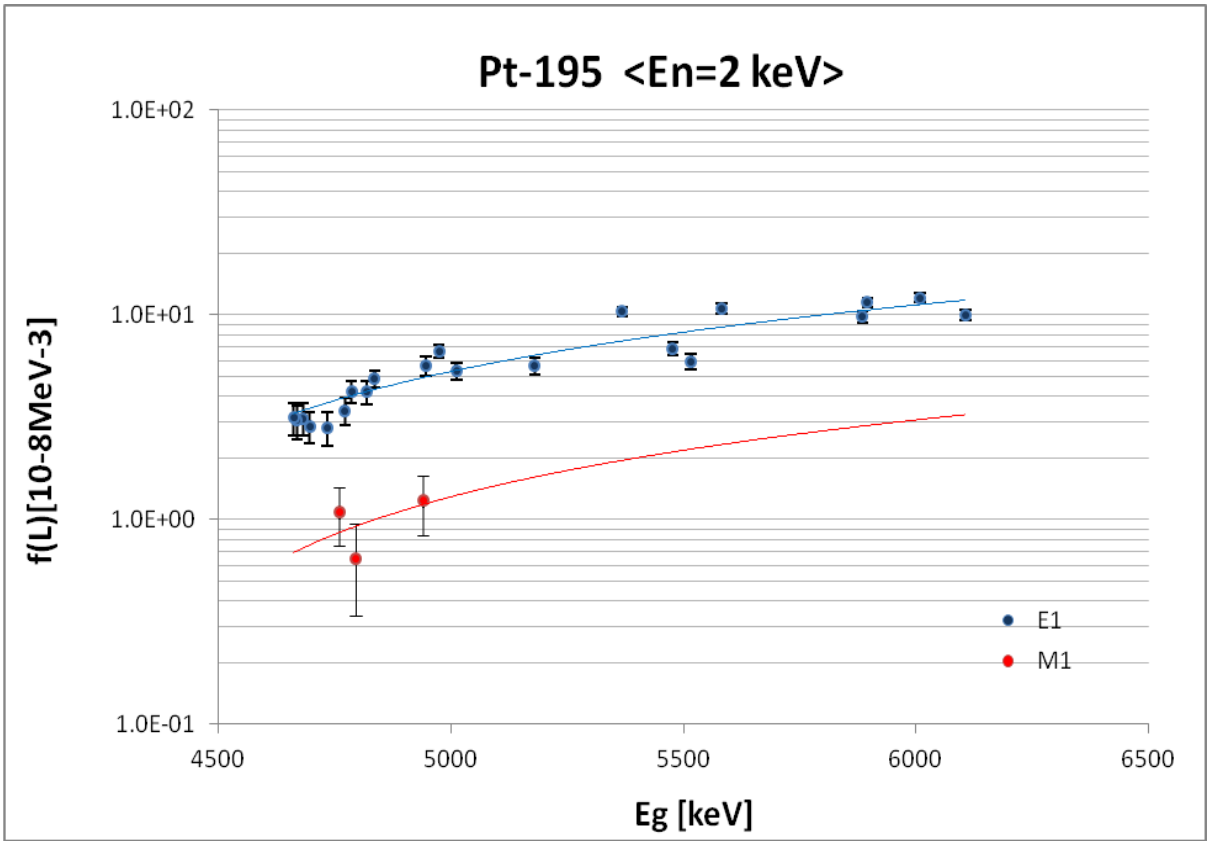
Pt-195 <En=2 keV>
1.0E+02
1.0E+01
1.0E+00
1.0E-01
f(L)[10-8MeV-3]
4500
5000
5500
6000
6500
Eg [keV]
E1
M1

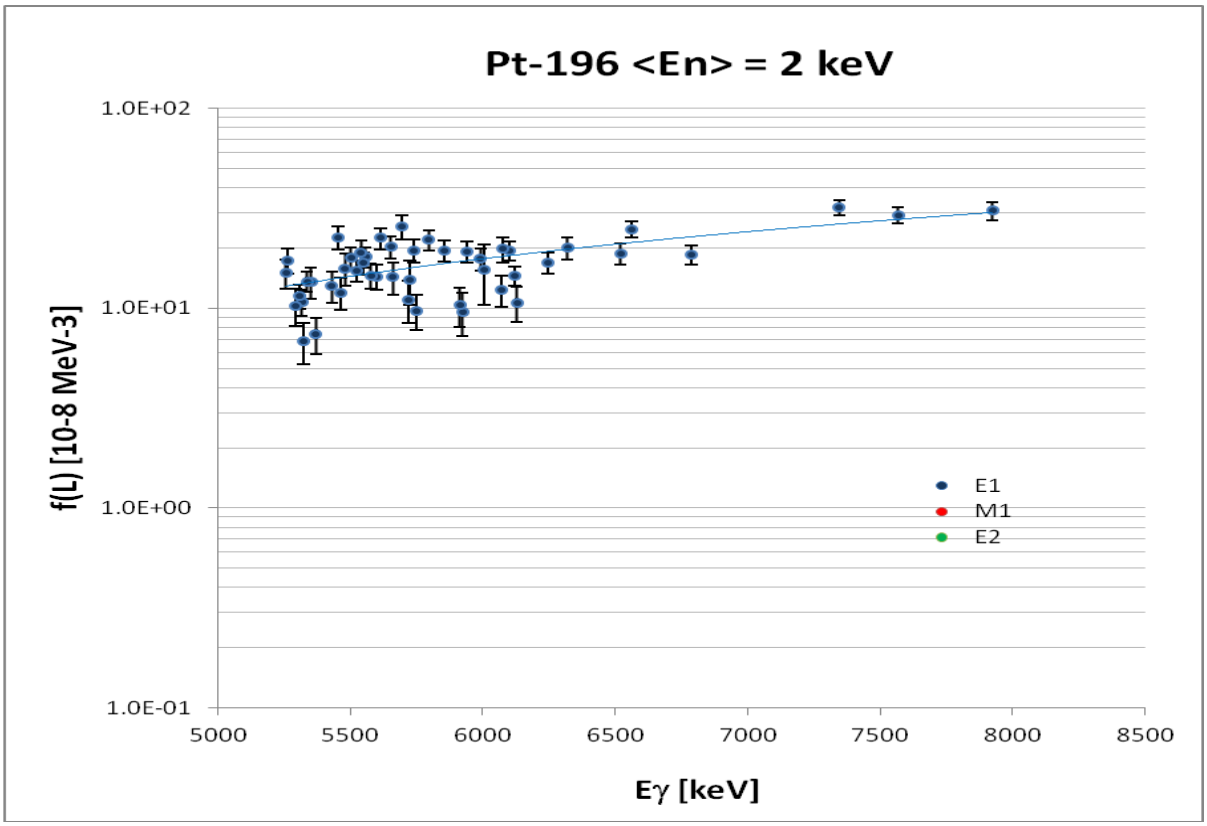
Pt-196 <En> = 2 keV
1.0E+02
1.0E+01
1.0E+00
1.0E-01
f(L) [10-8 MeV-3]
5000
5500
6000
6500
7000
7500
8000
8500
Eγ [keV]
E1
M1
E2

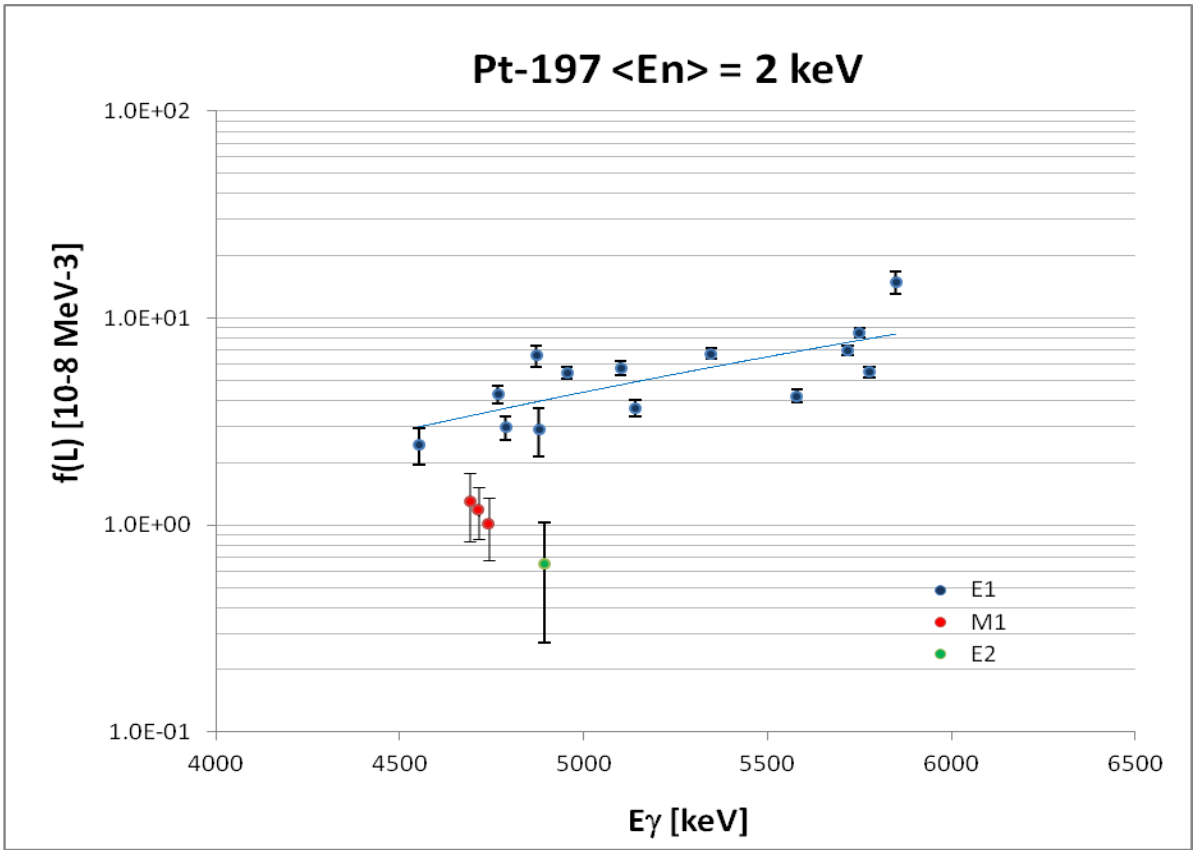
Pt-197 <En> = 2 keV
1.0E+02
1.0E+01
1.0E+00
1.0E-01
f(L) [10-8 MeV-3]
4000
4500
5000
5500
6000
6500
Eγ [keV]
E1
M1
E2

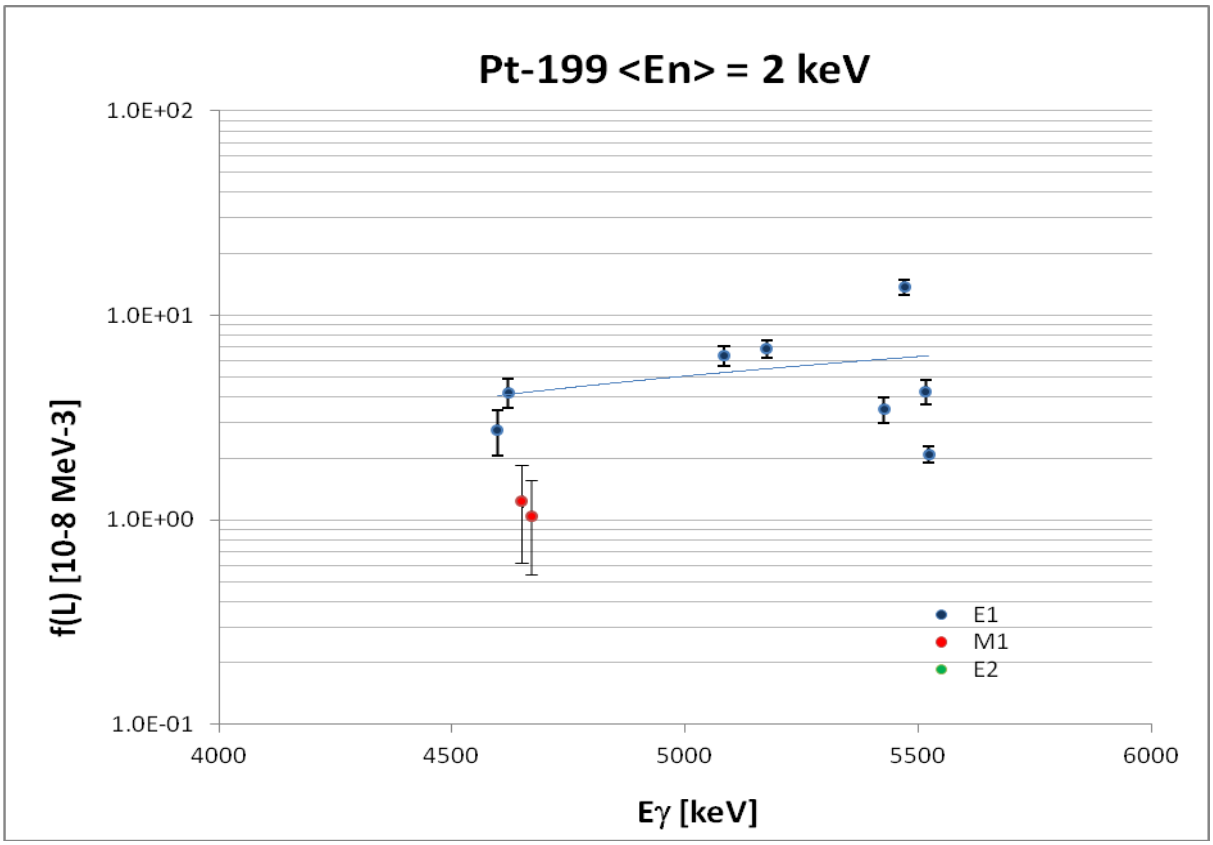
Pt-199 <En> = 2 keV
1.0E+02
1.0E+01
1.0E+00
1.0E-01
f(L) [10-8 MeV-3]
4000
4500
5000
5500
6000
Eγ [keV]
E1
M1
E2

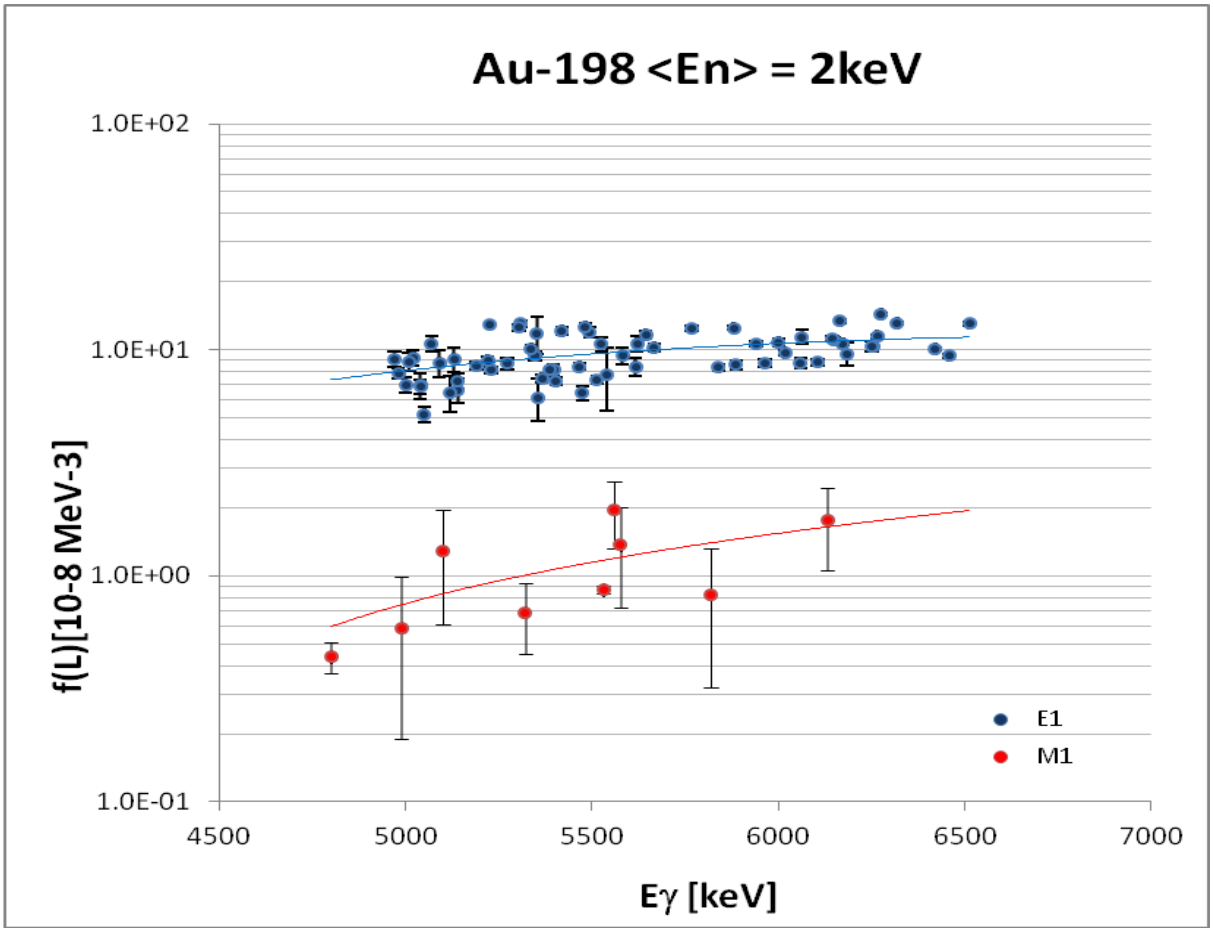
Au-198 <En> = 2keV
1.0E+02
1.0E+01
1.0E+00
1.0E-01
f(L)[10-8 MeV-3]
4500
5000
5500
6000
6500
7000
Eγ [keV]
E1
M1

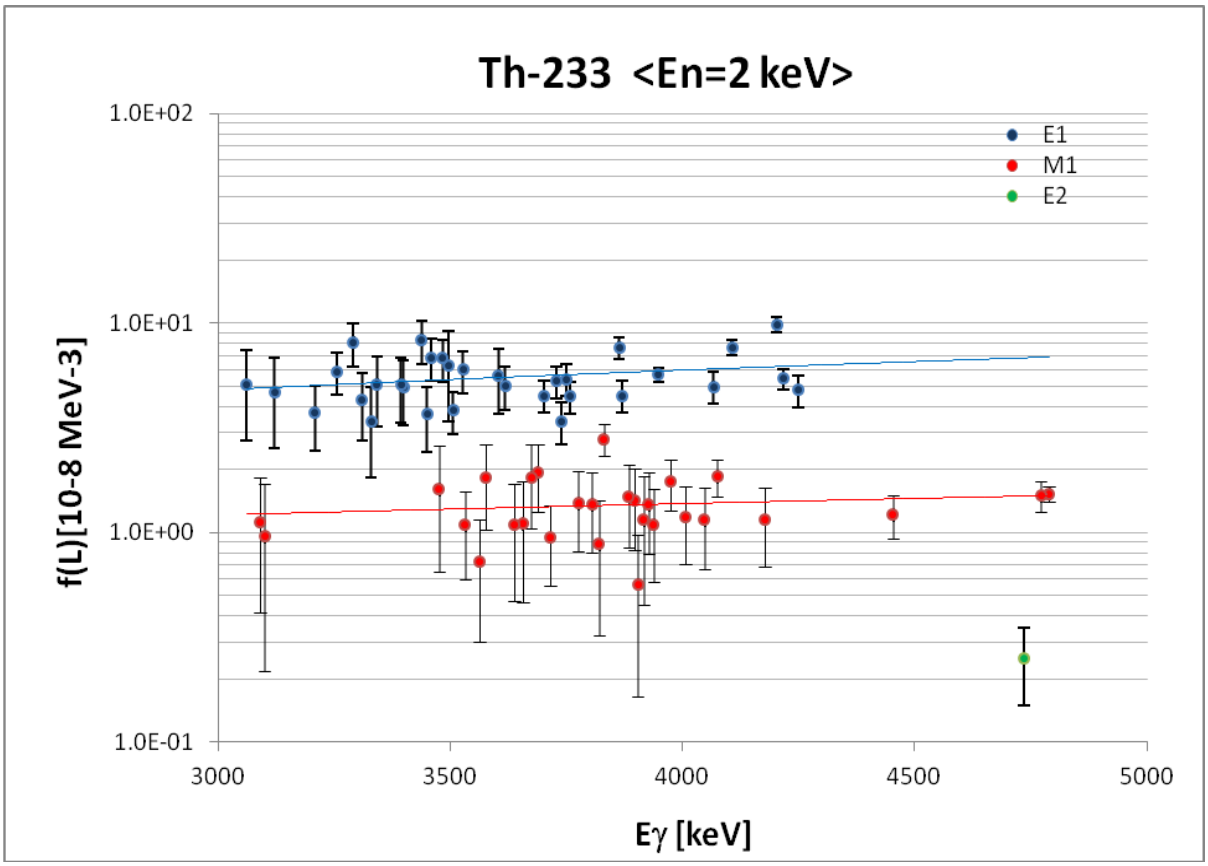
Th-233 <En=2 keV>
1.0E+02
1.0E+01
1.0E+00
1.0E-01
f(L)[10-8 MeV-3]
3000
3500
4000
4500
5000
Eγ [keV]
E1
M1
E2

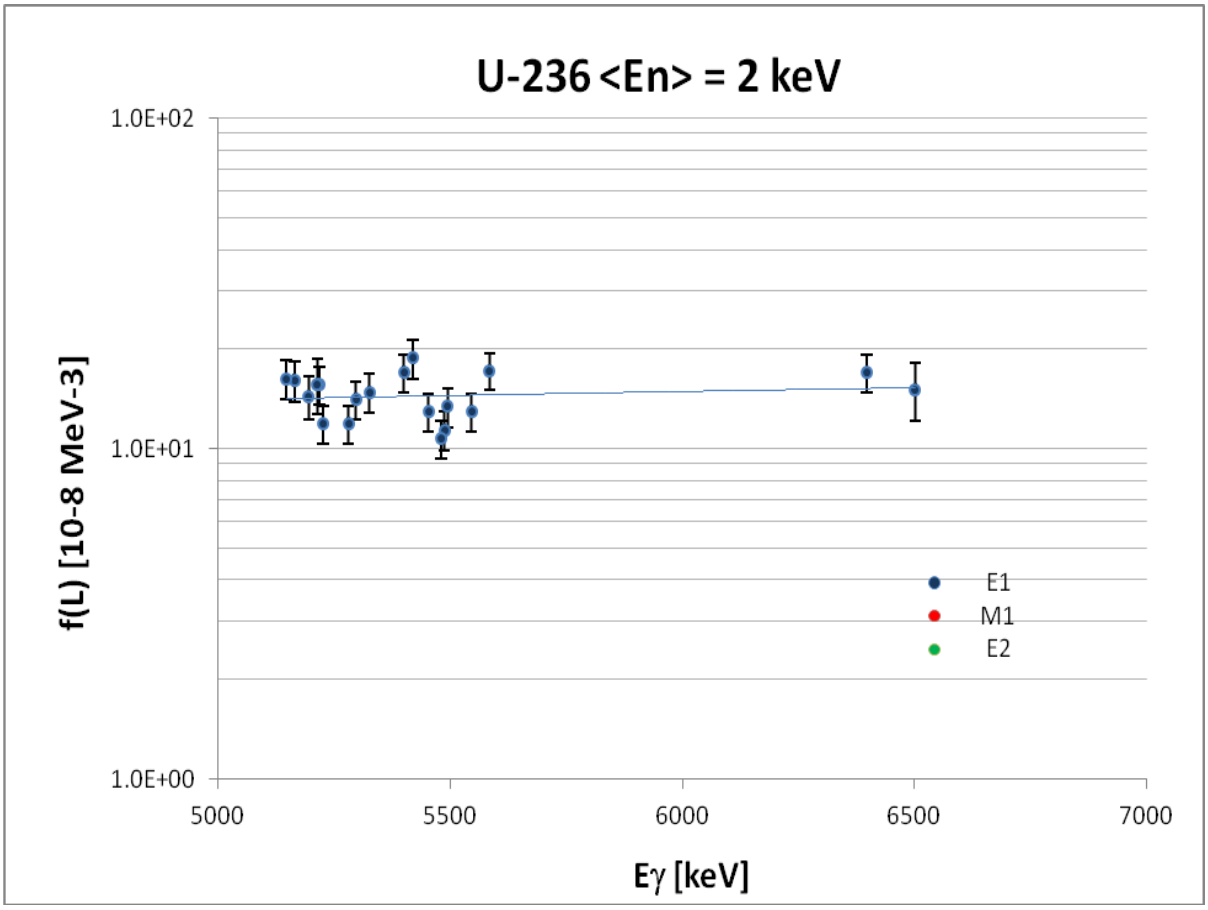
U-236 <En> = 2 keV
1.0E+02
1.0E+01
1.0E+00
f(L) [10-8 MeV-3]
5000
5500
6000
6500
7000
Eγ [keV]
E1
M1
E2

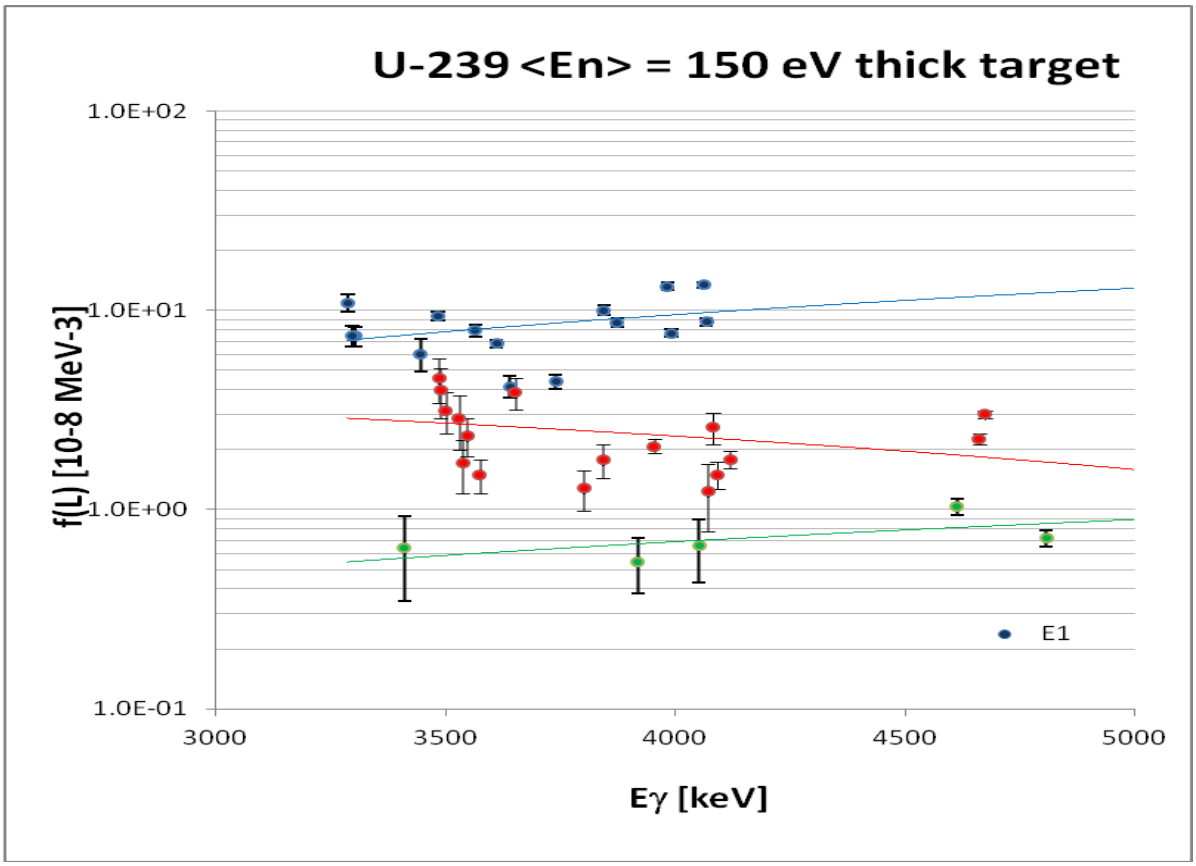
U-239 <En> = 150 eV thick target
1.0E+02
1.0E+01
1.0E+00
1.0E-01
f(L) [10-8 MeV-3]
3000
3500
4000
4500
5000
Eγ [keV]
E1

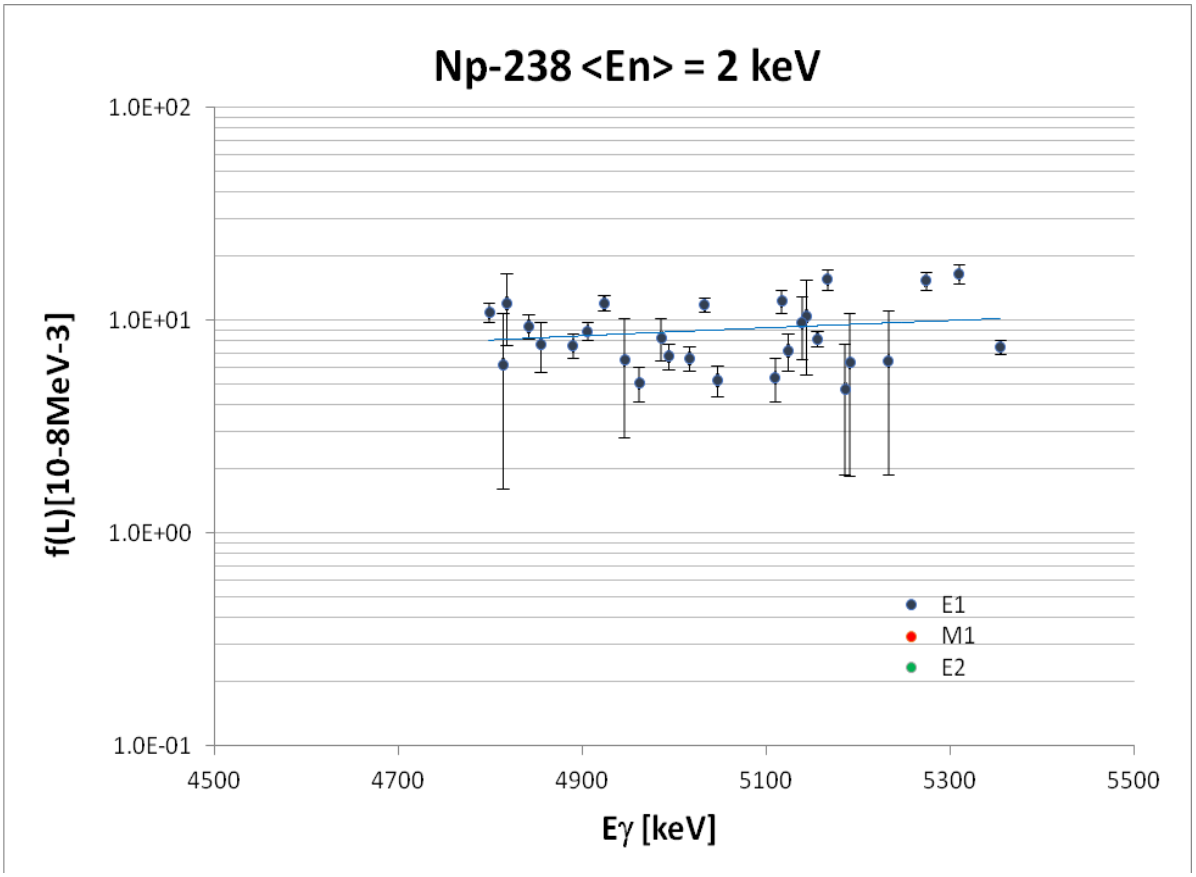
Np-238 <En> = 2 keV
1.0E+02
1.0E+01
1.0E+00
1.0E-01
f(L)[10-8MeV-3]
4500
4700
4900
5100
5300
5500
Eγ [keV]
E1
M1
E2

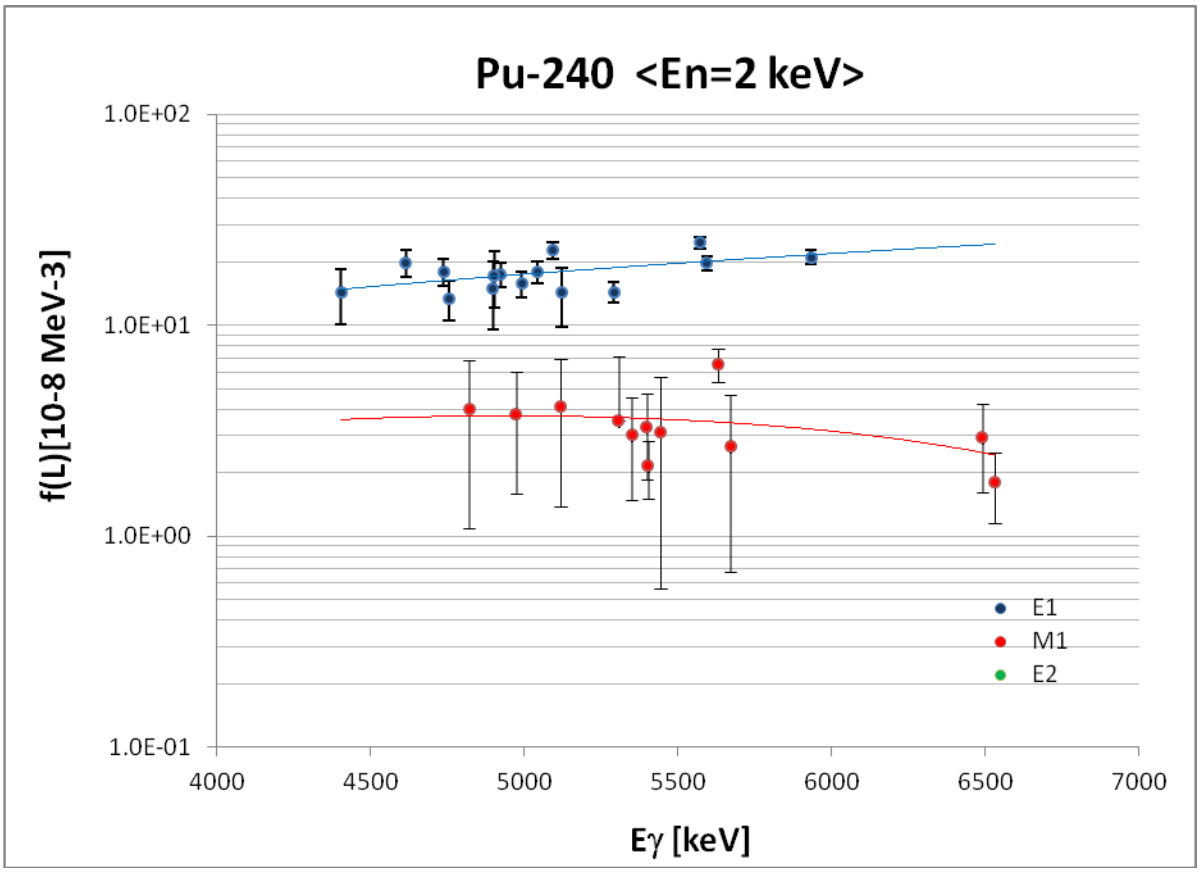
Pu-240 <En=2 keV>
f(L)[10-8 MeV-3]
1.0E+02
1.0E+01
1.0E+00
1.0E-01
4000
4500
5000
5500
6000
6500
7000
Eγ [keV]
E1
M1
E2